The Development of New Methods for Ion Transport for the Potential Future Treatment of Channelopathies and Cancers

by

Braeden Hourihan

BSc in Chemistry, University of New Brunswick, 2021

A Thesis Submitted in Partial Fulfillment
of the Requirements for the Degree of

Master of Science

in the Graduate Academic Unit of Chemistry

Supervisor: Barry Blight, PhD, Chemistry

Examining Board: Andreas Decken, PhD, Chemistry
Brian Hayden, PhD, Biology
Gilles Villemure, PhD, Chemistry, Chair

This thesis is accepted by the
Dean of Graduate Studies

THE UNIVERSITY OF NEW BRUNSWICK

December 2022

ABSTRACT

Channelopathies are diseases caused by disruption of the ion transport process within the cell; cystic fibrosis being one of the most well-known examples of these conditions. Developing new methods of synthetically transporting ions into cells with non-functioning protein channels is imperative for improving treatments for these diseases. Cancer drugs that function as ion transporters have also recently become of interest to scientists. These drugs work to induce cellular apoptosis of cancer cells by causing a rapid influx of ions to disrupt the cell's ion homeostasis and are proving to be efficient in treating cancer. During cancer treatment, lifesaving drugs, and dyes used to image tumors must be administered separately. Within the field of theranostics, scientists have sought out to combine therapeutic drugs and diagnostic tools to solve this problem, however, there has yet to be a drug developed that can both induce cellular apoptosis through ion transport, and act as a tumor imaging dye. Within this project we have developed the first reported example of using metal-organic frameworks as anion transporters, as well as the development of two new iridium (III) complexes that can act as both bioimaging dyes and as anion transporters for the potential future treatment of channelopathies and cancers.

ACKNOWLEDGEMENTS

I would like to thank Dr. Barry Blight for his supervision, guidance, and mentorship over the past three years. As my supervisor for multiple summer research projects, CHEM 2009, 3009, 4000, and my masters project he helped me to discover my love for research. I am also grateful for all the help I have received from Marta Tomas throughout this project and my time spent in the Blight group. She helped me to obtain all of my photophysical data, as well as mass spec and ^{13}C NMR for some of my compounds when I needed to move for my PhD. I am thankful to amazing people I met during my time in the Blight group including Holly, Erica, Sarah, and Harri who created a fun and enjoyable work environment that I looked forward to working in every day. I am also grateful for the help of Dr. Andreas Decken and Dr. Ghislain Deslongchamps for helping me throughout my masters by serving on my committee, and for their helpful comments on my research. Finally, I would like to extend my thanks Steven Cogswell and Dr. Hall in the microscopy unit in biology for all their help using the confocal microscope, and Dr. Anna Ignaszak for lending me equipment needed to complete my project.

Table of Contents

ABSTRACT ii
ACKNOWLEDGEMENTS iii
Table of Contents iv
List of Tables vi
List of Figures vii
List of Symbols, Nomenclature or Abbreviations xii
Chapter 1 1
Introduction 1
1.1 Metal-Organic Frameworks 1
1.2 Vesicles 5
1.3 Fluorescence and Bioimaging Dyes 10
1.4 Cyclometalated Iridium (III) Complexes 14
1.5 Ion Transport 20
1.6 Channelopathies 26
1.7 Synthetic Methods of Ion Transport 29
1.8 Project Goals 34
1.9 References 35
Chapter 2 41
MOFs as Anion Transporters for the Potential Treatment of Channelopathies and Cancers 41
2.1 Introduction 42
2.2 Experimental 45
2.3 Results and Discussion 49
2.4 Conclusion 63
2.5 Future Work 63
2.6 References 64
Chapter 3 67
Iridium (III) Complexes as Dual Bioimaging Dyes and Anion Transporters for Theranostics Applications 67
3.1 Introduction 68

3.2 Experimental 70
3.3 Results and Discussion 79
3.4 Conclusion 92
3.5 Future Work 92
3.6 References 93
Chapter 4 95
Conclusions and Future Work 95
4.1 Conclusions 95
4.2 Future Work 97
4.3 References 100
Appendices 101
Appendix I 101
CV

List of Tables

Table 1 Photophysical data for compounds 4 and 6 79

List of Figures

Figure 1.1 Structure of MOF-5 and MOF-177 open source from Wikimedia Commons 1

Figure 1.2 Structures of terephthalic acid, **1**, trimesic acid, **2**, and 2-methylimidazole, **3** 2

Figure 1.3 Chemical structures of POPC (top) and POPG (bottom) 7

Figure 1.4 Chemical structure of cholesterol 7

Figure 1.5 Comparison of the sizes of SUVs, LUVs, and GUVs 8

Figure 1.6 Apparatus used for the electroformation of GUVs 9

Figure 1.7 Jablonski diagram illustrating the photophysical processes responsible for fluorescence and phosphorescence 11

Figure 1.8 Structures of common families of organic fluorophores; Xanthene dyes, **4**, Oxazine dyes, **5**, Carbopyronine dyes, **6**, Rylene dyes, **7**, Cyanine dyes, **8**, and Bodipy dyes, **9** 12

Figure 1.9 Structure of simple $Ir(ppy)_3$ green emitting complex 15

Figure 1.10 Chemical structure of lipid mimetic iridium (III) complex synthesized by Quan et al. 17

Figure 1.11 Chemical structures of guanidine and thiourea iridium (III) complexes used to treat drug resistant cancer cells synthesized by Balonova et al. 20

Figure 1.12 Depiction of different type of passive transport (diffusion, facilitated diffusion, and osmosis), and active transport 23

Figure 1.13 Depiction of different types of secondary active transport 25

Figure 1.14 Diagram of healthy vs cystic fibrosis airways 28

Figure 1.15 The chemical structure of prodigiosin 31

Figure 1.16 Chemical structure of salinomycin 32

Figure 1.17 Structure of thiourea based anion transporter synthesized by Davis et al. 33

Figure 1.18 Structures of chloride ion transporters published by Busschaert et al. 34

Figure 2.1 Depiction of a MOF being used to transport chloride ions into a GUV filled with the chloride sensitive dye lucigenin 45

Figure 2.2 Structures of organic linker molecules of 18) MOF-808, 19) MOF UiO-67, and 20) MOF Zr-BTDZ 50

Figure 2.3 Confocal fluorescence images of GUVs anchored to no MOFs at 0 minutes, and 20 minutes after addition of NaCl, Right: Brightfield images taken at 0 minutes, and 20 minutes after addition of NaCl 52

Figure 2.4 Plot of Time (seconds) vs Normalized Fluorescence for the decrease in fluorescence of lucigenin dye within GUVs not anchored to MOFs after the addition of NaCl 53

Figure 2.5 Chemical structure of lucifer yellow dye 53

Figure 2.6 Confocal fluorescence images of GUVs filled with lucifer yellow dye and anchored to MOF-808 at 0 minutes, and 20 minutes after addition of NaCl, Right: Brightfield images taken at 0 minutes, and 20 minutes after addition of NaCl 54

Figure 2.7 Plot of Time (seconds) vs Normalized Fluorescence for the decrease in fluorescence of lucifer yellow dye within GUVs anchored to MOF-808 after the addition of NaCl 55

Figure 2.8 Confocal fluorescence images of GUVs filled with lucifer yellow dye and anchored to MOF UiO-67 at 0 minutes, and 20 minutes after addition of NaCl, Right: Brightfield images taken at 0 minutes, and 20 minutes after addition of NaCl 56

Figure 2.9 Plot of Time (seconds) vs Normalized Fluorescence for the decrease in fluorescence of lucifer yellow dye within GUVs anchored to MOF UiO-67 after the addition of NaCl 57

Figure 2.10 Left: Confocal fluorescence images of GUVs anchored to MOF-808 at 0 minutes, and 20 minutes after addition of NaCl, Right: Brightfield images taken at 0 minutes, and 20 minutes after addition of NaCl 58

Figure 2.11 Plot of Time (seconds) vs Normalized Fluorescence for the decrease in fluorescence of lucigenin dye within GUVs anchored to MOF-808 after the addition of NaCl 59

Figure 2.12 Left: Confocal fluorescence images of GUVs anchored to MOF UiO-67 at 0 minutes, and 20 minutes after addition of NaCl, Right: Brightfield images taken at 0 minutes, and 20 minutes after addition of NaCl 60

Figure 2.13 Plot of Time (seconds) vs Normalized Fluorescence for the decrease in fluorescence of lucigenin dye within GUVs anchored to MOF UiO-67 after the addition of NaCl 61

Figure 2.14 Left: Confocal fluorescence images of GUVs anchored to MOF UiO-67 at 0 minutes, and 20 minutes after addition of NaCl, Right: Brightfield images taken at 0 minutes, and 20 minutes after addition of NaCl 62

Figure 2.15 Plot of Time (seconds) vs Normalized Fluorescence for the decrease in fluorescence of lucigenin dye within GUVs anchored to MOF Zr-BTDZ after the addition of NaCl 63

Figure 3.1 Depiction of iridium (III) complexes being used as dual anion transporters and bioimaging dyes 70

Figure 3.2 Reaction scheme for the synthesis of compound **22** 74

Figure 3.3 Reaction scheme for the synthesis of compound **23** 74

Figure 3.4 Reaction scheme for the synthesis of compound **24** 75

Figure 3.5 Reaction scheme for the synthesis of compound **25** 76

Figure 3.6 Left: Compound **25** as an oily yellow solid, right: compound **25** under UV light 76

Figure 3.7 Reaction scheme for the synthesis of compound **26** 77

Figure 3.8 Reaction scheme for the synthesis of compound **27** 78

Figure 3.9 Left: Compound **27** and a yellow solid, right: compound under UV light 79

Figure 3.10 Confocal (left) and brightfield (right) images taken at 488 nm of compound 25 as a bioimaging dye in the lipid bilayer of GUVs 81

Figure 3.11 Confocal (left) and brightfield (right) images taken at 488 nm of compound 27 as a bioimaging dye in the lipid bilayer of GUVs 82

Figure 3.12 Confocal fluorescence images of GUVs without anion transporters at 0 minutes, and 20 minutes after addition of NaCl, Right: Brightfield images taken at 0 minutes, and 20 minutes after addition of NaCl 84

Figure 3.13 Plot of Time (seconds) vs Normalized Fluorescence for the decrease in fluorescence of lucigenin dye within GUVs without anion transporters after the addition of NaCl 85

Figure 3.14 Confocal fluorescence images of GUVs filled with lucifer yellow dye and compound 25 at 0 minutes, and 20 minutes after addition of NaCl, Right: Brightfield images taken at 0 minutes, and 20 minutes after addition of NaCl 86

Figure 3.15 Plot of Time (seconds) vs Normalized Fluorescence for the decrease in fluorescence of lucifer yellow dye within GUVs with compound 25 after the addition of NaCl 86

Figure 3.16 Confocal fluorescence images of GUVs filled with lucifer yellow dye and compound 27 at 0 minutes, and 20 minutes after addition of NaCl, Right: Brightfield images taken at 0 minutes, and 20 minutes after addition of NaCl 87

Figure 3.17 Plot of Time (seconds) vs Normalized Fluorescence for the decrease in fluorescence of lucifer yellow dye within GUVs with compound 27 after the addition of NaCl 88

Figure 3.18 Left: Confocal fluorescence images of GUVs with compound 25 at 0 minutes, and 20 minutes after addition of NaCl, Right: Brightfield images taken at 0 minutes, and 20 minutes after addition of NaCl 89

Figure 3.19 Plot of normalized fluorescence vs time over a period of 20 minutes for chloride ion transport studies conducted on compound 25 90

Figure 3.20 Left: Confocal fluorescence images of GUVs with compound 27 at 0 minutes, and 20 minutes after addition of NaCl, Right: Brightfield images taken at 0 minutes, and 20 minutes after addition of NaCl 90

Figure 3.21 Plot of normalized fluorescence vs time over a period of 20 minutes for chloride ion transport studies conducted on compound 27 91

List of Symbols, Nomenclature or Abbreviations

Abbreviation	Definition
µm	micrometer
Å	angstrom
ABC	ATP-binding cassette
ADP	adenosine diphosphate
ATP	adenosine triphosphate
BODIPY	boron-dipyrromethene
BSA	bovine serum albumin
℃	degrees Celsius
C_2H_2	acetylene
CFTR	cystic fibrosis transmembrane conductance regulator
CH_4	methane
ClC-1	skeletal muscle chloride channel
CLCN1	chloride voltage-gated channel 1
CO_2	carbon dioxide
CSC	cancer stem cell
DMSO	dimethyl sulfoxide
DNA	deoxyribonucleic acid
EDG	electron-donating group
ENaC	epithelial sodium channel
EWG	electron-withdrawing group
FPs	fluorescent proteins

GFP	green fluorescent protein
GUV	giant unilamellar vesicle
H_2	hydrogen
HOMO	highest occupied molecular orbital
Hz	hertz
Ir	iridium
ITO	indium tin oxide
KATP	adenosine triphosphate-sensitive potassium channel
Kir6.x	inwardly rectifying potassium channel subunits
LUMO	lowest unoccupied molecular orbital
LUV	large unilamellar vesicle
m^2g^{-1}	meters squared per gram
mg	milligram
mL	milliliter
mm	millimeter
mM	millimolar
MOF	metal-organic framework
mol	mole
$NaNO_3$	sodium nitrate
NF-κB	nuclear factor kappa B
nm	nanometer
Pd	palladium
pO_2	partial pressure of oxygen

POPC	1-palmitoyl-2-oleoyl-sn-glycero-3-phosphocholine
POPG	1-palmitoyl-2-oleoyl-sn-glycero-3-phospho-rac-(1-glycerol)
ppy	phenyl pyridine
Pt	platinum
ROS	reactive oxygen species
Ru	ruthenium
S3	segment 3
SGLT1	sodium-glucose transport proteins
SURx	sulfonylurea receptors
SUV	small unilamellar vesicle
Tpphz	tetrapyrido[3,2-a:2',3'-c:3",2"-h:2"',3"'-j]phenazine
V	volt
wt-FP	wild-type fluorescent protein
wt-GFP	wild-type green fluorescent protein
λ	wavelength

Chapter 1
Introduction

1.1 Metal-Organic Frameworks

First developed in the 1990s, metal-organic frameworks (MOFs) are 3-dimensional crystalline structures composed of organic ligands linked together by metal nodes.[1]

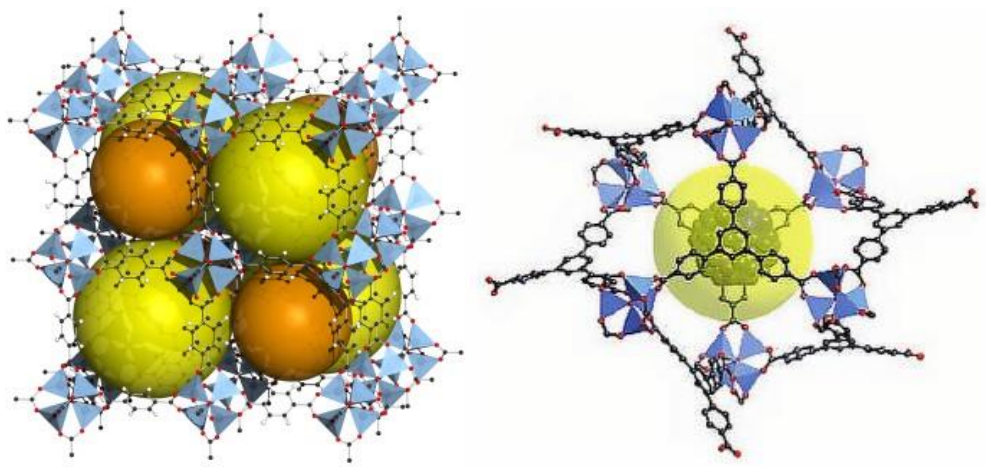

Figure 1.1: Structures of MOF-5 and MOF-177, open source from Wikimedia Commons, blue is indicative of metals, yellow and orange spheres demonstrate pore size.

These organic ligands typically composed of carbon and hydrogen, often in the forms of aromatic rings, and frequently include oxygen and nitrogen atoms as well. Some of the most used organic linkers for MOF synthesis include terephthalic acid (1,4-benzenedicarboxylic acid), trimesic acid (benzene-1,3,5-tricarboxylic acid), and 2-methylimidazole.[2]

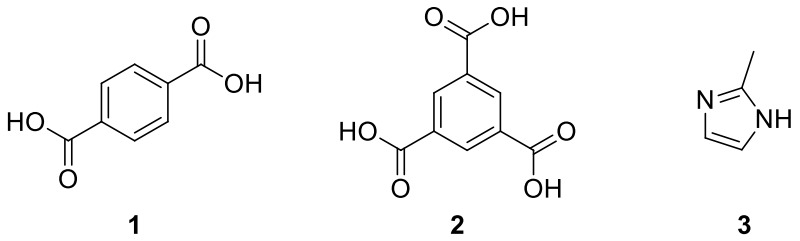

Figure 1.2: Structures of terephthalic acid, **1**, trimesic acid, **2**, and 2-methylimidazole, **3**

Since their development, thousands of MOFs have been synthesized due to the high chemical tunability of these structures.[3] Varying the metal nodes and organic ligands can lead to innumerable variations of MOFs that can be customized for specific applications.[4] Currently, the most common metal ions used in MOF synthesis include zinc (II), cobalt (II), copper (II), iron (III), and zirconium (IV); although not as common, MOFs have also been synthesized using other metals such as aluminum, titanium, iridium, and europium.[2,5,6,7,8]

The most popular way to create MOFs is by using solvothermal techniques.[9] The reaction temperature is the most crucial variable in the synthesis of MOFs. Solvothermal and non-solvothermal temperature ranges are commonly distinguished, and these factors influence the type of reaction setup that must be used. Hoskins and Robson have shown that most of the early studies on the synthesis of MOFs were conducted using low-temperature methods.[10] As a result, slow evaporation of the described solvent followed by a precipitation reaction and recrystallization was developed.[10] These techniques are frequently employed as a straightforward method to crystallize molecular and ionic compounds, because it is possible to modify the reaction circumstances such as the rate of crystal growth and nucleation. The critical nucleation concentration must be exceeded

to produce crystals from clear solutions.[9] This is commonly accomplished by adjusting the temperature or evaporating the solvent. Crystal growth occurs when particles larger than the critical radius are created.[10] Employing a concentration gradient is a useful technique. This is accomplished by stacking solutions (different solvent densities), slow diffusion of reactants into one another, and solvent evaporation of a solution of reactants.[10] Temperature can also be used as a variable to create concentration gradients; for example, the reaction mixture can be slowly cooled down or subjected to a temperature gradient. By using these techniques, large crystals appropriate for structure determination are frequently produced. Even at room temperature, MOFs have been created by simply combining the starting materials; examples of this include MOF-5, MOF-74, MOF-177, HKUST-1, and ZIF-8.10. This technique, which is also known as a direct precipitation reaction, demonstrates that some MOFs must crystallize in a short period. Unexpectedly, several of these MOFs, such as ZIF-8, have high chemical and thermal stabilities.[10] Variations in reaction temperature have a significant impact on product formation, and higher temperatures are frequently associated with denser, more condensed structures. To achieve appropriate crystallinity and reaction rates in some systems, an increase in reaction temperature may also be required, especially if kinetically more inert ions are used.[10] The crystal morphology can also be significantly influenced by the temperature, and prolonged reaction times can even lead to the degradation of the MOF. There have been significant improvements made in the synthesis of MOFs after more than two decades of study and development.[9] There are also several newly reported techniques, including electrochemical, microwave-assisted, mechanochemical, and microfluidic assembly.

Using modulators is another method to influence the structure of MOFs.[10,11] Kitagawa originally described the use of coordination modulation to regulate the size and form of MOFs. He called this strategy the "coordination modulation method," and the first known application of this technique was the employment of carboxylic acid additives to control the development of MOF crystals.[11] In this investigation, a predetermined amount of acetic acid was introduced to the crystallization mother liquor. Through competitive coordination with the metal clusters, acetic acid reduced the coordination between organic linkers and metal clusters, which affected the development of the crystals and lattice structure. Acetic acid continues to be a prominent option of modulator in this technique, which has now gained popularity for influencing the morphology of MOFs that are being manufactured.[11]

MOFs have certain advantageous structural characteristics, including high porosity, high surface area, variable pore size and geometry compared to conventional porous materials like activated carbons and zeolites. These characteristics make gas storage and separation one of the most prevalent and extensively researched uses of MOFs. Several gases, such as hydrogen (H_2), carbon dioxide (CO_2), acetylene (C_2H_2), and methane (CH_4) gases have been used in their testing.[12] A rising demand for energy resources has occurred because of the growing world population and economy. Years of exploitation of fossil fuels have led to a wide range of environmental issues, with climate change being the most pressing one. Researchers are now looking for novel energy carriers that will reduce our carbon footprint. Since hydrogen gas contains the maximum energy per mass of any fuel, it has been shown to be one possible substitute for typical fossil fuels.[12] The biggest obstacle to employing hydrogen gas is its relatively low

volumetric energy density at ambient temperatures, particularly when on board moving vehicles. This has led to the creation of novel and enhanced techniques for the effective storage of hydrogen gas under settings close to ambient temperatures.[12] Yaghi et al. reported the first instance of hydrogen storage in MOFs using MOF-5 in 2003. Hundreds of additional MOF materials have been researched for their potential in hydrogen storage over the past 20 years since this discovery.[12]

In summary, MOFs are a new and fascinating area of research that has gained popularity among chemistry researchers. This is primarily due to their unique characteristics like chemical tunability, large pore area and internal surface area, and thermal stability. They are easily synthesized using solvothermal methods and frequently employed for a variety of applications with gas storage being among the most common.

1.2 Vesicles

Vesicles are self-assembling structures that consist of fluid or gas enclosed by a lipid bilayer, a membrane composed of lipid molecules with hydrophilic heads and hydrophobic tails.[13] Vesicles can be unilamellar, meaning they only have one lipid bilayer, or they can be multilamellar, which means they have two or more lipid bilayers. These structures are naturally found within living cells and form during the processes of secretion (exocytosis), uptake (endocytosis) and transport of materials within the plasma membrane.[14] These vesicles are involved in various biological activities that are imperative to the cell's survival including playing roles in metabolism, transport, buoyancy control, and temporary storage of food and enzymes. They can also act as chemical reaction chambers.[13]

There are various types of vesicles within human cells. These include transport vesicles,[15] secretory vesicles,[16] extracellular vesicles,[17] and even gas vesicles.[13] Transport vesicles function to transport proteins made on ribosomes found in the rough endoplasmic reticulum to other structures within the cell such as lysosomes, peroxisomes, or even to destinations outside of the cell. These proteins travel inside the vesicles from one destination to another. Secretory vesicles help the cell to excrete various materials. Cells have many reasons to excrete materials. One reason is to dispose of wastes. Other reasons can be tied to the function of the cell. Within a larger organism, some cells are specialized to produce certain chemicals. These chemicals are stored in secretory vesicles and released when needed. An example of this includes when animal endocrine tissues release hormones into the bloodstream. These hormones are stored within secretory vesicles.

There are also extracellular vesicles that are secreted by cells into the extracellular space and are produced by all domains of life including complex eukaryotes, both Gram-negative and Gram-positive bacteria, mycobacteria, and fungi. The primary function of these vesicles is to deliver proteins, metabolites, and nucleic acids to recipient cells. Gas vesicles are yet another type of vesicle, and are used by Archaea, bacteria, and planktonic microorganisms,[13] and are believed to control the vertical migration of these organisms by regulating the gas content and causing buoyancy, or possibly to position the cell for maximum solar light harvesting.[13] Vesicles within cells have various methods of being formed. These can form when part of the membrane pinches off the endoplasmic reticulum or the Golgi complex, or when an object outside of the cell is surrounded by the cell membrane.

Vesicles can also be made synthetically; in which case they are also commonly called liposomes.[18] These vesicles are synthesized from lipids such as 1-palmitoyl-2-oleoyl-sn-glycero-3-phosphocholine (POPC)[18] and 1-palmitoyl-2-oleoyl-sn-glycero-3-phospho-rac-(1-glycerol)[18] shown in Figure 1.3. Cholesterol is also necessary for the synthesis of vesicles; its purpose is to add rigidity to make them more stable and less likely to break.[20]

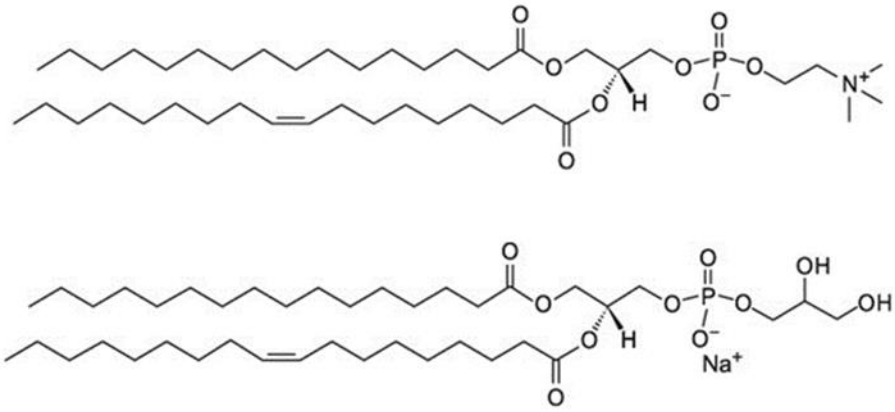

Figure 1.3: Chemical structures of POPC (top) and POPG (bottom).

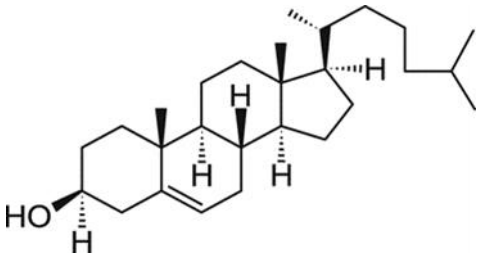

Figure 1.4: Chemical structure of cholesterol.

Synthetic vesicles can be made in different sizes including small unilamellar vesicles (SUVs) which are less than 100 nm in size, large unilamellar vesicles (LUVs) which range in size from 100 nm – 1 μm, and finally giant unilamellar vesicles (GUVs)

which typically range in size from 1 μm – 100 μm, and are the vesicles used in the studies of this thesis.[21]

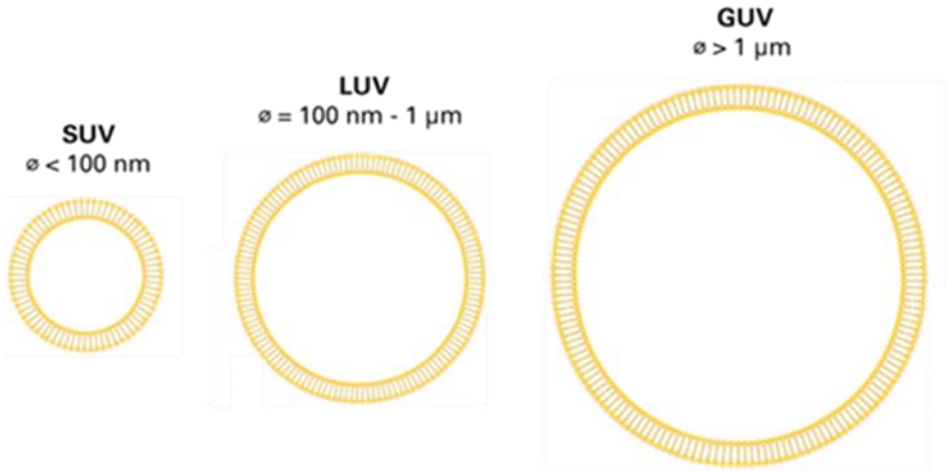

Figure 1.5: Comparison of the sizes of SUVs, LUVs, and GUVs.

The most common method for the synthesis of GUVs is electroformation, which was the technique used in this study. Electroformation is a technique during which a lipid film that is spread on indium-tin oxide (ITO)-coated glass slides peels away from the slides as a low voltage is passed through the apparatus (Figure 1.6), resulting in vesicles forming in solution. The charged polar heads of these molecules along with their long hydrophobic alkyl chain tails aggregate when exposed to water forcing the tails inward and the heads outward into the shape of a closed spherical capsule.[22,23,24,25]

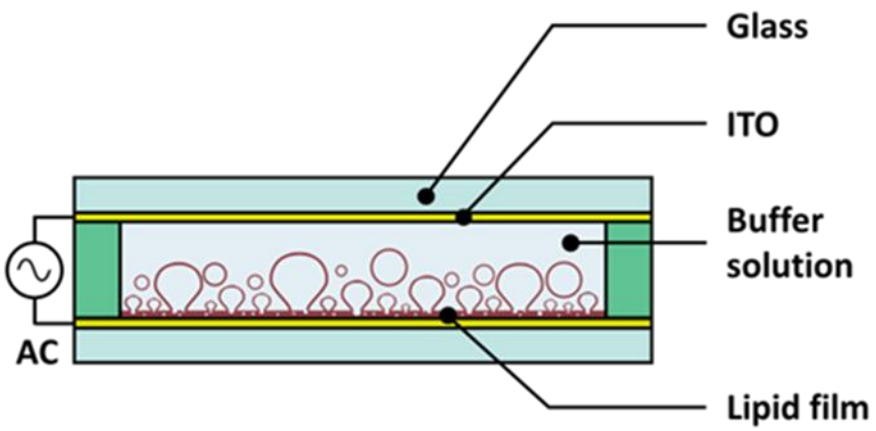

Figure 1.6: Apparatus used for the electroformation of GUVs.

The comparatively simple composition of GUVs has given scientists further insight into the complex mechanics of living cells, such as their biological membranes and the bodily functions they facilitate. The living cell is an active and complex unit, with various interconnected systems making it extremely difficult to design experiments on one specifically chosen aspect of the cell. Due to their similarity in size to living cells and their ability to be designed for specific experiments, it has become increasingly common to use GUVs as cell models in experiments, one example of this being the study of self-assembly processes that occur on the cellular membrane.[26] GUVs have also been used to test the capability of single molecule ion transporters.[27] This study demonstrated that GUVs due to their similarity in structure and size to human cells, can be used as a new method to demonstrate whether ion transporters can integrate within the cellular bilayer, and transport ions into the cell. Within the study, GUVs were electroformed in the presence of lucigenin, a chloride sensitive dye, which then becomes trapped within the aqueous interior of the GUVs.[27] The GUVs were also electroformed in the presence of the ion transporter to allow for its integration into lipid bilayer. The GUVs were then

imaged on a fluorescence confocal microscope, and chloride ions were added. Following the addition of the chloride ions, as ion transport was occurring, it could be visually observed on the microscope through the decrease in fluorescence of the lucigenin dye within the vesicles.[27]

Synthetic vesicles, and GUVs specifically, are becoming more commonly studied as more new applications are discovered, and they play an integrative role in the research conducted in this thesis.

1.3 Fluorescence and Bioimaging Dyes

Luminescence is a phenomenon where there is an emission of light from a substance and is caused by electronically excited states. Luminescence can be further divided into the categories of fluorescence and phosphorescence depending on the excited states involved.[28] Fluorescence is a result of the excitation of singlet states, where an electron in the excited orbital is paired by opposite spin to a second electron in the ground state orbital.[28] Phosphorescence on the other hand is the emission of light from triplet states, in which the electron in the excited orbital has the same spin orientation as the ground state electron.[28] Such transitions to the ground state are spin-forbidden, resulting in emission rates that are relatively low compared to fluorescence. This suggests that phosphorescence takes place on a time scale of at least milliseconds and can often be seen as long as seconds.

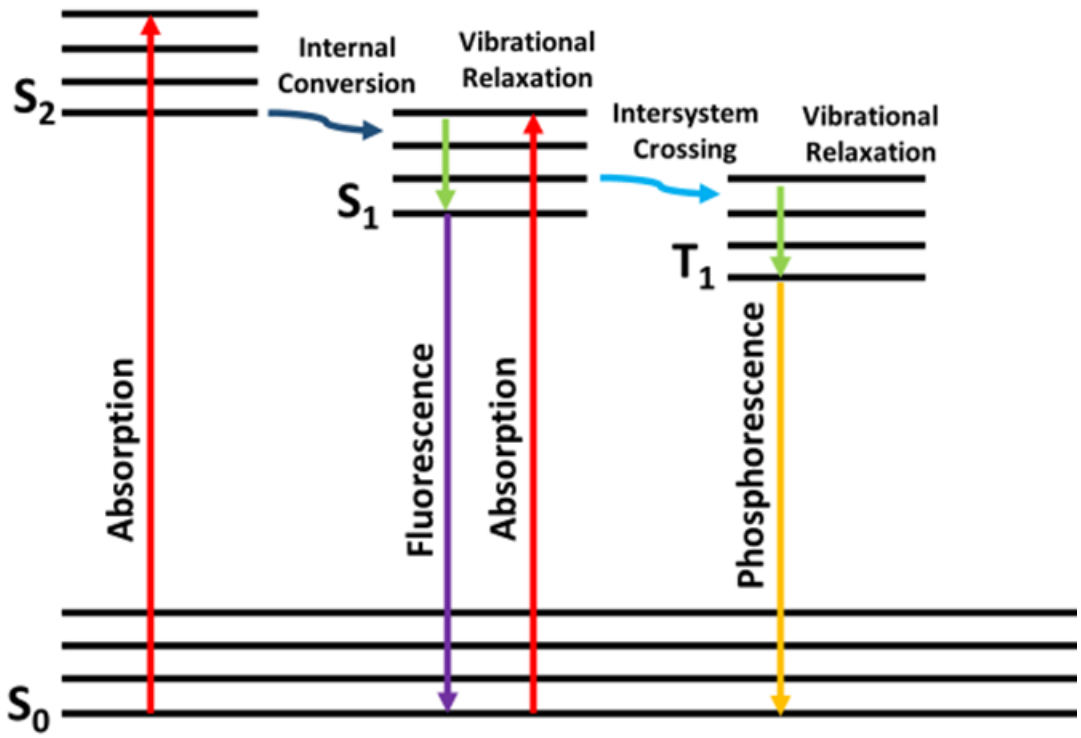

Figure 1.7: Jablonski diagram illustrating the photophysical processes responsible for fluorescence and phosphorescence.[28]

Fluorophores are fluorescent compounds that can re-emit light upon excitation. These compounds can absorb light energy of a certain wavelength, and then this light absorption causes electronic excitation of the molecules.[29] When a molecule's electrons return to their ground state, the fluorophore can re-emit the absorbed light energy at a longer wavelength. These compounds typically consist of molecules with aromatic groups, or planar or cyclic molecules with several π bonds.[29] There are several classes of commonly used fluorophores two of which include organic dyes and biological fluorophores. There are a few families of common organic fluorophores including xanthene dyes[30], oxazine dyes[31], carbopyronine dyes[32], rylene dyes[33], cyanine dyes[34], and bodipy dyes[35]. The general structures of each family of organic fluorophore can be seen

in Figure 1.8. Altering the different functional groups of these structures gives a variety of different organic fluorophores with varied fluorescent properties and the different pi conjugated systems between the structures give a range of different colours and properties.

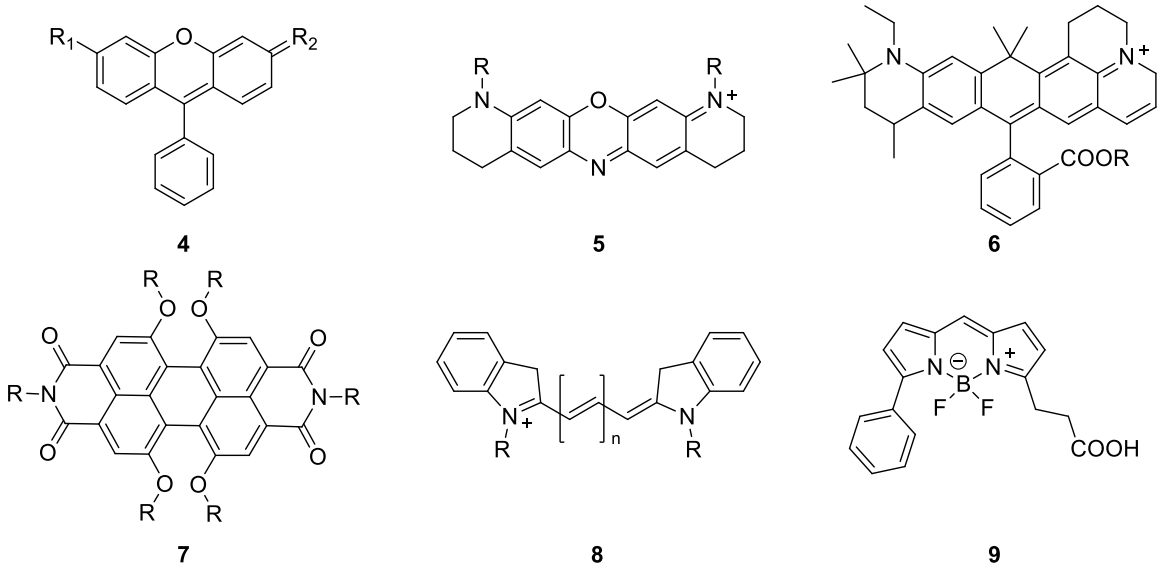

Figure 1.8: Structures of common families of organic fluorophores; Xanthene dyes, **4**, Oxazine dyes, **5**, Carbopyronine dyes, **6**, Rylene dyes, **7**, Cyanine dyes, **8**, and Bodipy dyes, **9**.

Organic fluorophores have many advantageous properties including good wavelength selection, small size (1-2 nm), as well as commercial availability and low cost. This class of fluorescent dyes comes with disadvantages as well including the fact that it is necessary at times to “tag” them to the feature to be observed, that they can photobleach, and that they are foreign organic objects that are often toxic when inserted into biological samples.[29]

Fluorescent proteins are another class of commonly used fluorophores. In 1961, fluorescent proteins were first discovered by Shimomura and Johnson when they were able to isolate the wild-type green fluorescent protein (wt-GFP) from the bioluminescent Aequorea victoria species of jellyfish. Shimomura was later awarded the Nobel Prize in chemistry in 2008 for his role in the discovery.[36] Typically, fluorescent proteins consist of a small organic chromophore covalently linked to and surrounded by a barrel of 11 β-sheet proteins and 6 α-helices. Since the initial discovery of wt-GFP, a variety of more advanced fluorescent proteins (FPs) have been developed by inducing mutations in the original wt-GFP. These mutations affect the folding efficiency and colour of the protein, and have led to drastically improved fluorescence, brightness and photostability. Currently there are several GFP mutants and other FPs which emit a spectrum of colour from blue to red. The main advantage of FPs lies in the fact that the chromophore forms spontaneously upon protein folding without the need for any additional enzymatic synthesis. This means that it is possible to express the GFP gene into cells and even entire organisms.[36] Other advantages that come with fluorescent proteins include good wavelength selection, and the fact that they are natural, so they are not toxic to cells or to the human body. Fluorescent proteins, however, are not as bright as other fluorophores and suffer from low stability.[37]

One of the biggest disadvantages that comes with a variety of classes of fluorophores is a process known as photobleaching. Photobleaching is an irreversible process that occurs when a fluorophore permanently enters what is known as a non-emitting dark state which then renders the fluorophore inactive. Photobleaching that results in fluorescence quenching can occur when the fluorophore enters the reactive

triplet state in the presence of molecular oxygen, which then interacts with the fluorophore by the formation of radical ions in solution.[38] Fluorophores that are resistant to photobleaching are highly desirable as they can remain fluorescent for significantly longer periods of time and are thus much more reliable.

One of the most common uses for fluorophores is in bioimaging applications. They are commonly used to stain tissues, cells, or materials in a variety of analytical methods like fluorescent imaging and spectroscopy. Additionally, fluorophores have become well-known for their capacity to help visualize tumors in cancer patients.[39] Over the past two decades, fluorescence imaging has attracted more interest as a reliable way to find many malignancies. Fluorescence imaging has the potential to provide doctors with high resolution images with improved contrast, enabling them to diagnose and treat cancer patients more accurately.[39] Fluorescence imaging can detect non-advanced, and even pre-cancerous tumors where imaging based on white light or radiation disregarded them. Early identification and treatment of cancer are crucial to the patient's prognosis.[39] Through a technique known as active targeting, these dyes can identify tumors by selectively delivering the dye to diseased over healthy tissue. This distribution to diseased over healthy tissue has proven useful in both diagnostic imaging and therapy.[39]

1.4 Cyclometalated Iridium (III) Complexes

Cyclometalated iridium (III) complexes are typically composed of an iridium (III) metal center bound to two cyclometalated ligands such as 2-phenylpyridine, and one bidentate ligand such as a diamine.[40] The chemical nature of this family of complexes can be readily tuned by chemical variations of the coordinated ligands, thus allowing tuning

of properties such as charge, lipophilicity, and solubility, as well as photoluminescent characteristics.[40] In fact, it is known that iridium complexes can be tuned to be emissive across the entire range of the visible spectrum, from blue to red, and further in the near-infrared region. Their colour can be tuned by altering the cyclometalated ligands on the iridium complexes. Ligands with electron-withdrawing groups (EWG) will typically result in an iridium complex with a larger HOMO-LUMO energy gap, whereas ligands with electron-donating groups (EDG) or with extending π-conjugation on the ligands will have small HOMO-LUMO energy gaps and high λ_{max}. This is because the colour that the iridium complex emits is due to the size of the HOMO – LUMO gap. These complexes are triplet state emitters, which makes them phosphorescent given that their ground state is of singlet spin multiplicity.[40]

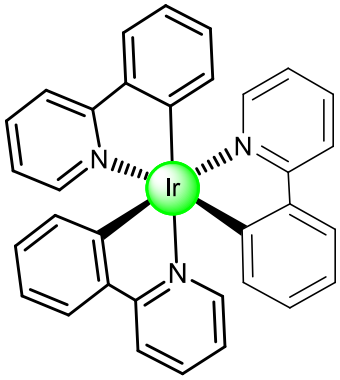

Figure 1.9: Structure of a simple $Ir(ppy)_3$ green emitting complex.

Iridium (III) cyclometalated complexes have been investigated for their use as fluorescent dyes as they have many advantageous properties over the traditional organic fluorophores. These advantages include longer luminescent lifetimes, high chemical, and photochemical stabilities so they are not as prone to photobleaching as other bioimaging dyes, colour tunability, good membrane permeability, and high Stokes shift values. These

characteristics put together have the possibility to create highly effective bioimaging dyes.[41,42]

The use of iridium (III) complexes as bioimaging dyes is not new as there have been many reported cases of their use for various biological applications.[42] To ensure the lipophilicity of iridium (III) complexes used for biological applications, it has become common to add a long alkyl chain to their structures, commonly termed “lipid mimetic” iridium (III) complexes.[42,43] These aid in the solubility of these compounds as well as enables them to integrate within the membrane of cells. In a recent study published in 2020 in the *Journal of Inorganic Biochemistry*, by Quan et al., a new iridium (III) complex was synthesized for dual use as sensor and as fluorescent dye.[42] This complex proved to be superior to normal organic fluorophores due to advantages such as longer luminescent lifetimes, high chemical, and photochemical stabilities, colour tunability and high Stokes shift values. Due to the long carbon chain on the structure of this complex (Figure 1.10) it was able to efficiently incorporate into the lipid bilayer of liposomes to function as a bioimaging dye and could be visualized on a fluorescence microscope at concentrations as low as 0.5 mol %. The authors were also able to provide evidence that the addition of the fluorescent dye to the liposomes does not affect the integrity of their lipid bilayer. They increased the concentration of the dye up to 5 mol% and noticed that the fluorescence of the liposomes was directly proportional to the mol% of dye used, and that the liposomes remained intact even with the increase in dye concentration.[42]

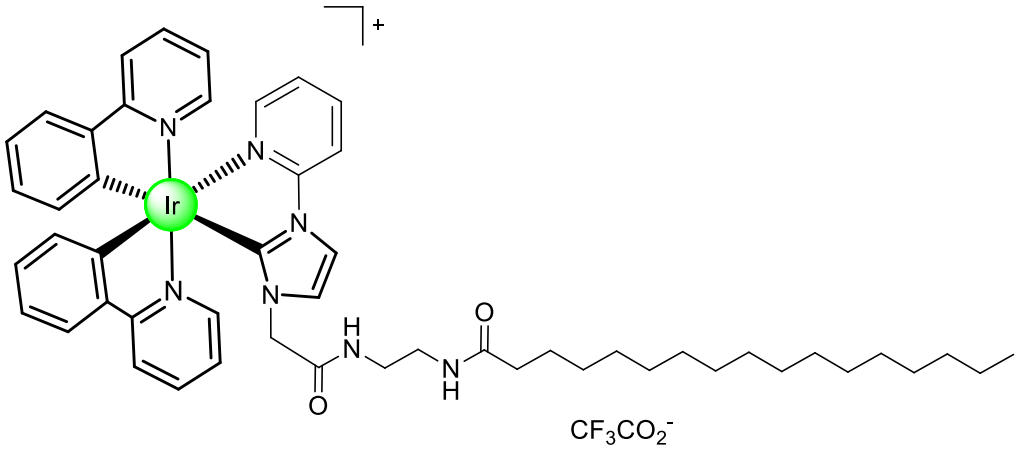

10

Figure 1.10: Chemical structure of lipid mimetic iridium (III) complex synthesized by Quan et al.

The potential for using cyclometalated iridium (III) complexes as sensors has also been explored.[44,45] Molecular oxygen is a key regulator of healthy cells, and maintaining its equilibrium is crucial for organisms. Hypoxia (oxygen deficiency) is caused when a body's steady oxygen supply is disrupted, and it is thought that this condition is closely related to several serious illnesses, including arteriosclerosis, cerebral infarction, ischemic heart disease, chronic kidney disease, and diabetic retinopathy. Due to an imbalance between oxygen supply and consumption, tumor tissue is also known to be hypoxic. Accurate methods to assess the intracellular and in vivo oxygen status are urgently needed to clarify the role of hypoxia in the etiology of these disorders. Since Wilson and colleagues' ground-breaking work employing oxygen-dependent phosphorescence quenching of Pd-porphyrin to detect biological oxygen, numerous phosphorescent probes have been created. The most common phosphorescent oxygen probes currently in use are Pd- and Pt-porphyrin derivatives, as well as Ru (II)

complexes. However, Ir(III) complexes have recently emerged as a novel class of oxygen probe for intracellular and in vivo oxygen sensing. The fact that Ir(III) complexes are chemically stable, exhibit strong phosphorescence with a very high quantum yield, and allow for the tuning of the emission colour by altering the ligand structure, attracted a lot of interest when they were first being considered as emitting materials for organic light emitting diode devices. These characteristics are advantageous for an oxygen probe as well. In 2010, employing a red emitting iridium complex, the first attempt to use Ir(III) complexes for intracellular and in vivo oxygen sensing was made. HeLa cells cultured with this complex under low pO_2 showed bright phosphorescence in phosphorescence microscopic pictures. When the air was saturated, the emission intensity considerably dropped, indicating that live cells were responding to the presence of oxygen. These investigations also showed that Ir (III) complexes ingested by cells preferentially aggregate in a particular organelle based on their molecular structure and provide the potential for organelle-specific oxygen sensing.[45]

In addition to their use as bioimaging dyes and sensors, cyclometalated iridium (III) complexes have also been tested for their use in theranostics applications. During cancer treatment, lifesaving drugs and dyes used to image tumors must be administered separately. Within the field of theranostics, scientists have sought to combine therapeutic drugs and diagnostic tools to solve this problem. Iridium (III) compounds have been created to serve as both cancer cell killers and dyes for tumor imaging. Following the synthesis of guanidine and thiourea derivatives of these complexes and testing them on drug-resistant cancer cell lines, Balonova et al. (Figure 1.11) showed this capacity in iridium (III) complexes in 2019.[46] Due to their biological activity, guanidine and thiourea

moieties have attracted interest in medicine. Further study has been done on the antimicrobial and anticancer effects of guanidines, which are employed in the medication metformin (N,N-dimethylbiguanide), which is often used in the treatment of type 2 diabetes. Although thioureas have long been employed for anion sensing, they are now also well-known in medicine for their potential as an anticancer agent. This is mostly because of the sulfur atom in thiourea, which is crucial for living organisms. Iridium complexes themselves are of great interest as potential cancer therapeutics because they produce a 3D scaffold, enabling structural diversity beyond the "flatter" organic molecules or platinum complexes typically employed in cancer therapy. They provide a chance for simultaneous imaging because of their rich and controllable luminescence properties; and they also provide a chance for photogeneration of singlet oxygen within cells. Iridium complexes can cause cell death by a variety of mechanisms, including the production of reactive oxygen species (ROS) and interaction with nuclear factor kappa B (NF-κB), a protein known to control the transcription of DNA. The human ovarian cancer cell lines EFO-21, EFO-27, and COLO-704 and their cisplatin-resistant sublines were evaluated for their effects on the viability of the compounds to determine their biological activity. The results of this study suggest that thiourea and guanidine-based iridium (III) complexes have the potential to be used in the future as anticancer medications because they have shown promising low dose responses in the early research stages of human in vitro cell assays. The information gathered from these assays could open new potential therapeutic pathways in the fight against drug-resistant ovarian cancer.[46]

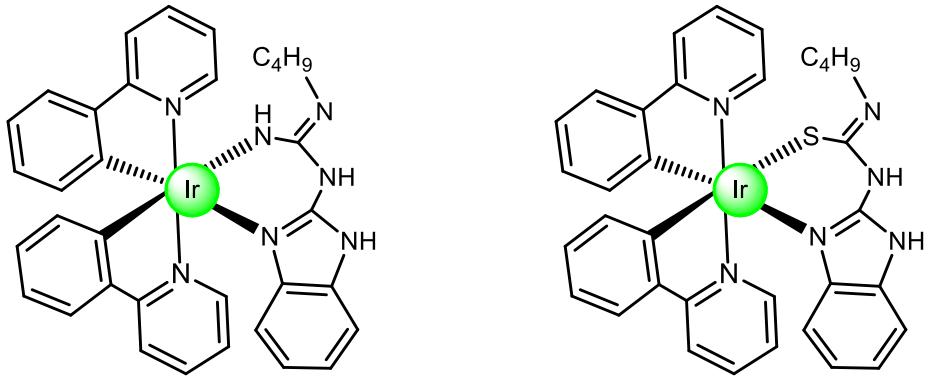

11 **12**

Figure 1.11: Chemical structures of guanidine and thiourea iridium (III) complexes used to treat drug resistant cancer cells synthesized by Balonova et al.

1.5 Ion Transport

The transport of materials across the lipid bilayer of cells is among one of the most important biological processes within the human body. Transport across the cellular membrane can be divided into passive transport and active transport.[47] Passive transport occurs in the absence of energy, and can be further divided into three categories, diffusion, facilitated diffusion, and osmosis.[47,48] During diffusion, a molecule simply diffuses across the phospholipid bilayer, and then dissolves in the aqueous solution at the other side of the membrane. No membrane proteins are involved, and the direction of transport is determined simply by the relative concentrations of the molecule inside and outside of the cell.[47] From an area with a high concentration of the molecule to an area with a lower concentration, the net flow of molecules is always down the gradient of their concentration. Thus, passive diffusion is a nonselective mechanism that allows any

molecule that can dissolve in the phospholipid bilayer to traverse the plasma membrane and equilibrate between the interior and exterior of the cell. It is crucial to note that only tiny, mostly hydrophobic compounds can diffuse through a phospholipid bilayer.[47] As a result, small polar but uncharged molecules like water and ethanol as well as gases like oxygen and carbon dioxide can permeate across the plasma membrane. However, the hydrophobic core of the phospholipid bilayer prevents other biological molecules from dissolving across the membrane. As a result, larger uncharged polar molecules like glucose, as well as charged molecules of any size, are unable to traverse the plasma membrane by passive diffusion (including small ions such as calcium, sodium, potassium, and chloride).[47] Instead, the activity of transport by channel proteins is required for the passage of these molecules across the membrane, and as a result, regulate the flow of most biological molecules into and out of the cell. Another method of movement within cells is osmosis. Like passive diffusion, it merely requires a concentration gradient and does not rely on proteins to aid in movement. Osmosis, as opposed to passive diffusion, includes the diffusion of water from a high concentration location to a low concentration area.[48]

When molecules like small counterions and larger uncharged polar molecules (such as glucose), which cannot simply diffuse across the lipid bilayer, must traverse the cell membrane, facilitated diffusion takes place.[47] To facilitate the transfer of these molecules and ions, channel proteins or carrier proteins must be active. Specific molecules are bound by carrier proteins and transferred on one side of the membrane. The conformational adjustments they go through next enable the molecules to cross the

membrane and exit on the other side. These proteins oversee moving a variety of molecules across the cellular membrane, including amino acids and nucleosides.

Ion channels, also known as channel proteins, simply create open membrane pores that allow tiny molecules with the right size and charge to readily move through the lipid bilayer. Ion channels' three main characteristics play a key role in how they work.[47] First, transportation through channels happens very quickly. Open channels may accommodate more than a million ions per second, which is a thousand times the pace at which carrier proteins can transport one ion. Second, because only ions with the right size and charge may flow through the channel's small pores, ion channels are extremely selective. The movement of sodium, potassium, calcium, and chloride ions across the membrane is consequently made possible by certain channel proteins. Third, most ion channels are not always open. Ion channel opening is instead controlled by "gates" that momentarily open in response to stimuli. Voltage-gated channels open in reaction to shifts in the plasma membrane's electric potential, whereas ligand-gated channels open in response to the binding of neurotransmitters or other signaling molecules.[48]

Active transport is the type of transport that requires energy to proceed. This process is often coupled with ATP hydrolysis and is used to transport molecules or ions from an area of low concentration to an area of high concentration, against the typical concentration gradient.[47]

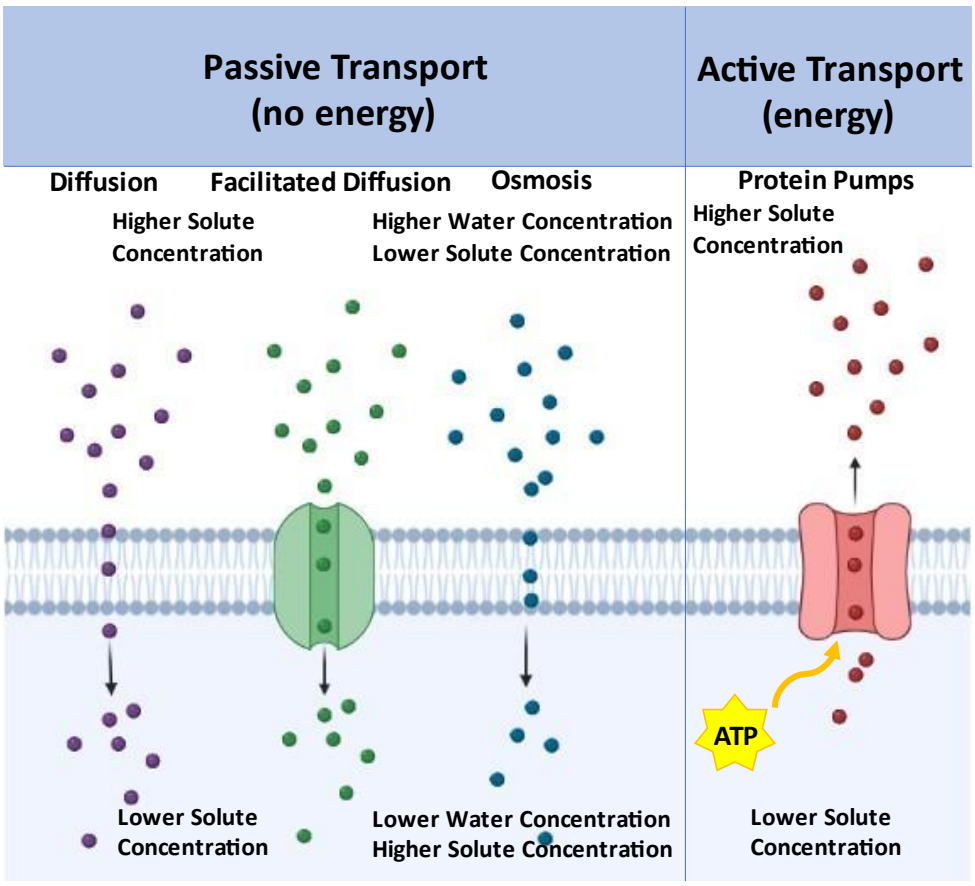

Figure 1.12: Depiction of different type of passive transport (diffusion, facilitated diffusion, and osmosis), and active transport.

Active transport can be further divided into two categories, primary active transport,[48] and secondary active transport.[50] Secondary active transport often uses potential energy from an electrochemical potential difference,[50] whereas primary active transport uses energy from ATP to function. Sodium, potassium, magnesium, and calcium ions are transported during primary active transport. The sodium-potassium pump is one instance of primary active transport in action. Three Na+ ions are removed from the cell by a transport pathway in a biological membrane, while two potassium ions are introduced into the cell against the gradients of their respective concentrations.[49]

There is no direct ATP connection during secondary active transport. Instead, as the ions are pumped into and out of the cell, the electrochemical potential difference provides the energy that powers the transport. One ion is permitted to go down its electrochemical gradient during secondary active transport. As a result, there is a rise in entropy, which can be converted into energy. The transport of a second ion, such as H+ ions, against its gradient is boosted, for instance, when sodium ions move down the electrochemical gradient across the plasma membrane. Therefore, coupled transport or cotransport are other names for secondary active transport.[50] As shown in Figure 1.13, there are two categories of secondary active transporters, symporters and antiporters.[51] Symporters transport ions or molecules in the same direction, but antiporters allow for the opposite direction transport of two separate ions or molecules, one into the cell and the other out of the cell.[51] The sodium-calcium exchanger in the membranes of heart muscle cells is an illustration of an antiporter. This antiporter permits one calcium ion to be actively transported out of the cell after allowing three sodium ions to enter the cell along the concentration gradient. Calcium ions migrate in the opposite direction from sodium ions.[52] The glucose symporter SGLT1, which is present in the interior lining of the small intestine, the heart, the brain, and the S3 region of the proximal tubule in each nephron, is an illustration of the symport mechanism. This transporter delivers two sodium ions and one glucose (or galactose) molecule to the cell.[53]

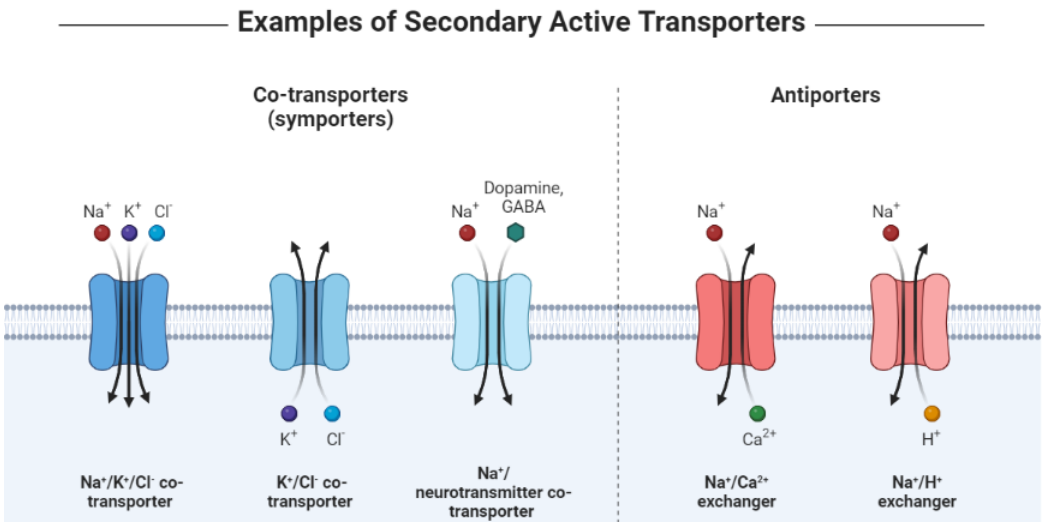

Figure 1.13: Depiction of different types of secondary active transport.

All transport of molecules in and out of cells is important, but the transport of ions across cellular membranes is a particularly important biological process. Specifically, ions such as potassium, sodium, calcium, and chloride are the most biologically important within the human body and are imperative for proper cellular functioning and signaling. The transport of cations into and out of cells is common, but the transport of anions is not as common, with chloride and bicarbonate ions being the most biologically important within the human body. Anions like iodide and bromide are used within the body under specific conditions, but not nearly as commonly as chloride. Ion transport underlies many important physiological processes that occur within the human body including the regulation of cell volume, excitation, and propagation of electrical signals in nerve and muscle cells, the secretion of fluids by organs such as the intestine and kidney, and the electrolyte levels in the blood.[47] When ion transport within the cells of the human body becomes disrupted, it can lead to the development of life-threatening diseases often referred to as “channelopathies”.[54]

1.6 Channelopathies

"Channelopathies" are a group of diseases caused by the dysfunction of ion channel subunits or their interacting proteins. These diseases can be inherited genetically or acquired by other disorders, drugs, or toxins, though mutations in the genes encoding ion channels, which impair ion channel function, are the most common cause of these diseases. As ion channels are necessary structures in most human cells, they are distributed throughout the human body meaning they can result in a wide variety of diseases. Channelopathies are incredibly difficult to classify due to the wide range of genetic and phenotypic variability, so they are often grouped by the organ system that is most impacted by the disruption in ion transport. Channelopathies can affect the nervous system (epilepsy), cardiovascular system (congenital long QT system), respiratory system (cystic fibrosis), endocrine system (diabetes), urinary system (Bartter syndrome), and the immune system (Morvan's syndrome).[54]

Ion channels are essential for neural signaling, and as a result, channelopathies are seen in an increasing range of neurological diseases. Primary skeletal muscle illnesses are among the earliest genetically identified and best known channelopathies. The clinical spectrum of these muscular disorders ranges from flaccid paralysis (muscle hypo excitability) to myotonia (muscle hyperexcitability). Patients with myotonia congenita experience episodes of extremely stiff muscles due to delayed relaxation brought on by persistent electrical activity in the muscle. One gene, chloride voltage-gated channel 1 (CLCN1), which codes for the skeletal muscle chloride channel ClC-1, has loss-of-function mutations that lead to both the dominant (Thomsen disease) and recessive (Becker disease) forms of the disease. In skeletal muscle cells, ClC-1 channels help to

repolarize the membrane after action potentials by stabilizing the resting membrane potential. Potassium ions leave the cell and go into the extracellular fluid and transverse tubular system when action potentials are evoked. The Nernst equation predicts that when extracellular potassium levels increase, the membrane has a propensity to depolarize. When ClC-1 channels are functionally lost, the inward chloride current needed to counteract the depolarization brought on by potassium buildup in the transverse tubules is reduced, which causes spontaneous repetitive action potential firing and a slower rate of repolarization.[54]

One of the most well-known examples of channelopathy diseases is cystic fibrosis, a disease characterized by excessive build-up of mucus within the organs of the body that leads to organ damage and often a shortened lifespan. Cystic fibrosis specifically is caused by a disruption in the functioning of two ion channels, the cystic fibrosis transmembrane conductance regulator (CFTR), a protein responsible for chloride transport, and the epithelial sodium channel (ENaC), a protein responsible for sodium transport. In healthy airways, there is a balance between the transport of chloride ions by the CFTR and the transport of sodium ions by the ENaC. The ENaC mediated absorption of NaCl and H_2O facilitates proper hydration of airway surfaces essential for effective mucociliary clearance. In cystic fibrosis airways, the CFTR does not function properly, so deficient CFTR-mediated chloride transport and fluid secretion as well as increased ENaC-mediated sodium and fluid absorption leads to airway surface dehydration, hyper concentrated mucus, and impaired mucociliary clearance.[54-56]

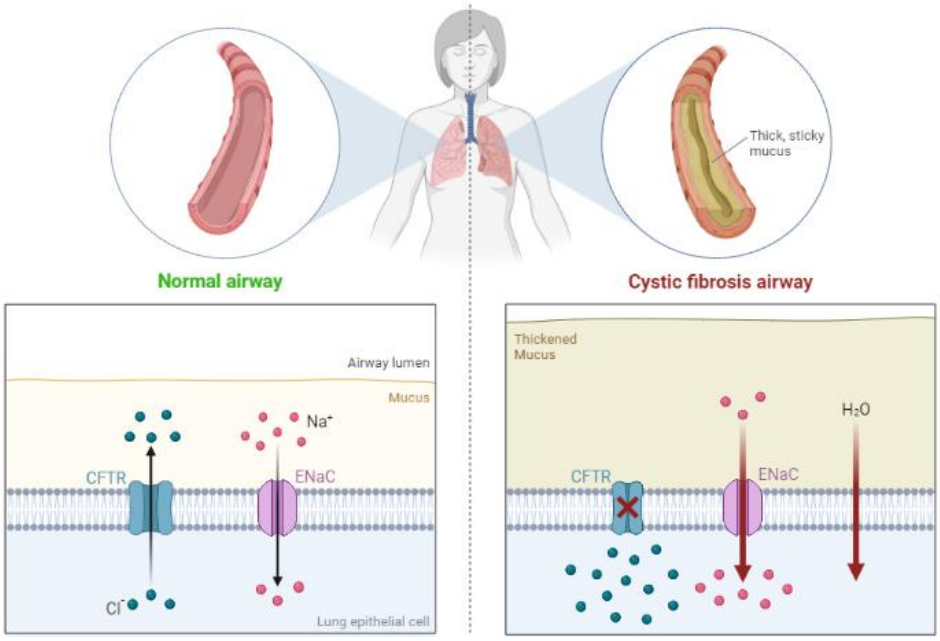

Figure 1.14: Diagram of healthy vs cystic fibrosis airways.

Insulin release from pancreatic cells depends heavily on electrical activity. Ion channel electrical activity is used by endocrine cells, like neurons and other excitable cells, to maintain or control a variety of physiological processes. It is becoming more and more clear that ion channel defects can lead to endocrine illnesses, even ones that are not often thought of as channelopathies. From familial hyperinsulinemic hypoglycemia to neonatal diabetes mellitus, a wide range of insulin secretory diseases are impacted by the adenosine triphosphate-sensitive potassium (KATP) channel (also known as congenital hyperinsulinism). Four inwardly rectifying potassium channel subunits (Kir6.x), which form the pore, and four sulfonylurea receptors (SURx), which control channel activity, make up the hetero-octameric complex known as the KATP channel. The pancreas, brain, heart, smooth muscle, and skeletal muscle are only a few examples of the organs and/or tissues that have KATP channels. The KATP channel, which is made up of the Kir6.2

and SUR1 subunits in pancreatic cells, plays a crucial role in controlling the release of insulin. While sulfonylurea and Mg-nucleotides regulate the channel activity through the SUR1 subunit, ATP, phosphatidylinositol 4,5-bisphosphate, and the Kir6.2 subunit directly affect the Kir6.2 subunit. The KATP channel's activity is principally governed by the intracellular [ATP]/[ADP] ratio. As intracellular [ATP] rises because of increased glucose metabolism, ATP binds to Kir6.2 to block KATP channels, which causes membrane depolarization, calcium influx, and insulin secretion. In contrast, Mg-ADP activates KATP channels through the SUR1 subunit when blood glucose levels are low, causing potassium efflux, membrane hyperpolarization, and decreased excitability in pancreatic cells. The KATP channel couples' electrical activity to metabolism in this way.[54]

The list of channelopathies is continuously growing as we advance in our understanding of the role's ion channels play within the human body. There is research being conducted suggesting that certain cancers, psychiatric disorders, gastrointestinal diseases, and additional nervous system disorders could soon be added to the list. Better understanding of the structure and function of ion channels and their related proteins should elucidate the mechanisms that can provide molecular targets for intervention in the pathophysiological process of diseases in this rapidly growing field of medicine.[54]

1.7 Synthetic Methods of Ion Transport

Amongst many other applications, synthetic methods of ion transport have been developed to function as therapeutic agents for the treatment of a variety of diseases

including channelopathies and cancer.[57,58] One of these methods includes the development of single molecule ion transporters. Single molecule ion transporters that can embed themselves within the lipid bilayer of cells have been quite successful in treating certain diseases. Many of these have been developed specifically to cause apoptosis in cancer cells. Maintenance of ion homeostasis is extremely important for the survival of all cells. Cancer cells establish a unique ion homeostasis beneficial for their growth and proliferation, but there is a multitude of evidence showing that disrupting this delicate ion homeostasis can serve as a lynch pin to start a cascade of signaling events ultimately leading to cancer cell death. These single molecule ion transporters also have the potential to function as therapeutic agents for diseases like cystic fibrosis.[59]

Single molecule ion transporters can be naturally occurring or synthetically made. One example of a naturally occurring single molecule ion transporter used for cancer treatment is prodigiosin, which can be seen in Figure 1.15. Prodigiosin is the red pigment produced as a secondary metabolite by many bacteria species including Serratia marcescens, as well as other Gram-negative, gamma proteobacteria such as Vibrio psychroerythrus and Hahella chejuensis. It has been isolated and highly studied as the molecule has antibacterial, antiprotozoal, anti-tumor and anti-inflammatory activity. The anti-tumor abilities of prodigiosin come from the fact that it can function as an ion transporter. Prodigiosin and its analogues are known to induce cancer cell death by altering intracellular pH gradients through HCl transport.[60]

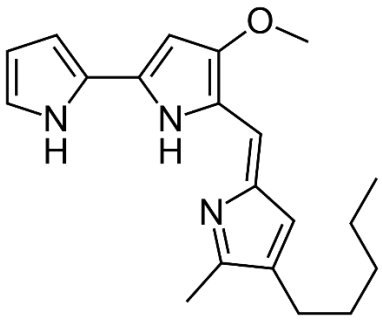

13

Figure 1.15: The chemical structure of prodigiosin.

Another example of naturally occurring ion transporters for cancer treatment is salinomycin, which is a K+ ionophore antibiotic isolated from Streptomyces albus and known for more than 30 years. It has been used in veterinary medicine as an antimicrobial against Gram negative bacteria and coccidioides. In 2009, Gupta et al. identified salinomycin in a screening among 16,000 compounds, as having a strong anti-cancer activity, particularly against cancer stem cells. Salinomycin kills cancer stem cells in different types of human cancers by interfering with ATP-binding cassette (ABC) drug transporters, the Wnt/β-catenin signaling pathway, mitochondrial function, and other cancer stem cell (CSC) pathways. By comparing the chemical structures and cellular effects of this drug with those of valinomycin (K+ ionophore) and nigericin (K+/H+ exchanger), these authors concluded that salinomycin mediates K+/H+ exchange across the inner mitochondrial membrane. Clinically, this drug has been able to induce partial regressions in heavily pre-treated and therapy-resistant cancer patients.[59,61]

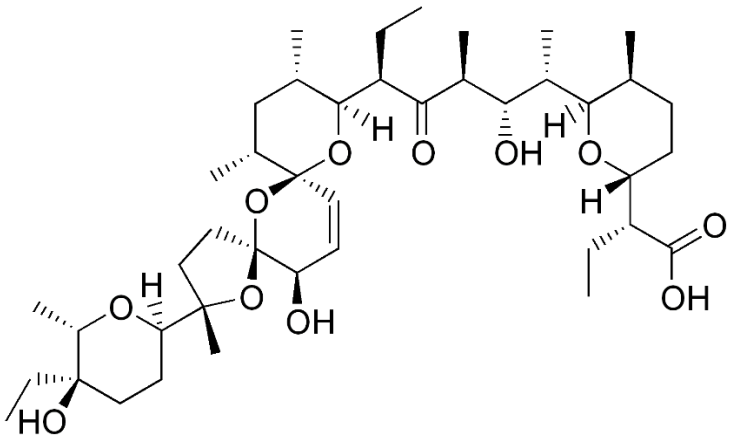

14

Figure 1.16: Chemical structure of salinomycin.

There are many examples of highly effective, synthetically made ion transporters as well for applications as cancer drugs, and they have also been investigated for the potential treatment of diseases like cystic fibrosis. In a study published *in Angewandte Chemie* in 2014, Davis et al. were able to develop an ion transporter that was able to transport ions at a rate only slightly slower than the CFTR, the protein that is defective in cystic fibrosis. This structure has a trans decalin scaffold with two attached thiourea structures (Figure 1.17). This structure was based on a previously reported structure that had urea molecules in the place of the thiourea molecules. Davis et al. wanted to show that the thiourea version of already reported urea-based anion transporters could transport ions at an increased rate. Within this study, they were able to prove that thiourea based anion transporters can transport anions more than ten times faster than their urea counterparts.[62,63]

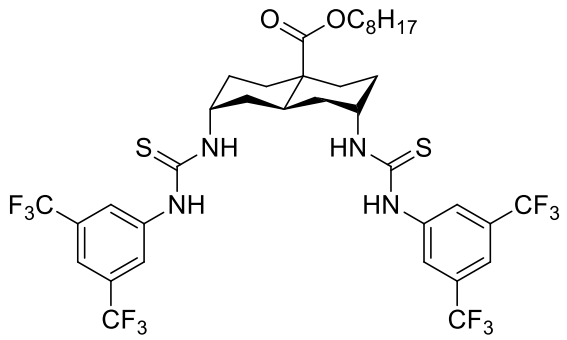

15

Figure 1.17: Structure of thiourea based anion transporter synthesized by Davis et al.

Synthetic ion transporters have also been developed to not only cause cancer cell apoptosis but to also disrupt autophagy, as shown by a study published in 2017 in *Nature* by Busschaert et al. Autophagy is a process by which cells undergo a "self-eating" process to clean out damaged and diseased cells to regenerate new cells. It is known that levels of autophagy in cancer cells are generally higher than those in normal cells, leading to suggestions that autophagy-disrupting agents may be potentially useful in the treatment of cancers. Within this study 6 squaramide based anion transporters were synthesized. To test the potential for these compounds to function as anion transporters, POPC vesicles were synthesized, and then suspended in a 489 mM external $NaNO_3$ solution with 5 mM sodium phosphate (pH 7.2), and chloride efflux was induced by the addition of a DMSO solution of the anion transporter (1 mol% of lipid) was monitored using a chloride selective electrode. All 6 anion transporters were able to integrate into the lipid bilayer of the vesicles and transport the chloride ions. Shown in Figure 1.18, from left to right, are the two compounds that showed the fastest and second fastest rates of chloride transport. Multiple previous studies have shown that disruption of ion

homeostasis, particularly via chloride influx, can induce apoptosis. To test if the anion transporters within this study could accelerate cellular apoptosis, HeLa and A549 cells were separately exposed to three of the tested anion transporters, including the two shown in Figure 1.18, and the results demonstrated that all three compounds could induce apoptosis. Despite synthesizing 6 anion transporters, only one (Figure 1.19, left) could both disrupt autophagy in cells and cause cellular apoptosis.[64]

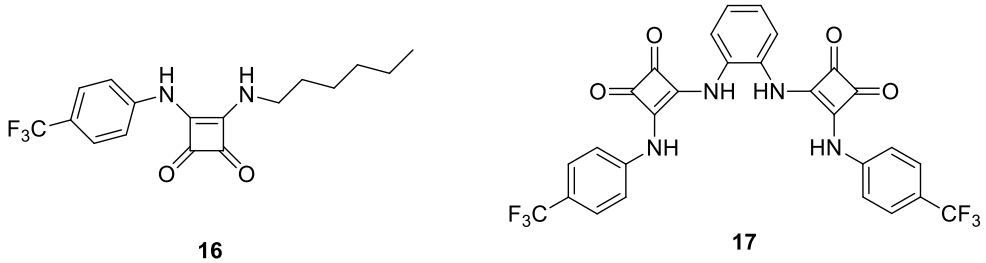

Figure 1.18: Structures of chloride ion transporters published by Busschaert et al.

1.8 Project Goals

The goals of this thesis were to develop new and effective methods of ion transport for the potential future use in treating diseases such as channelopathies like cystic fibrosis or possibly cancer.

Due to the abilities of MOFs to store small molecules such as hydrogen and carbon dioxide, as well as their abilities to anchor to GUVs, we put forward the idea that since MOFs could function small molecule incorporation, this could potentially be expanded to small ion incorporation, thus allowing for ion transport. We aimed to test this theory following a literature procedure wherein we electroformed GUVs in the presence of lucigenin, a chloride sensitive fluorescent dye, causing it to become trapped

within the GUVs aqueous interior. GUVs were also formed in the presence of MOFs allowing them to become anchored to the lipid bilayer of the GUVs. Then, while imaging on a confocal microscope, MOF mediated ion transport could be visualized by the decrease in fluorescence of the lucigenin dye in the presence of chloride ions. In this thesis we aim to report the first ever evidence of MOFs to be used as chloride ion transporters with potential future applications in the treatment of channelopathies and cancers.

In addition to demonstrating the abilities of MOFs to function as anion transporters, we were interested in advancing the field of theranostics. Cyclometalated iridium (III) complexes have been investigated for their use as dual bioimaging dyes and potential future cancer drugs, however, there is yet to be a drug developed that can both induce cellular apoptosis through ion transport, and act as a tumor imaging dye. Two new iridium (III) complexes were synthesized, modelled after known anion transporters, as well as known iridium (III) complexes synthesized for the purpose of functioning as bioimaging dyes. These complexes will be tested for chloride ion transport following the same literature procedure used for the MOFs, the only difference being that the GUVs were formed in the presence of the iridium complexes to allow them to become integrated into the GUVs lipid bilayer.

1.9 References

1. X. Zhang, Z. Chen, X. Liu, S. L. Hanna, X. Wang, R. Taheri-Ledari, A. Maleki, P. Li, O. K. Farha, *Chem. Soc. Rev*., **2020**, 49, 7406-7427.

2. P. Rocío-Bautista, P. González-Hernández, V. Pino, J. Pasán, A. Afonso, *TrAC Trends Anal. Chem*., **2017**, 90, 114–134.

3. S. M. Moosavi, A. Nandy, K. M. Jablonka et al. *Nat. Commun*., **2020**, 11, 4068.

4. C. Wang, D. Liu, W. Lin, *J. Am. Chem. Soc*., **2013**, 135 (36), 13222–13234.

5. T. Wu, N. Prasetya, K. Li, *Journal of Membrane Science*, **2020**, 615, 118493.

6. H. L. Nguyen, *New J. Chem*., **2017**, 41, 14030-14043.

7. K. Fan, S. Bao, W. Nie, C. Liao, L. Zheng, *Inorg. Chem*., **2018**, 57 (3), 1079–1089.

8. L. Han, Y. Kong, G. Hou, H. Chen, X. Zhang, H. Zheng, *Inorg. Chem*., **2020**, 59 (10), 7181–187.

9. N. Stock, S. Biswas, *Chem. Rev*., **2012**, 112 (2), 933–969.

10. B. F. Hoskins, R. Robson, *J. Am. Chem. Soc*., **1990**, 112, 1546.

11. Y. Han, H. Yang, and X. Guo, "Synthesis Methods and Crystallization of MOFs", in Synthesis Methods and Crystallization. London, United Kingdom: IntechOpen, **2020**.

12. H. Li, L. Li, R. Lin, W. Zhou, Z. Zhang, S. Xiang, B. Chen, *EnergyChem*, **2019**, 1 (1), 100006.

13. A. E. Walsby, *Microbiological Reviews*, **1994**, 58 (1), 94–144.

14. N. S. Parkar, B. S. Akpa, L. C. Nitsche, L. E. Wedgewood, A. T. Place, M. S. Sverdlov, O. Chaga, R. D. Minshall, *Antioxid Redox Signal*., **2009**, 11(6).

15. J. E. Rothman, F. T. Wieland, *Science*, **1996**, 272 (5259), 227-234.

16. D. Njus, P. M. Kelley, G. J. Harnadek, *Biochimica et Biophysica Acta (BBA) - Reviews on Bioenergetics*, **1986**, 853 (3–4), 237-265.

17. G. van Niel, G. D'Angelo, G. Raposo, *Nat. Rev. Mol. Cell Biol*., **2018**, 19, 213–228.

18. M. Doktorova, F. A. Heberle, B. Eicher, R. F. Standaert, J. Katsaras, E. London, G. Pabst, D. Marquardt, *Nat. Protoc*., **2018**, 13 (9), 2086-2101.

19. K. Murzyn, T. Róg, M. Pasenkiewicz-Gierula, *Biophys. J*., **2005**, 88 (2), 1091-103.

20. X. Zhang, K. M. Barraza, J. L. Beauchamp, *Proceedings of the National Academy of Sciences*, **2018**, 115 (13), 3255-326.

21. C. Lin, C. Li, Y. Sheng, D. T. Wu, H. Tsao, *Langmuir*, **2012**, 28 (1), 689–700.

22. M. I. Angelova and D. S. Dimitrov, *Faraday Discuss. Chem. Soc*., **1986**, 81, 303–311.

23. H. Stein, S. Spindler, N. Bonakdar, C. Wang and V. Sandoghdar, *Front. Physiol*., **2017**, 8 (63).

24. J. Steinku¨hler, P. D. Tillieux, R. L. Knorr, R. Lipowsky and R. Dimova, *Sci. Rep*., **2018**, 8, 11838.

25. A. Witkowska, L. Jablonski and R. Jahn, *Sci. Rep*., **2018**, 8, 9422.

26. Fenz SF, Sengupta K, *Integr. Biol. (Camb)*, **2012**, 4 (9), 982-95.

27. H. Valkenier, N. López Mora, A. Kros, A. P. Davis, *Angewandte Chemie*, **2015**, 54 (7), 2137-2141.

28. J. R. Lakowicz, *Principles of Fluorescence Spectroscopy (3rd ed.) Springer*, **2006**.

29. Juan Carlos Stockert, Alfonso Blázquez-Castro (2017). "Chapter 3 Dyes and Fluorochromes". *Fluorescence Microscopy in Life Sciences. Bentham Science Publishers*. pp. 61–95. ISBN 978-1-68108-519-7. Retrieved 24 December 2017.

30. Y. Yang, J. O. Escobedo, A. Wong, C. M. Schowalter, M. C. Touchy, L. Jiao, W. E. Crowe, F. R. Fronczek, R. M. Strongin, *J. Org. Chem*., **2005**, 70 (17), 6907–6912.

31. Lee SF, Vérolet Q, Fürstenberg A. Improved super-resolution microscopy with oxazine fluorophores in heavy water. *Angew. Chem. Int. Ed*. Engl., **2013** Aug 19;52(34):8948-51.

32. K. Kolmakov, V. N. Belov, C. A. Wurm, B. Harke, M. Leutenegger, C. Eggeling, S. W. Hell, *Eur. J. Org. Chem*., **2010**, 2010 (19), 3593-3610.

33. T. Weil, M. A. Abdalla, C. Jatzke, J. Hengstler, K. Müllen, *Biomacromolecules*, **2005**, 6 (1), 68–79.

34. G. T. Dempsey, M. Bates, W. E. Kowtoniuk, D. R. Liu, R. Y. Tsien, X. Zhuang, *J. Am. Chem. Soc*., **2009**, 131 (51), 18192–18193.

35. A. Loudet, K. Burgess, *Chem. Rev*., **2007**, 107 (11), 4891–4932.

36. A. Roda, *Anal Bioanal. Chem*., **2010**, 396, 1619–1622.

37. C. P. Toseland, *J. Chem. Biol*., **2013**, 6 (3), 85-95.

38. Q. Zheng, S. Jockusch, Z. Zhou, S. C. Blanchard, *Photochemistry and Photobiology*, **2014**, 90 (2), 448-454.

39. S. M. Usama, K. Burgess, *Acc. Chem. Res*. **2021**, 54 (9), 2121–2131.

40. C. Caporale, M. Massi, *Coordination Chemistry Reviews*, **2018**, 363, 71-91.

41. K. Lu, H. Chou, C. Hsieh, Y. O. Yang, H. Tsai, H. Tsai, L. Hsu, C. Chen, I. Chen, C. Cheng, *Adv. Mater*., **2011**, 23 (42), 4933-4937.

42. L. M. Quan, A. I. Mechler, P. J. Barnard, *Journal of Inorganic Biochemistry*, **2020**, 206, 111047.

43. J. R. Shakirova, A. Sadeghi, A. A. Koblova, P. S. Chelushkin, E. Toropainen, S. Tavakoli, L. Kontturi, T. Lajunen, S. P. Tunik, A. Urtti, *RSC Adv*., **2020**, 10, 14431.

44. S. Zhang, M. Hosaka, T. Yoshihara, K. Negishi, Y. Iida, S. Tobita, T. Takeuchi, *Cancer Res*., **2010**, 70 (11), 4490-8.

45. J. Zhou, J. Li, K. Y. Zhang, S. Liu, Q. Zhao, *Coordination Chemistry Reviews*, **2022**, 453, 214334.

46. S. J. Thomas, B. Balónová, J. Cinatl, M. N. Wass, C. J. Serpell, B. A. Blight, M. Michaelis, *ChemMedChem*, **2020**, 15 (4), 349-353.

47. Cooper GM. *The Cell: A Molecular Approach. 2nd edition*. Sunderland (MA): Sinauer Associates; **2000**. Transport of Small Molecules.

48. Marta Zaccaria, Claudio Ronco, in *Critical Care Nephrology (Third Edition)*, **2019**.

49. Luis Reuss, *in Seldin and Giebisch's The Kidney (Fourth Edition)*, **2008**.

50. E. Shechter, *Biochimie*, **1986**, 68 (3), 357-65.

51. M. G. Wolfersberger, *J. Exp. Biol*., **1994**, 196, 5–6.

52. Joseph Feher, *in Quantitative Human Physiology (Second Edition)*, **2017**.

53. S. B. Poulsen, R. A. Fenton, T. Rieg, *Curr. Opin. Nephrol. Hypertens*., **2015**, 24 (5), 463-9.

54. Kim JB. *Channelopathies. Korean J Pediatr*., **2014** Jan;57(1):1-18.

55. A. Edelman, E. Saussereau, *Arch Pediatr*., **2012**.

56. M. A. Mall. *Eur. Respir. J*., **2020**, 56(6).

57. E. Oosterwijk, R. Gillies, Philos. Trans. R. Soc. Lond. *B Biol. Sci*., **2014**, 369 (1638).

58. A. Arcangeli, J. Yuan, *Am. J. Physiol. Cell Physiol*., **2011**, 301, C253–C254.

59. V. Kaushik, J. S. Yakisich, A. Kumar, N. Azad, A. K. V. Iyer, *Cancers*, **2018**, 10, 360.

60. T. Danevčič, M. Borić Vezjak, M. Zorec, D. Stopar, *PLoS One*, **2016**, 11 (9).

61. Tomas Koltai, Salvador Harguindey, in *An Innovative Approach to Understanding and Treating Cancer: Targeting pH*, **2020**.

62. C. M. Dias, H. Valkenier, A. P. Davis, *Eur. J. Chem*., **2018**, 24 (23), 6262-6268

63. H. Valkenier, L.W. Judd, H. Li, S. Hussain, N. Sheppard, A. P. Davis, *J. Am. Chem. Soc*., **2014**, 136, 12507.

64. N. Busschaert, S. Park, K. Baek, Y. P. Choi, J. Park, E. N. W. Howe, J. R. Hiscock, L. E. Karagiannidis, I. Marques, V. Félix, W. Namkung, J. L. Sessler, P. A. Gale, I. Shin, *Nat. Chem*., **2017**, 9, 667–675

Chapter 2
MOFs as Anion Transporters for the Potential Treatment of Channelopathies and Cancers

Braeden Hourihan, and Barry A. Blight

Braeden Hourihan was responsible for all experimental data obtained in this chapter.

2.1 Introduction

Ion transport across the lipid bilayer of cellular membranes is a common and important biological process that occurs within the human body.[1,2] Ions like sodium, potassium, calcium, and chloride are among the most predominantly found ions within biological systems,[3] and are imperative for cellular functioning and signaling. Despite the necessity for these ions to be transported into and out of cells, they are unable to easily diffuse through the cellular membrane like oxygen or carbon dioxide and need the help of ion channels.[4] These ion channels consist of large proteins that span the width of the membrane and form open pores, allowing small molecules of the appropriate size and charge to pass freely through the lipid bilayer.[4] When these ion channels do not function properly it leads to the development of diseases known as channelopathies, which are a group of diseases caused by the dysfunction of ion channel subunits or their interacting proteins. These diseases can be inherited or acquired by other disorders, drugs, or toxins.[3,4] One of the most well-known examples of channelopathy diseases is cystic fibrosis,[3] a disease characterized by the development of excessive mucus that can lead to damage in many of the body's organs, and often a shortened lifespan. In healthy airways, there is a balance between the cystic fibrosis transmembrane conductance regulators (CFTR) transport of chloride ions and the epithelial Na+ channel (ENaC) transport of sodium ions. The ENaC mediated absorption of NaCl and H_2O facilitates proper hydration of airway surfaces which is essential for effective mucociliary clearance. In cystic fibrosis airways, the transport of chloride ions by the CFTR is impaired, so deficient CFTR-mediated chloride transport and increased ENaC-mediated sodium transport and fluid absorption leads to airway surface dehydration, hyper concentrated

mucus, and impaired mucociliary clearance, resulting in the common symptoms of this disease.[5,6] Ion transport is an important process when it comes to cancer as well. Ion homeostasis is extremely important for the survival of cells, cancer cells, specifically, establish a unique ion homeostasis beneficial for their growth and proliferation. There is a multitude of evidence showing that disrupting this delicate ion homeostasis can serve as a lynch pin to start a cascade of signaling events ultimately leading to cancer cell death.[7,8] While cystic fibrosis and cancer at first glance may not seem to have a lot in common, both are diseases where synthetic methods of ion transport are being investigated for potential treatment.

Metal-organic frameworks (MOFs) are supramolecular structures that consist of metal ions coordinated to organic linker molecules to form 2D or 3D crystalline structures. They have become a well-known area of research within chemistry due to their various advantageous features, including high porosity, large amounts of internal surface area, and high chemical tunability, meaning that their structure can be changed to fit different functions by simply altering the metal nodes and organic linker molecules.[8] MOFs have been used in a variety of applications including drug storage and delivery, other biomedical applications including biocatalysis, bioimaging, as well as anticancer applications, catalysis, the storage, and separation of gases such as hydrogen gas, methane, and carbon dioxide, chemical sensors, as well as the purification of natural gases and water.[9]

As previously mentioned, MOFs can be used in bioimaging applications. One of these applications was published in 2021 by the Blight group at the University of New Brunswick.[10] When giant unilamellar vesicles (GUVs) are electroformed in the presence

of MOFs, they become anchored to the MOFs, causing them to become immobilized. When the GUVs are left to float freely, they are highly mobile, so getting clear images on a confocal microscope can be challenging. Anchoring them to MOFs allows for clear and consistent images of the GUVs since they can no longer move leading to easier imaging sessions.[10] MOFs can be used in a variety of applications, including small molecule uptake, and acting as anchors to immobilize GUVs for bioimaging purposes. This led to the goal of my first project which was to demonstrate that MOFs, when anchored to GUVs can disturb the lipid bilayer enough to act as a new and effective method of ion transport for the potential future treatment of channelopathies and cancer.

GUVs are structures that consist of fluid or gas enclosed by a lipid bilayer, a membrane made up of hydrophilic heads and hydrophobic tails and are greater than 1 μm in diameter. They are typically prepared through electroformation,[11-14] a process during which vesicles will peel away from indium-tin oxide (ITO)-coated glass slides and enter the surrounding solution as a low voltage is passed through the apparatus. GUVs are fascinating because of their ability to function as a model for cell membranes due to their similarity in size as well as their comparatively simple composition.[15] Within this study GUVs were used as a model to demonstrate ion transport by MOFs. Using a modified literature procedure,[16] GUVs were electroformed in the presence of a chloride sensitive dye called lucigenin, which subsequently became trapped within the GUVs aqueous interior. The ion transport process consisted of nitrate/chloride ion exchange, as both the aqueous interior of the GUVs, and exterior solution contained nitrate. While imaging with a confocal microscope, sodium chloride was added to the GUVs and the lucigenin dye within the GUVs was quenched in the presence of chloride ion transport. Within this

study, three MOFs were tested for chloride transport, two of which indicated promising abilities of MOF particles as ion transporters. This new development could lead to a new class of synthetic ion transporters with the potential to function as future therapeutic agents for the treatment of cystic fibrosis or cancer.

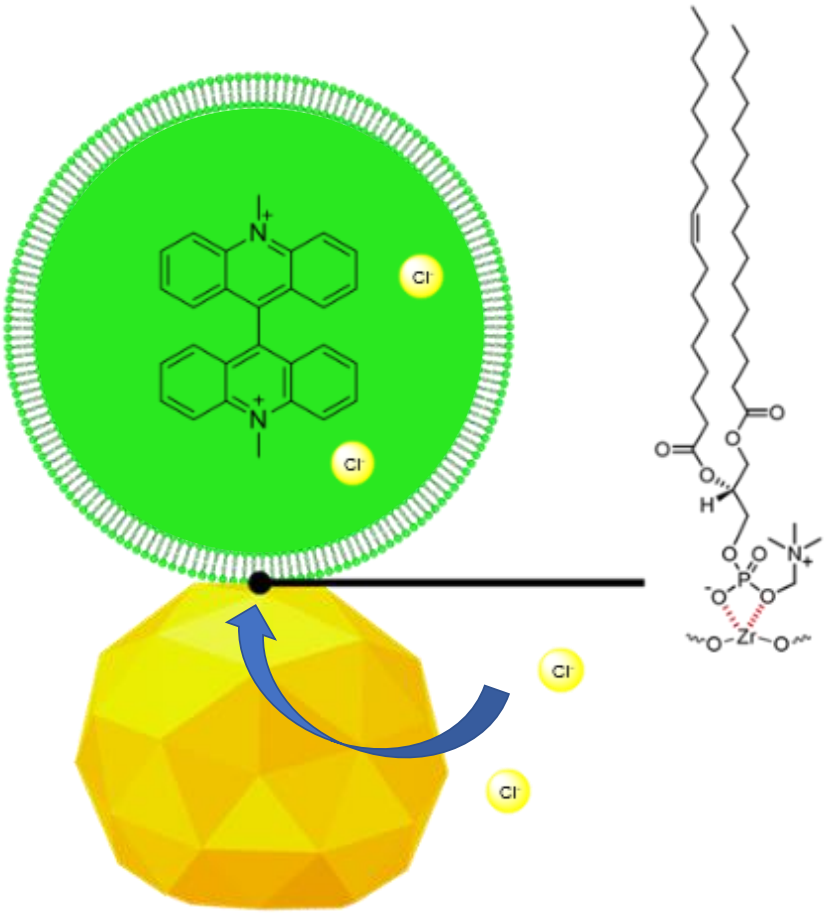

Figure 2.1: Depiction of a MOF being used to transport chloride ions into a GUV filled with the chloride sensitive dye lucigenin.

2.2 Experimental

General:

Materials. All reagents were purchased from Sigma Aldrich, Fisher Scientific or Avanti Polar Lipids and used as received, unless otherwise stated. The peristaltic pump was 3D printed using a modified literature procedure.[17]

Giant Unilamellar Vesicle Preparation. GUVs were grown using a literature-based electroformation technique. 1-Palmitoyl-2-oleoyl-sn-glycero-3-phosphocholine (POPC), and 1 palmitoyl-2-oleoyl-sn-glycero-3-phospho-rac-(1-glycerol) (sodium salt) (POPG) were purchased from Avanti Polar Lipids (dissolved in chloroform to a concentration of 10 mg/mL), and cholesterol was purchased from Sigma Aldrich and used without any further purification. For a typical lipid mix: lipids POPC and POPG, and cholesterol were mixed in a 4 : 1 : 1 molar ratio, and this solution was made to an overall concentration of 1 mg/mL.

Confocal Imaging. Confocal imaging was performed at the UNB Microscopy and Microanalysis Facility with a Leica TCS-SP2 CLSM microscope using Leica confocal software package version 2.61 build 1537. Images were collected with the excitation wavelength of 458 nm and fluorescence was collected in a 500 - 600 nm band range for lucigenin and lucifer yellow fluorescent dyes. Images and data extracted using the freeware software package ImageJ.[18]

MOF Synthesis

MOF 808. Synthesized according to literature procedure.[19] Trimesic acid (0.11 g, 0.50 mmol) and ZrOCl2·8H2O (0.16 g, 0.50 mmol) in a solvent mixture of DMF/formic acid

(20 mL/20 mL) were placed in a 60-mL screwcapped glass jar, which was heated at 100 °C for 7 days. Crystals were collected and washed three times with 10 mL of fresh DMF (Yield: 0.098 g, 70% based on $ZrOCl_2 \cdot 8H_2O$). MOF-808 was rinsed with 10 mL of anhydrous DMF three times per day for 3 days and immersed in 10 mL of anhydrous acetone for 3 days, during which time the acetone was replaced three times per day. Acetone exchanged crystals were activated on a supercritical CO_2 dryer, followed by evacuation at 150 °C for 24 h.

MOF UiO-67. Synthesized according to literature procedure.[20] An 8-dram vial was loaded with ZrCl4, one third of the DMF, and concentrated HCl before being sonicated for 20 minutes until fully dissolved. The ligand and the remainder of the DMF were then added and the mixture was sonicated an additional 20 minutes before being heated at 80 °C overnight. The resulting solid was then filtered over a fine frit and washed first with DMF (2x 30 mL) and then with EtOH (2x 30 mL). The sample was filtered for several hours to remove all residual solvent. The samples were activated by first heating to 90 °C under vacuum until a pressure of 100 mtorr was reached.

MOF Zr-BTDZ. Synthesized according to literature procedure.[21] L-proline (0.052 g, 0.45 mmol, 4 eq), ligand (0.048 g, 0.11 mmol, 1 eq), zirconium chloride (0.026 g, 0.11 mmol, 1 eq) and DMF (5 ml) were added to a 50 ml PYREX reagent bottle and sonicated for 10 minutes. Concentrated HCl (0.01 ml) was added, and the mixture was sonicated for a further 10 minutes before being placed in the oven at 120 °C for 24 hours. The bulk material was collected from the bottle upon completion, centrifuged once with fresh DMF (30 ml) and twice with acetone (2 x 30 ml), before being dried under vacuum ([Zr6O4(OH)4(L7)6]n, 0.058 g, 0.018 mmol, 98%).

GUV formation and Ion Transport Studies:

GUVs were synthesized using literature procedures.[10] The non-conductive sides of two indium tin oxide (ITO) – coated glass slides were marked with a 15 mm diameter circle in the center of each. An aliquot of ~10 µL of lipid mixture (4:1:1 POPC/POPG/Chol, all dissolved in chloroform) was gently spread on the conductive side of each slide within the circle with the tip of a micro syringe while a gentle flow of air was passed over it until the chloroform evaporated. The slides were then placed in a desiccator for ~30 minutes to further remove the solvent from the residue. A 2 mm thick O-ring with a 15 mm diameter was covered in a minimum amount of silicon grease and affixed to one of the 2 slides over the drawn circle. Approximately 350 µL of an electroformation solution (0.8 mM Lucigenin, 225 mM $NaNO_3$, 200 mM sucrose, in water), was added to an Eppendorf tube, with a microspatula tip (approx. 5 mg) of MOF, which was then sonicated, added to the O-ring chamber, and left to settle for 10-15 minutes. The conductive sides of both slides were fixed (sandwiched) together and placed into a NANION Vesicle Prep Pro apparatus, a sinusoidal AC electric field at 10 Hz was applied for electroswelling the lipid films. The sample was shielded from external light during this time. In the first phase of the electroswelling process, the amplitude of the applied field was linearly increased from 0.1 V to 0.5 V over 30 min, while the temperature was increased from 21 °C to 35 °C. The voltage was then increased further over the next 15 minutes to 1.6 V. Thereafter, the amplitude of the AC field was kept constant at 1.6 V for 2 h to grow the vesicles. Finally, during the last 5 minutes, the voltage was slowly lowered to 0 V. Once the electroformation was complete, the slides were carefully

removed from the Nanion Vesicle Prep Pro and separated. The aliquot within the O-ring was transferred to a centrifuge tube containing 0.6 µL of a resuspension solution (225 mM $NaNO_3$, 200 mM glucose, in water) using a disposable pipette with the tip cut off at the 5 mL mark to make a larger opening to prevent lysing of the vesicles. The mixture was then transferred from the centrifuge tube into the wells of the imaging chamber using the same pipette (filled 2 wells), and a peristaltic pump set to a flow rate of 0.4 mL/min was used to replace the resuspension solution, to help remove excess lucigenin dye. The imaging wells were then covered in tin foil while transported to the microscopy room, to prevent photobleaching of the lucigenin. While imaging with a confocal microscope (458 nm laser at 15%), 25 µL of 1 M NaCl solution in 200 mM glucose and 225 mM $NaNO_3$ in water was slowly added down the wall of the imaging wells to avoid disturbing the immobilized GUVs. Confocal images were then taken every 10 seconds for 20 minutes to observe quenching of the lucigenin dye.

2.3 Results and Discussion

Three MOFs were tested for ion transport within this study: MOF-808, MOF UiO-67, and MOF Zr-BTDZ. MOF-808 is composed of zirconium metal nodes and trimesic acid organic linkers (Scheme 2 A), MOF UiO-67 is composed of Zr nodes and [1,1'-biphenyl]-4,4'-dicarboxylic acid linkers (Scheme 2 B), and MOF Zr-BTDZ is composed of Zr nodes, and a linker containing a heterocyclic ring, attached to two alkyne groups, and ending in benzene rings with carboxylic acids (Scheme 2 C).

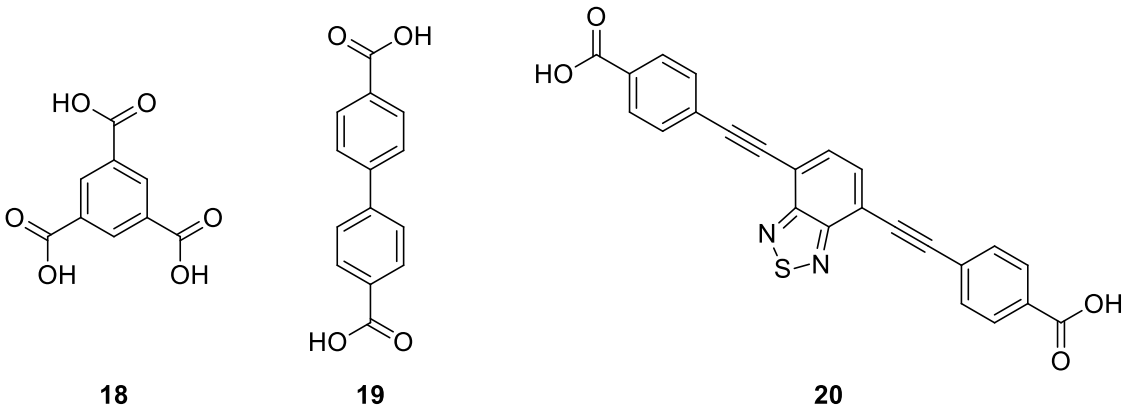

Figure 2.2: Structures of organic linker molecules of 18) MOF-808, 19) MOF UiO-67, and 20) MOF Zr-BTDZ.

These MOFs were chosen for a variety of reasons. MOF-808 and MOF Zr-BTDZ were both used within the study to demonstrate that MOFs can be used to anchor GUVs for bioimaging purposes, so there was an established history of the ability of these MOFs to anchor GUVs.[10] MOF-808 is also easily synthesized in a one pot reaction in water[17] by combining cost effective components,[17] the reaction is easy to scale up,[16] and it is known to have large pore diameter of 18.4 Å and an apparent surface area of 2060 m^2g^{-1}.[22,23] MOF Zr-BTDZ has a pore diameter of 13 Å, which is slightly smaller than MOF-808, but has an apparent surface area of 2130 m^2g^{-1}.[22] MOF Zr-BTDZ is also a fluorescent MOF, which gives the MOF its own diagnostic handle for the microcopy experiments.[21] Finally, MOF UiO-67 is known for having excellent adsorption properties due to its internal surface area of 2815 m^2g^{-1} with pore diameters of 10.9 Å (tetrahedral pore) and 21.6 Å (octahedral pore), according to calculations.[23,24] Due to the large available surface areas and accessible pore sizes, these MOFs were tested for their abilities to transport ions while GUVs were immobilized for imaging.

Lucigenin Control Experiment:

Control experiments were conducted to confirm that the any decrease in fluorescence of lucigenin dye within GUVs was from chloride ion transport. GUVs were formed in the presence of the chloride sensitive lucigenin dye, but in the absence of MOF. Chloride was then added to the imaging slide with the GUVs and imaged on the confocal microscope to prove that GUVs filled with lucigenin that are not in the presence of an anion transporter will remain consistently fluorescent. This also demonstrates that the lucigenin dye does not leak from the GUVs due to the addition of chloride ions and illustrates that the dye does not photo bleach over the 20 minutes imaging session. This control experiment was done in triplicate, GUVs A and B were imaged within the same session (Figure 2.3), whereas GUV C was imaged individually (S6). As shown in the confocal images in Figure 2.3, GUVs A and B show no change in fluorescence 20 minutes after the chloride was added. Normalized fluorescence was then plotted against time for all three GUVs, as shown in Figure 2.4. There was little to no change in fluorescence of the lucigenin dye after 20 minutes which helps to suggest that the decrease in fluorescence observed during the chloride transport experiments using MOFs was not due to dye leaking from the GUVs due to the addition of chloride ions causing defects in the lipid bilayer or from photobleaching of the dye.

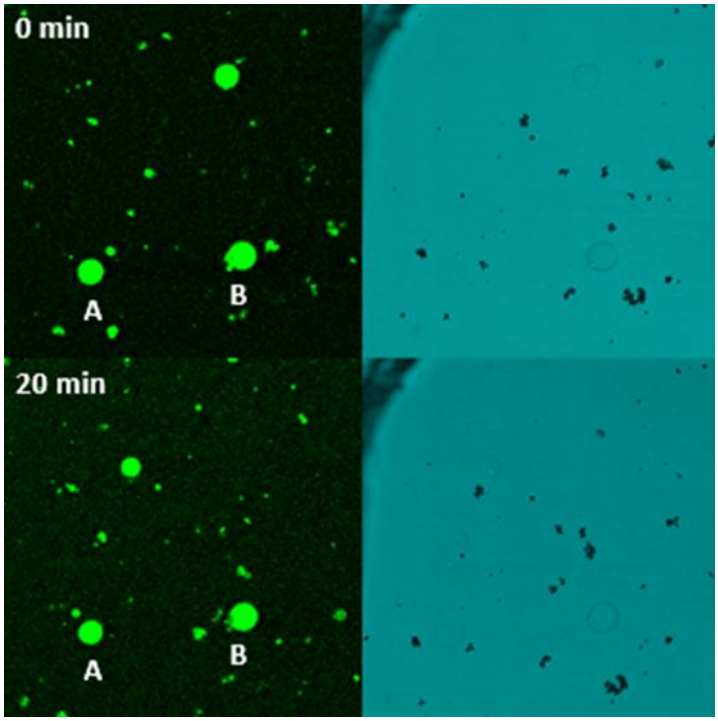

Figure 2.3: Confocal fluorescence images of GUVs anchored to no MOFs at 0 minutes, and 20 minutes after addition of NaCl, Right: Brightfield images taken at 0 minutes, and 20 minutes after addition of NaCl.

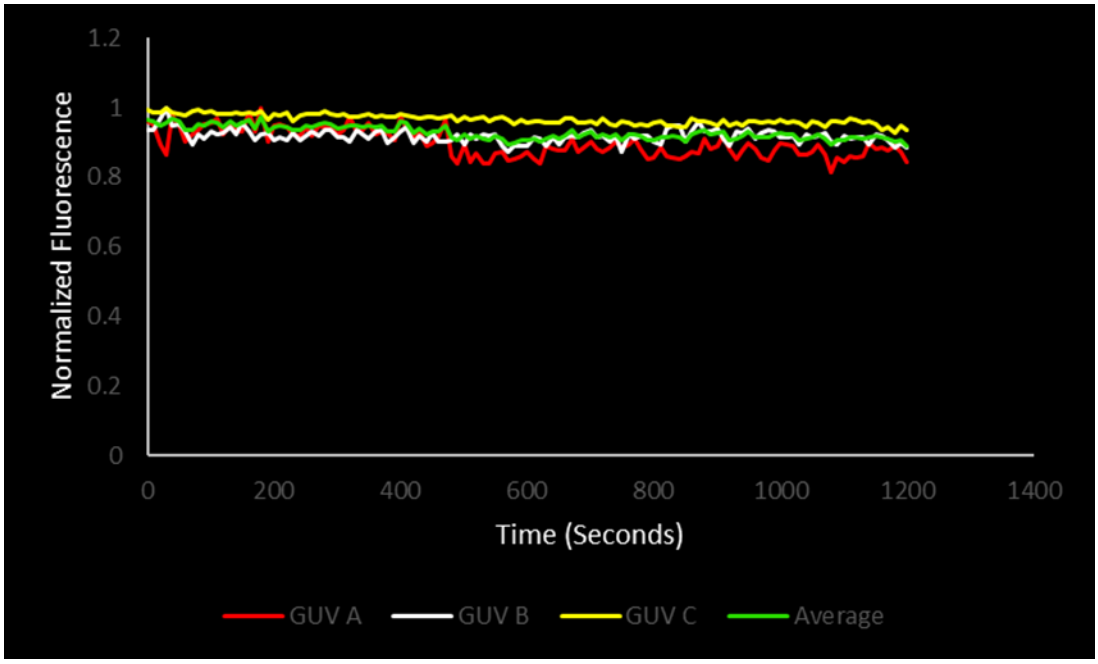

Figure 2.4: Plot of Time (seconds) vs Normalized Fluorescence for the decrease in fluorescence of lucigenin dye within GUVs not anchored to MOFs after the addition of NaCl.

Lucifer Yellow Control Experiment:

Another control experiment was conducted to rule out the possibility that an interaction between the GUVs and MOFs might cause the lucigenin dye to leak causing the appearance of the dye quenching. To prove that the dye was not leaking from the GUVs the control experiment was conducted using lucifer yellow dye rather than lucigenin dye. Lucifer yellow (Figure 2.5) is a commonly used bioimaging dye however it is not sensitive to chloride ions so it will not quench in the presence of chloride.

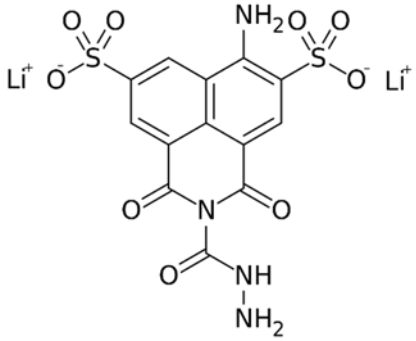

21

Figure 2.5: Chemical structure of lucifer yellow dye.

Chloride ions were added to the supernatant containing lucifer yellow filled GUVs and imaged for 20 minutes. The lucifer yellow dye is not chloride sensitive, so if the lucigenin dye was quenching due to the interaction with the MOF causing the dye to leak, then there would be a decrease in fluorescence of the lucifer yellow dye as well. If ion transport was occurring, the fluorescence of the lucifer yellow dye should remain consistent, but the fluorescence of the lucigenin dye should decrease under the same

conditions. This experiment was completed for MOF-808, MOF UiO-67, and MOF Zr-BTDZ. For MOF-808 the experiment was done in triplicate, and GUVs A (Figure 2.6), B, and C (S10 and S11) were all imaged separately. At 0 minutes, and 20 minutes the fluorescence appears to remain constant, and when normalized fluorescence was plotted against time (Figure 2.7) it is evident from the graph that there is no decrease in fluorescence of the lucifer yellow dye. This further suggests that the any decrease in fluorescence of the lucigenin dye was in fact due to ion transport.

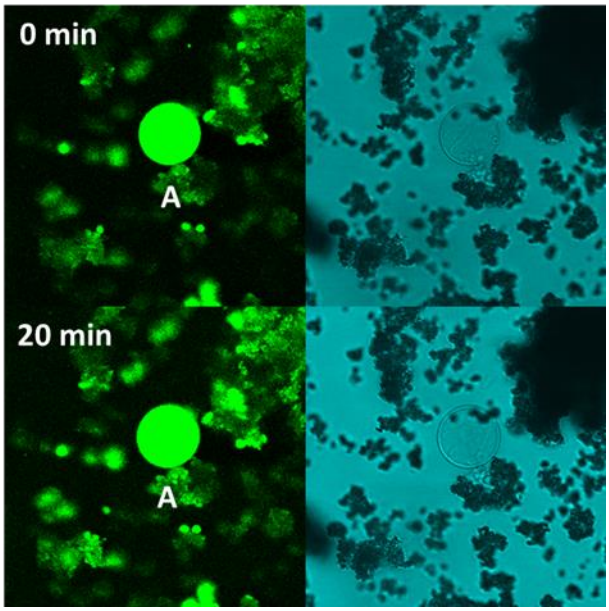

Figure 2.6: Confocal fluorescence images of GUVs filled with lucifer yellow dye and anchored to MOF-808 at 0 minutes, and 20 minutes after addition of NaCl, Right: Brightfield images taken at 0 minutes, and 20 minutes after addition of NaCl.

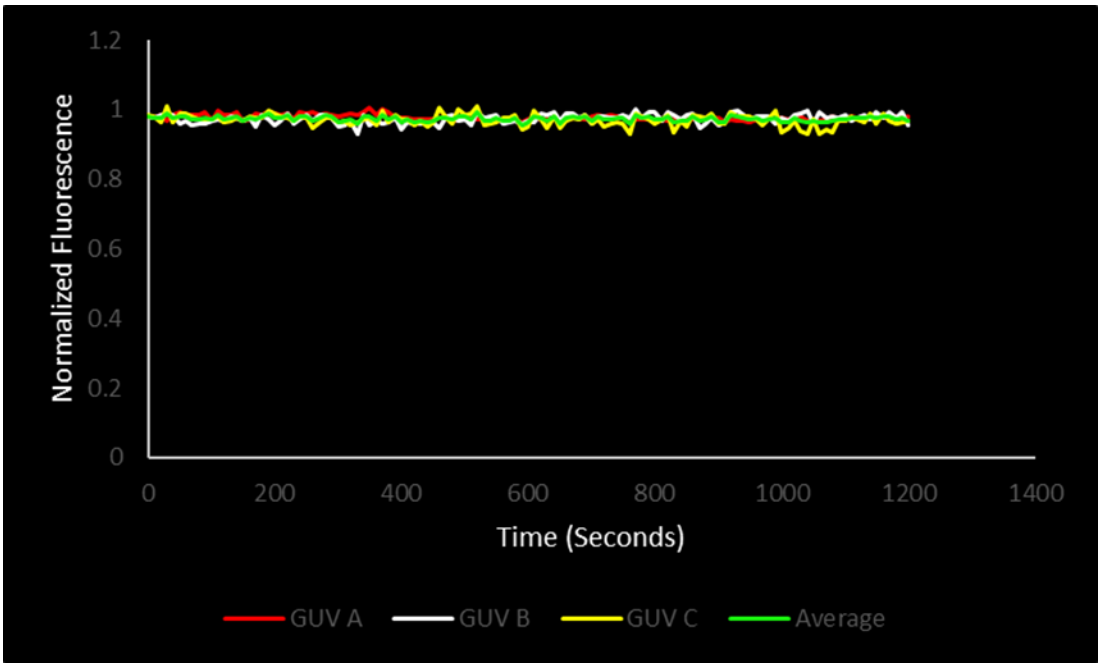

Figure 2.7: Plot of Time (seconds) vs Normalized Fluorescence for the decrease in fluorescence of lucifer yellow dye within GUVs anchored to MOF-808 after the addition of NaCl.

This control experiment was conducted with MOF UiO-67 as well. GUVs A and B (Figure 2.8) were imaged within the same session and GUV C (S11) was imaged separately. The results were the same as with MOF-808 and there was no apparent change in fluorescence between the images taken at 0 minutes before the chloride was added, and 20 minutes after it was added. The normalized fluorescence was plotted vs time (Figure 2.9) for this experiment as well and it is evident from the data that there is no leaking of the lucifer yellow dye, further suggesting that quenching of the lucigenin dye within the experiment was due to ion transport.

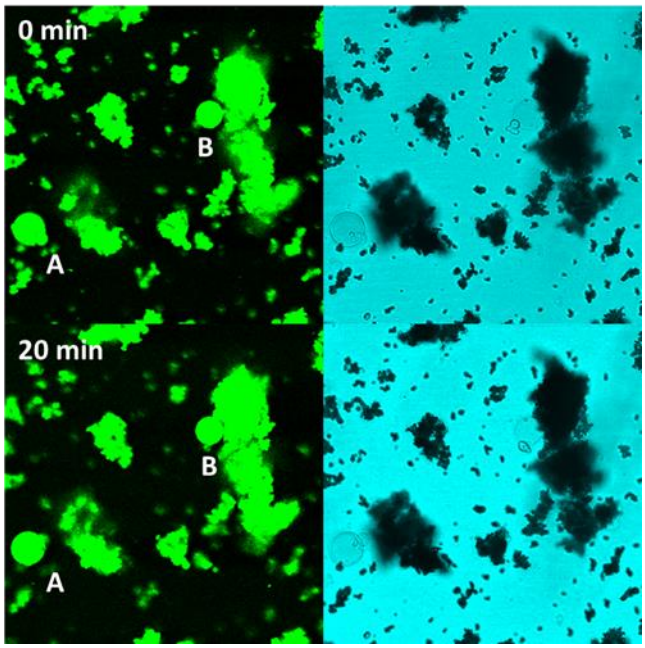

Figure 2.8: Confocal fluorescence images of GUVs filled with lucifer yellow dye and anchored to MOF UiO-67 at 0 minutes, and 20 minutes after addition of NaCl, Right: Brightfield images taken at 0 minutes, and 20 minutes after addition of NaCl.

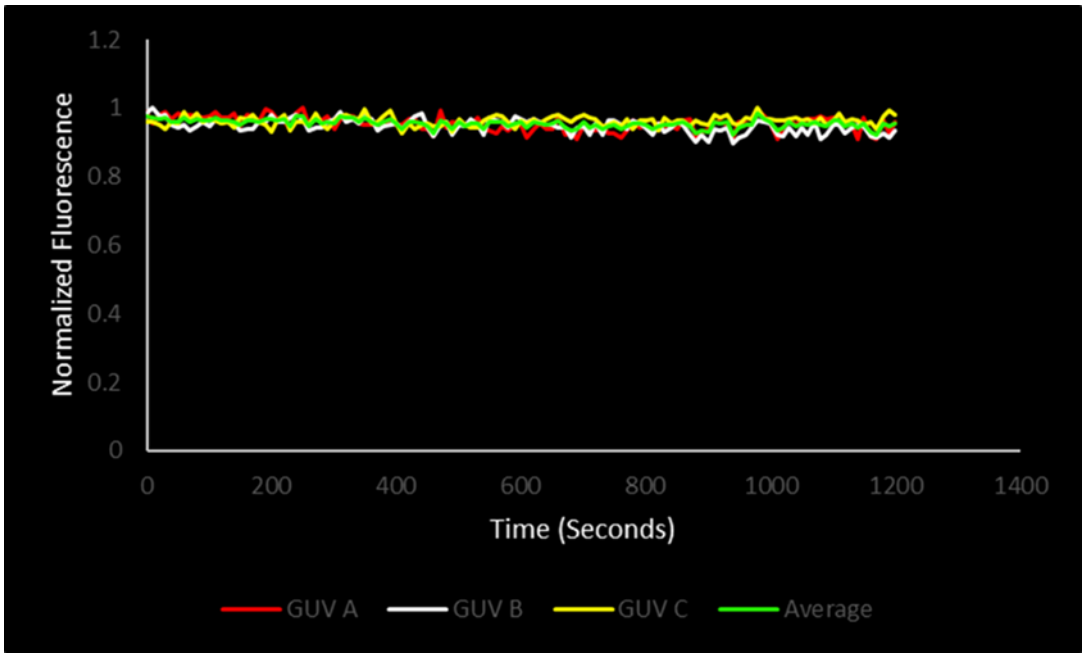

Figure 2.9: Plot of Time (seconds) vs Normalized Fluorescence for the decrease in fluorescence of lucifer yellow dye within GUVs anchored to MOF UiO-67 after the addition of NaCl.

The control experiment with lucifer yellow was conducted with MOF Zr-BTDZ (S12) as well in anticipation that there may be anion transport, and despite MOF Zr-BTDZ showing no indication of anion transport, this control experiment serves to further prove that MOFs do not disturb the lipid bilayer of GUVs enough to cause the dye to leak out in the presence of chloride ions, further reinforcing that trials with MOFs 808 and UiO-67 were in fact showing evidence of ion transport capabilities.

MOF-808:

The first MOF tested for chloride transport was MOF-808. This experiment was done in triplicate and GUVs A and B were imaged within the same session (Figure 2.10), and GUV C was imaged in a separate session (S1). In both imaging sessions, the decrease in fluorescence of the lucigenin dye within the GUVs anchored to the MOFs is evident. The bright field images indicate that the GUVs are still fully intact suggesting that the quenching is not due to defects within the GUVs. The lucigenin dye does not fully quench, however the decrease in fluorescence is sufficient to quantify. Normalized fluorescence was plotted against time for the three trials (Figure 2.11), GUV A shown in red, GUV B shown in white, and GUV C shown in yellow. There is a steady decrease in the fluorescence over the 20-minute imaging session, in the case of GUV B (Figure 2.10) the fluorescence decreases from 100% to 60% indicating that despite being slow, there is chloride ion transport occurring. GUV A quenched much faster than GUV B, and this can be attributed to the size difference between the GUVs. GUV A due to its smaller size has

less lucigenin dye within its interior, and if MOF-808 transports chloride ions at a consistent rate, then the lucigenin dye would be quenched quicker than in a larger GUV.

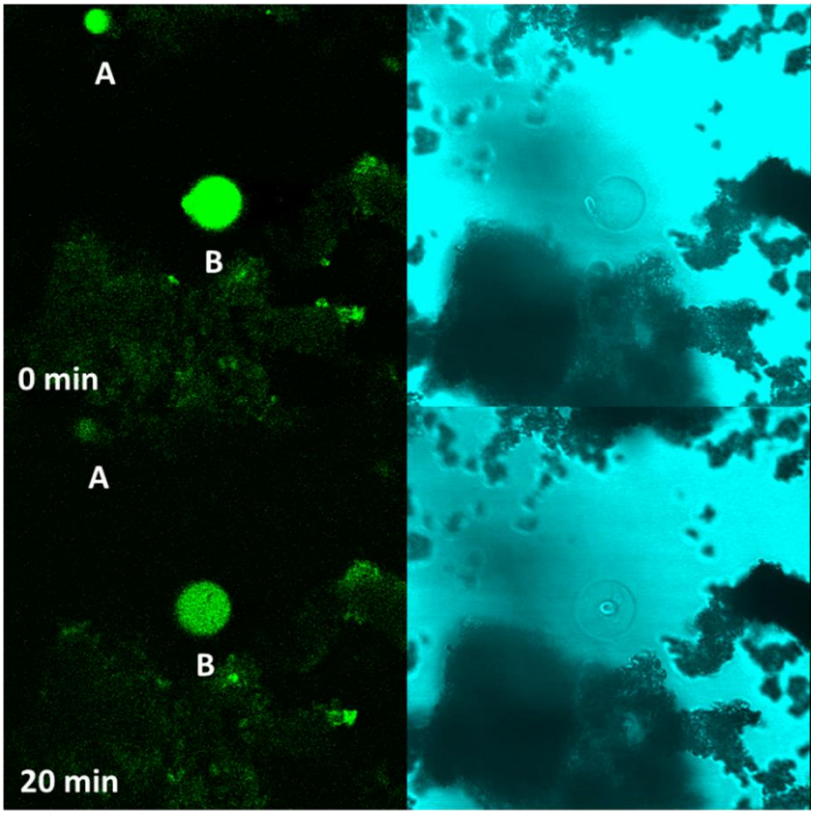

Figure 2.10: Left: Confocal fluorescence images of GUVs anchored to MOF-808 at 0 minutes, and 20 minutes after addition of NaCl, Right: Brightfield images taken at 0 minutes, and 20 minutes after addition of NaCl.

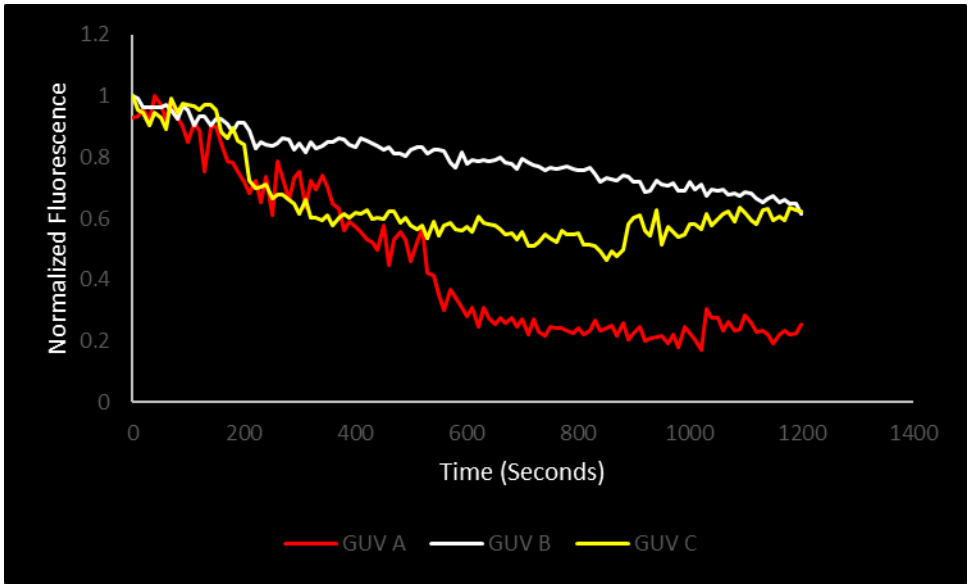

Figure 2.11: Plot of Time (seconds) vs Normalized Fluorescence for the decrease in fluorescence of lucigenin dye within GUVs anchored to MOF-808 after the addition of NaCl.

MOF UiO-67:

The next MOF tested was MOF UiO-67. GUVs A (Figure 2.12), B, and C (S2 and S3) were imaged in separate sessions. This experiment was completed three times and by comparing the images of GUV A taken at 0 minutes and 20 minutes there is a clear decrease in fluorescence of the lucigenin dye. This decrease in fluorescence was plotted as normalized fluorescence vs time (Figure 2.13) and indicates the presence of ion transport from the MOF UiO-67. For these three trials the quenching of the lucigenin dye was more inconsistent. This could be due to discrepancies in the sizes of the MOFs anchored to the GUVs, as well as how many points of contact there are between MOF and GUV. GUV C according to Figure 2.13 has an initiation phase where there is no initial ion transport until 350 seconds. This could potentially be due to the GUV not

initially being fully anchored to the MOF within this trial. Then once the GUV becomes fully anchored ion transport proceeds.

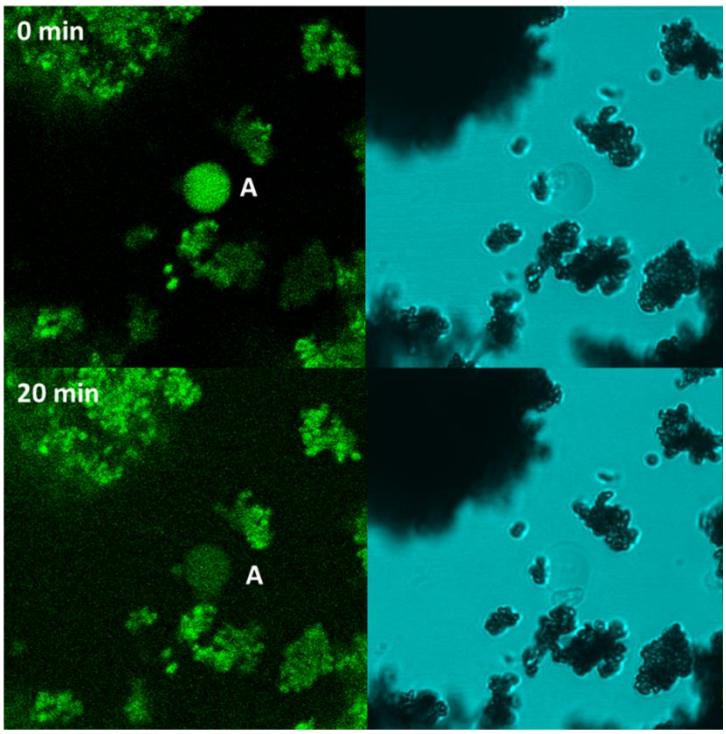

Figure 2.12: Left: Confocal fluorescence images of GUVs anchored to MOF UiO-67 at 0 minutes, and 20 minutes after addition of NaCl, Right: Brightfield images taken at 0 minutes, and 20 minutes after addition of NaCl.

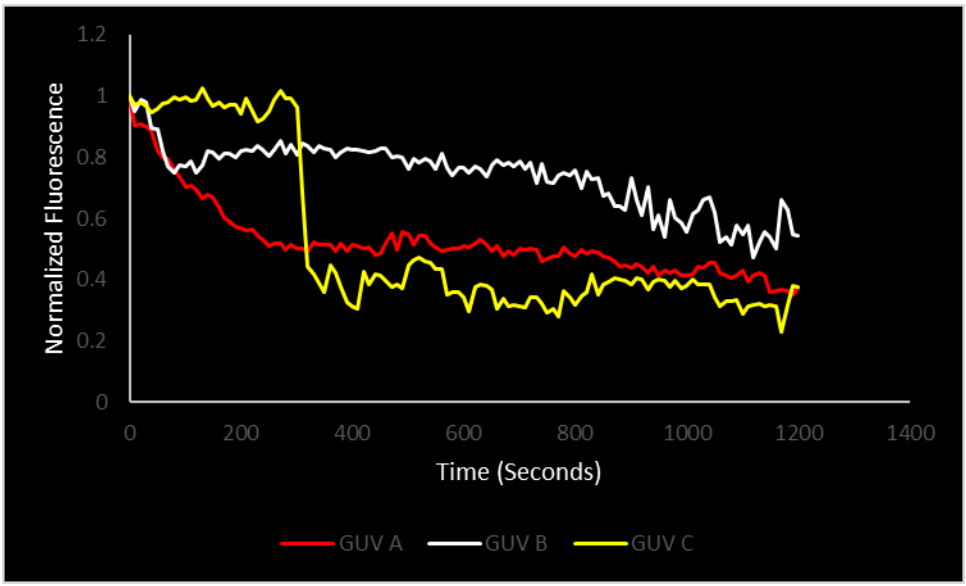

Figure 2.13: Plot of Time (seconds) vs Normalized Fluorescence for the decrease in fluorescence of lucigenin dye within GUVs anchored to MOF UiO-67 after the addition of NaCl.

MOF Zr-BTDZ:

The last MOF that was tested was MOF Zr-BTDZ, GUVs A (S4), B (Figure 2.14), and C (S5) were all imaged in separate sessions. Unlike MOF-808 and MOF UiO-67, there does not appear to be any change in fluorescence between the images taken at 0 minutes and the images taken at 20 minutes, this suggests that MOF Zr-BTDZ is not capable of transporting ions. Normalized fluorescence was, again, plotted vs time (Figure 2.15) and the plot appears like the control experiments where there is clearly no decrease in fluorescence indicating the absence of ion transport with this MOF. MOF Zr-BTDZ has a smaller pore size than both MOF-808 and MOF UiO-67 which could play a role in its inability to transport ions. This MOF differs in that it also has ligands that interpenetrate the interior pore. Most MOFs have open pore structures whereas the

ligands of MOF Zr-BTDZ cross through these open pores, resulting in a smaller pore size. This results in more electron density within the MOF which could cause repulsion of the chloride ions not allowing for chloride ion uptake, and an inability to transport ions across the bilayer of the GUVs.

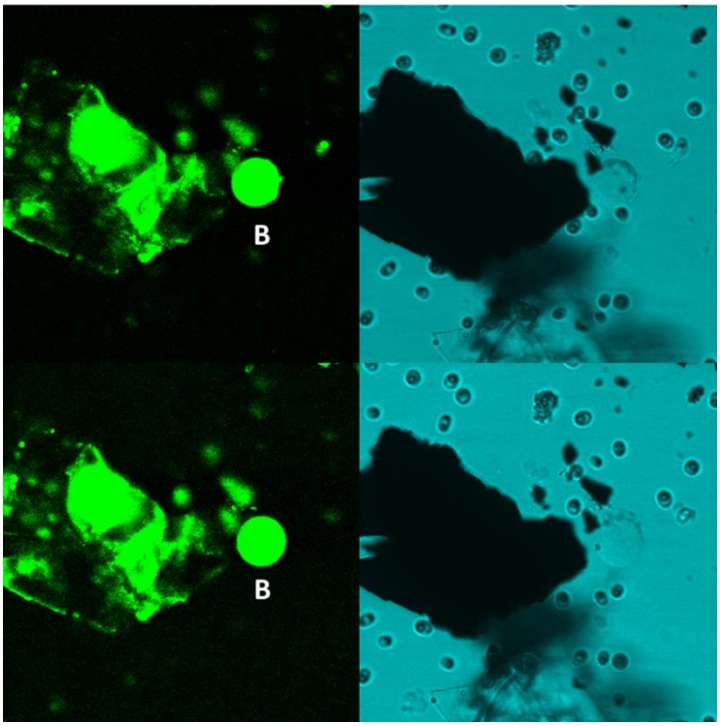

Figure 2.14: Left: Confocal fluorescence images of GUVs anchored to MOF UiO-67 at 0 minutes, and 20 minutes after addition of NaCl, Right: Brightfield images taken at 0 minutes, and 20 minutes after addition of NaCl.

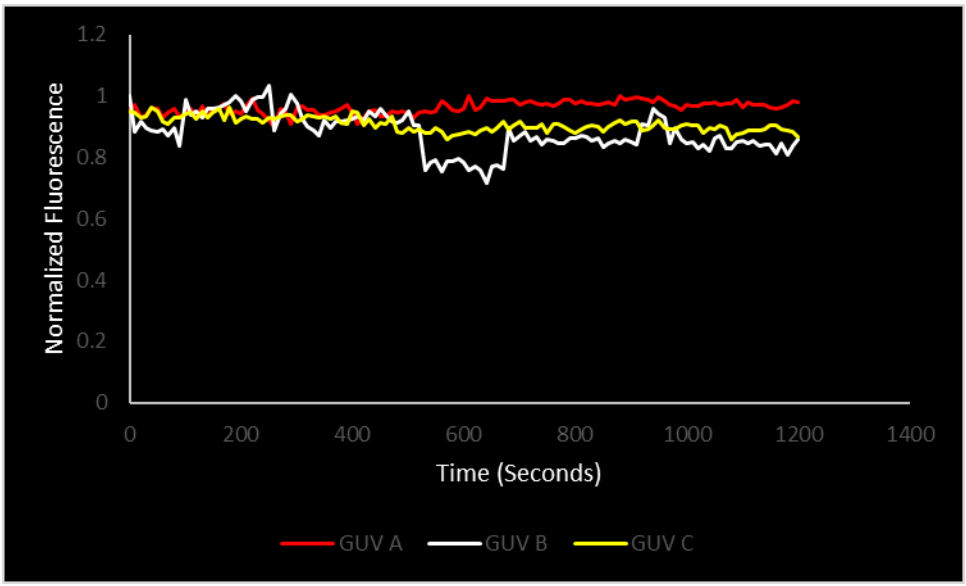

Figure 2.15: Plot of Time (seconds) vs Normalized Fluorescence for the decrease in fluorescence of lucigenin dye within GUVs anchored to MOF Zr-BTDZ after the addition of NaCl.

2.4 Conclusion

In summary, we have demonstrated the first reported evidence of macroscopic MOF particles that can function as chloride ion transporters. By anchoring three different MOFs to GUVs, we were not only able to prove that MOFs can transport anions but that they can do so rapidly. The ability of both MOFs 808 and UiO-67 to transport chloride ions gives us a new class of synthetic ion transporters to potentially be developed into new methods of treatment for diseases such as cystic fibrosis or cancer.

2.5 Future work

There is still much work that needs to be done to continue to prove this concept. Only three MOFs have been tested, all of which are zirconium MOFs. It would be useful

to test a variety of other MOFs using other metal nodes such as iron, copper, and zinc, as these are some of the most used metal nodes in MOFs. It would also be useful to test a variety of MOFs with varying organic linker molecules (e-rich/e-poor) as well to see how these might affect the MOFs ability for anion transport.

We have also only tested MOFs for anion transport using chloride ions, it would be beneficial to test MOFs for their ability to transport other anions as well including the bicarbonate ion as it and chloride are among the most important anions transported into and out of cells within the human body. Although not as important biologically, it would also be useful to test other anions such as iodide, and even bromide ions. MOFs could also have the potential to transport cations across the lipid bilayer of GUVs. Sodium, potassium, calcium, and even proton transport within cells is imperative for their functions, so it would be useful to test these MOFs for cation transport in addition to the already proven study of anion transport.

Finally, we are not completely certain of the mechanism that underlies the ability of MOFs 808 and UiO-67 to transport chloride ions, so control experiments need to be developed to discover what characteristic of MOFs allows them to function as anion transporters.

2.6 References

1. T. L. Overton, J. P. Rourke, M. T. Weller, F. A. Armstrong. *Inorganic Chemistry, Ch 26; Oxford University Press*: Oxford, **2018**

2. J. T. Davis, P. A. Gale, R. Quesada, *Chem. Soc. Rev*., **2020**, 49, 6056-6086

3. Cooper GM. *The Cell: A Molecular Approach. 2nd edition*. Sunderland (MA): Sinauer Associates; **2000**. Transport of Small Molecules.

4. E. Gouaux and R. Mackinnon. *Science*. **2005**, 310 (5753), 1461-1465.

5. J.A. Jarzembowski, in *Pathobiology of Human Disease*, **2014**

6. M. A. Mall. *Eur Respir J*. **2020**, 56(6).

7. N. Busschaert, S. Park, K. Baek, Y. P. Choi, J. Park, E. N. W. Howe, J. R. Hiscock, L. E. Karagiannidis, I. Marques, V. Félix, W. Namkung, J. L. Sessler, P. A. Gale, and I. Shin, *Nat Chem*. **2017**, 9(7), 667.

8. V. Kaushik, J. S. Yakisich, A. Kumar, N. Azad, A. K. V. Iyer, *Cancers*. **2018**, 10, 360.

9. R. Freund, O. Zaremba, G. Arnauts, R. Ameloot, G. Skorupskii, M. Dincă, A. Bavykina, J. Gascon, A. Ejsmont, J. Goscianska, M. Kalmutzki, U. Lächelt, E. Ploetz, C. S. Diercks, S. Wuttke. *Angew. Chem. Int. Ed*. **2021**, 60 (45), 23975-24001.

10. C. S. Jennings, J. S. Rossman, B. A. Hourihan, R. J. Marshall, R. S. Forgan, and B. A. Blight, *Soft Matter*. **2021**,17, 2024.

11. M. Treyer, P. Walde and T. Oberholzer, *Langmuir*, **2002**, 18, 1043–1050.

12. P. Peterlin, G. Jaklic and T. Pisanski, Meas. *Sci. Technol*., **2009**, 20, 055801.

13. R. Lipowsky, *Nature*, **1991**, 349, 475–481.

14. J. Lee, S. Choi, C. Doe, A. Faraone, P. A. Pincus and S. R. Kline, *Phys. Rev. Lett*., **2010**, 105, 038101.

15. S. F. Fenz, K. Sengupta. *Integr. Biol*. **2012**, 4 (9), 982–995.

16. A. P. Davis, A. Kros, N. L. Mora, H. Valkenier, *Angew. Chem. Int. Ed*. **2015**, 54(7), 2137.

17. A. Jönsson, A. Toppi, M. Dufva, The FAST Pump, *HardwareX*, **2020**, 8

18. C. A. Schneider, W. S. Rasband, K. W. Eliceiri, NIH Image to ImageJ: 25 years of image analysis. *Nature Methods*, **2012**, 9(7), 671–675

19. H. Furukawa, F. Gandara, Y. Zhang, J. Jiang, W. L. Queen, M. R. Hudson, and O. M. Yagh. *J. Am. Chem. Soc*. **2014**, 136, 4369−4381.

20. M. J. Katz, Z. J. Brown, Y. J. Colón, P. W. Siu, K. A. Scheidt, R. Q. Snurr, J. T. Hupp, and O. K. Farha. *Chem. Commun*. **2013**, 49, 9449-9451

21. R. J. Marshall, Y. Kalinovskyy, S. L. Griffin, C. Wilson, B. A. Blight, and R. S. Forgan. *J. Am. Chem. Soc*. **2017**, 139, 17, 6253–6260.

22. R. Thür, N. V. Velthoven, V. Lemmens, M. Bastin, S. Smolders, D. De Vos, and I. F. J. Vankelecom. *ACS Appl. Mater. Interfaces*. **2019**, 11 (47), 44792–44801.

23. H. Furukawa, F. Gándara, Y. Zhang, J. Jiang, W. L. Queen, M. R. Hudson, and O. M. Yaghi. *J. Am. Chem. Soc*. **2014**, 136 (11), 4369–4381.

24. C. Ardila-Suárez, D. R. Molina V., H. Alem, V. G. Baldovino-Medrano, G. E. Ramírez-Caballero. *Phys. Chem. Chem. Phys*., **2020**, 22, 12591-12604.

25. X.W. Gu, J.X. Wang, E. Wu, H. Wu, W. Zhou, G. Qian, B. Chen, and B. Li. *J. Am. Chem. Soc*. **2022**, 144 (6), 2614–2623.

26. V. S. D. Devulapalli, R. P. McDonnell, J. P. Ruffley, P. B. Shukla, T.Y. Luo, M. L. De Souza, P. Das, N. L. Rosi, J. K. Johnson, E. Borguet. *Eur. J. Chem*. **2022**. 15 (1).

Chapter 3
Iridium (III) Complexes as Dual Bioimaging Dyes and Anion Transporters for Theranostics Applications

Braeden Hourihan, Marta Tomas, Holly Howe, and Barry A. Blight

Braeden Hourihan was responsible for the design, synthesis, characterization, and experimental studies of all compounds in this chapter. Marta Tomas contributed by obtaining additional characterization information such as emission and excitation spectra, quantum yields, lifetimes, and CNMR and mass spec for compound ***27****. Holly Howe helped to resynthesize compounds for characterization throughout the project.*

3.1 Introduction

Ion transport is an extremely important process for the survival of cells. Maintaining a specific ion homeostasis inside the cells as well as in the extracellular matrix is essential for the upkeep of membrane potential, cell shape, and proper functioning of several cellular pathways.[1] Cancer cells, however, are known to alter this ion homeostasis in a way that is specifically beneficial for their growth and migration.[1] It is well documented that cancer cells are highly resistant to cellular apoptosis, a form of programmed cell death that is needed for maintaining tissue homeostasis.[1,2] Altering the new ion homeostasis established by cancer cells serves as a catalyst to start a cascade of signaling events that eventually leads to cellular apoptosis; thus much effort has recently gone into using ion transporters as potent apoptosis inducers that can be used to treat cancer.[1]

One method that scientists have used to alter ion homeostasis in cancer cells is through constructing molecules that can either activate or deactivate existing ion transporters and ion channels within the cellular membrane.[1] Studies have shown that this method can sensitize cancer cells to drugs that are known to be otherwise ineffective. More recently, scientists have also developed ion transporters that can work independently, inserting themselves in the membranes of cancer cells and cause an influx of ions that disrupts the cell's ability to properly function by altering various cellular pathways.[1]

Theranostics is an emerging field in medicine that works towards developing drug delivery systems that combine diagnostics and therapeutics.[3] This field has recently

become popular because it has lead to the development of therapeutics that work to target specific cells, genes, and proteins, and can also be used with little to no changes for diagnostic imaging to aid in precision medicine.[3] Iridium (III) complexes have recently become of interest in this field due to their many advantageous photophysical properties. These complexes have large Stokes shifts, high quantum yields, long lifetimes, and are resistant to photobleaching making them excellent candidates for bioimaging.[4] Fluorescent cancer targeting agents have been researched extensively, yet, there has been no attempt to develop a fluorescent ion transporter for potential use in cancer treatment.[5] In this paper we describe the first example of two new fluorescent anion transporters that have the potential to be used for diagnostic imaging towards the induction of cellular apoptosis.

This study demonstrates the synthesis and anion transport studies of two new iridium (III) complexes[4] that are embedded within a cellular membrane. Determination of their efficacy as bioimaging dyes was carried out by inserting the iridium complexes within the lipid bilayer of giant unilamellar vesicles (GUVs) and imaging with a confocal microscope. The ion transport abilities of these compounds were tested by again inserting the iridium complex into the lipid bilayer of GUVs, and then forming these vesicles in the presence of lucigenin, a chloride sensitive dye. While imaging with a confocal microscope sodium chloride was added to the GUVs and the lucigenin dye within the GUVs was quenched in the presence of chloride ion transport. The results from this study have indicated that these iridium (III) complexes can function as both efficient ion transporters, and promising bioimaging dyes. This advancement could pioneer a new

class of compounds that provide the ability to examine both if the ion transporter is actively targeting tumors, as well as provide a way to directly monitor treatment.

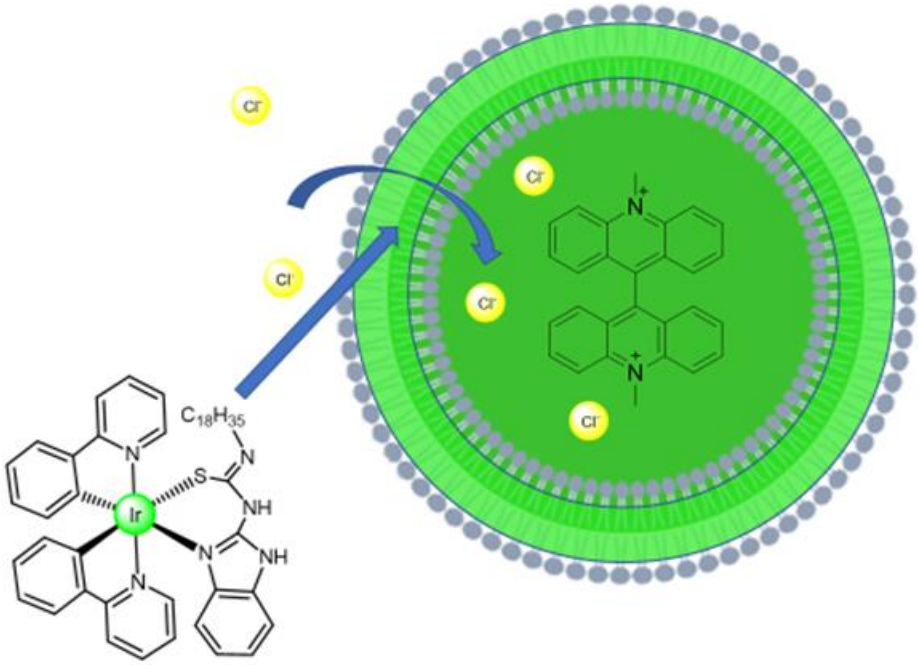

Figure 3.1: Depiction of iridium (III) complexes being used as dual anion transporters and bioimaging dyes.

3.2 Experimental

General:

Materials. All reagents were purchased from Sigma Aldrich, Fisher Scientific or Avanti Polar Lipids and used as received, unless otherwise stated. The peristaltic pump was 3D printed using a modified literature procedure.[6] Analytical thin layer chromatography was done on precoated TLC plates Alugram Sil G/UV254. Column chromatographic purifications were done with silica gel, ultrapure, 60-200 μm (60 Å).

NMR. ^{1}H (400 MHz) and ^{13}C (100 MHz) NMR spectra were recorded on a JEOL ECS 400 spectrometer in deuterated solvents chloroform-d, and DMSO-d6. All chemical shifts are reported in δ (ppm) referenced to tetramethylsilane, Si $(CH_3)_4$, and peak multiplicities are denoted as singlet (s), doublet (d), triplet (t), quartet (q), or multiplet (m). Copies of NMR spectra can be found in the Appendix.

Mass Spectrometry. High-resolution mass spectral data was obtained by the Mass Spectrometry Laboratory, Dalhousie University, Halifax, Canada. High-resolution mass spectra were recorded on a Bruker Daltonics MicrOTOF instrument. The ionization method used for low-res and highres analysis was positive or negative electrospray ionization (ESI).

UV-visible Absorption. Absorption spectra were recorded at room temperature using an Agilent Cary 4000 UV-vis double beam spectrophotometer.

Photophysical data. Steady-state emission and excitation spectra were recorded at 298 K using an Edinburgh Instruments FS5 spectrometer. All samples for steady-state measurements were excited at 360 nm. Photoluminescence quantum yields were determined through direct method using the integrating sphere.

Giant Unilamellar Vesicle Preparation. GUVs were grown using a literature-based -technique. 1-Palmitoyl-2-oleoyl-sn-glycero-3-phosphocholine (POPC), 1-palmitoyl-2-

oleoyl-sn-glycero3-phospho-rac-(1-glycerol) (sodium salt) (POPG) and cholesterol were purchased from Avanti Polar Lipids (dissolved in chloroform to a concentration of 10 mg/mL). For a typical lipid mix: lipids POPC and POPG, and cholesterol were mixed in a 4: 1: 1 molar ratio, and this solution was made to an overall concentration of 1 mg/mL.

Confocal Imaging. Confocal imaging was performed at the UNB Microscopy and Microanalysis Facility with a Leica TCS-SP2 CLSM microscope using Leica confocal software package version 2.61 build 1537. Images were collected with the excitation wavelength of 458 nm and fluorescence was collected in a 500 - 600 nm band range for lucigenin and lucifer yellow fluorescent dyes.

Ion Transport Studies:

GUVs were synthesized using literature procedures. The non-conductive sides of two indium tin oxide (ITO) – coated glass slides were marked with a 15 mm diameter circle in the center of each. An aliquot of ~10 µL of lipid mixture (4:1:1 POPC/POPG/Chol, 0.4 mol% transporter, all dissolved in chloroform) was gently spread on the conductive side of each slide within the circle with the tip of a micro syringe while a gentle flow of air was passed over it until the chloroform evaporated. The slides were then placed in a desiccator for ~30 minutes to further remove the solvent from the residue. A 2 mm thick O-ring with a 15 mm diameter was covered in a minimum amount of silicon grease and affixed to one of the 2 slides over the drawn circle. Approximately 350 µL of an electroformation solution (0.8 mM Lucigenin, 225 mM $NaNO_3$, 200 mM sucrose, in water), was added to the O-ring chamber. The conductive sides of both slides were fixed

(sandwiched) together and placed into a NANION Vesicle Prep Pro apparatus, a sinusoidal AC electric field at 10 Hz was applied for electroswelling the lipid films. The sample was shielded from external light during this time. In the first phase of the electroswelling process, the amplitude of the applied field was linearly increased from 0.1 V to 0.5 V over 30 min, while the temperature was increased from 21 °C to 35 °C. The voltage was then increased further over the next 15 minutes to 1.6 V. Thereafter, the amplitude of the AC field was kept constant at 1.6 V for 2 h to grow the vesicles. Finally, during the last 5 minutes, the voltage was slowly lowered to 0 V. Once the electroformation was complete, the slides were carefully removed from the Nanion Vesicle Prep Pro and separated. The aliquot within the O-ring was transferred to a centrifuge tube containing 0.6 µL of a resuspension solution (225 mM $NaNO_3$, 200 mM glucose, in water) using a disposable pipette with the tip cut off at the 5 mL mark to make a larger opening to prevent lysing of the vesicles. The imaging chamber was filled with a 1 mg/mL aqueous solution of BSA serum and left for a minimum of 30 minutes to create a coating to immobilize the GUVs. The mixture was then transferred from the centrifuge tube into the wells of the imaging chamber using the same pipette (filled 2 wells), and a peristaltic pump set to a flow rate of 0.4 mL/min was used to replace the resuspension solution, to help remove excess lucigenin dye. The imaging wells were then covered in tin foil while transported to the microscopy room, to prevent photobleaching of the lucigenin. While imaging with a confocal microscope (458 nm laser at 15%), 25 µL of 1 M NaCl solution in 200 mM glucose and 225 mM $NaNO_3$ in water was slowly added to the imaging wells. Confocal images were then taken every 10 seconds for 20 minutes to observe quenching of the lucigenin dye.

Synthesis:

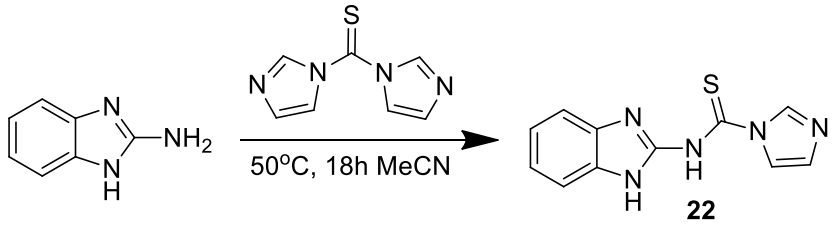

Figure 3.2: Reaction scheme for the synthesis of compound **22**.

Compound **22** – Synthesized using a literature procedure.[7] To a solution of 2-aminobenzimidazole (50 mg, 0.38 mmol, 1 eq), in MeCN (~5 mL), was added thiocarbonyl diimidazole (TCDI) (87.1 mg, 0.49 mmol, 1.3 eq). The reaction was left to stir at 50°C for 18 hours. The reaction mixture was then cooled to room temperature and stirred for 3 hours. The pale-yellow precipitate was filtered, washed with MeCN (2 x 50 mL), and dried under vacuum, giving a yield of 80%.

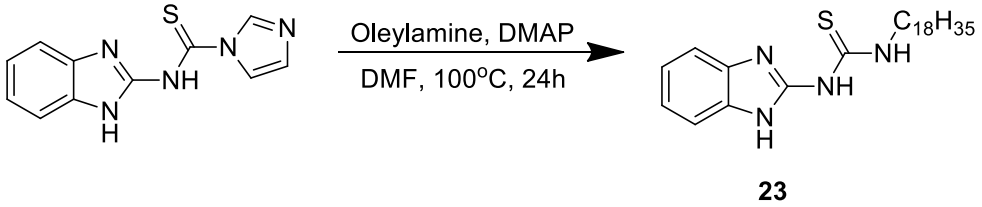

Figure 3.3: Reaction scheme for the synthesis of compound **23**.

Compound **23** – Formed following a modified literature procedure.[7] To a solution of compound **22** (0.4118 g, 1.69 mmol, 1eq) in DMF (~25 mL) was added DMAP (0.021 g, 0.17 mmol, 10 mol%) followed by dropwise addition of oleylamine (0.67 mL, 2 mmol, 1.2eq) while stirring. The reaction was stirred at 100°C for 15 h. The reaction was then cooled to room temperature and the solvent was removed in vacuo. The remaining solid was redissolved in ethyl acetate and washed with water, dried with $MgSO_4$, and filtered.

Column chromatography was then performed in hexanes/ethyl acetate (2:1) to give the pure product in a yield of 68%.

^{1}H NMR (400 MHz, 298 K, chloroform-d) δ (ppm): 11.15 (s, 3H), 7.40 (m, 2H), 7.08 (m, 2H), 5.27 (dt, 2H), 3.60 (q, 2H), 1.94 (m, 4H), 1.61 (m, 2H), 1.22 (m, 22H), 0.81 (m, 3H).

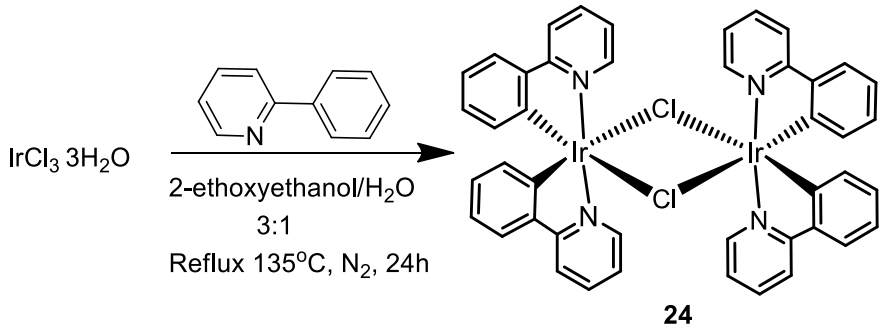

Figure 3.4: Reaction scheme for the synthesis of compound **24**.

Compound **24** – Synthesized using a literature procedure.[8] Iridium (III) chloride trihydrate (0.1 g, 0.28 mmol, 1 eq), and 2-phenylpyridine (42.5 µL, 0.29 mmol, 2.1 eq) were dissolved in a 3:1 mixture of 2-ethoxyethanol and water. The reaction mixture was stirred at 135°C for 24 hours under a nitrogen atmosphere. After cooling the reaction to room temperature, the yellow precipitate was filtered, and dried under vacuum, giving a yield of 88%.

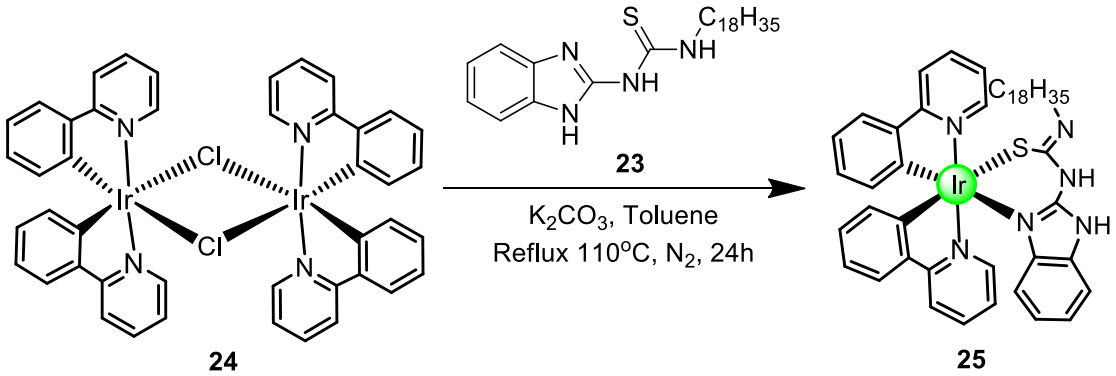

Figure 3.5: Reaction scheme for the synthesis of compound **25**.

Compound **25** – To a solution of compound **24** (0.1 g, 0.09 mmol, 1eq) in toluene (~15 mL) were added compound **23** (0.0885 g, 0.2 mmol, 2.1eq) and K_2CO_3 (0.089 g, 0.64 mmol, excess). The reaction mixture was stirred overnight at 110°C under a N_2 atmosphere. After cooling to room temperature, the solvent was removed in vacuo and the remaining solid was redissolved in ethyl acetate. The organic phase was washed with water (2 x 20 mL), dried with $MgSO_4$, and filtered. Column chromatography was performed in hexanes/ethyl acetate to give the pure product. The purified product was obtained in a 90% yield as a bright yellow oil.

^{1}H NMR (400 MHz, 298 K, chloroform-d) δ (ppm) 9.57 (d, 2H), 8.36 (d, 1H), 7.85 (d, 1H), 7.63 (t, 2H), 7.52 (dd, 3H), 6.96 (m, 2H), 6.86 (t, 2H), 6.79 (t, 2H), 6.69 (m, 1H), 6.59 (m, 1H), 6.47 (dd, 2H), 6.24 (d, 1H), 5.69 (s, 1H), 5.36 (m, 2H), 3.38 (s, 2H), 2.01 (m, 4H), 1.51 (dd, 2H), 1.25 (m, 22H), 0.85 (m, 3H).

HRMS m/z calculated: 943.4073. Found: 943.4063 [M+]

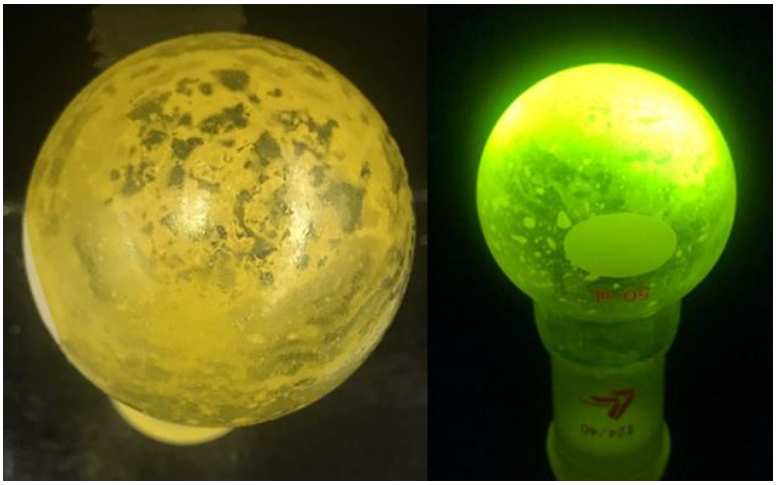

Figure 3.6: Left: Compound **25** as an oily yellow solid, right: compound **25** under UV light.

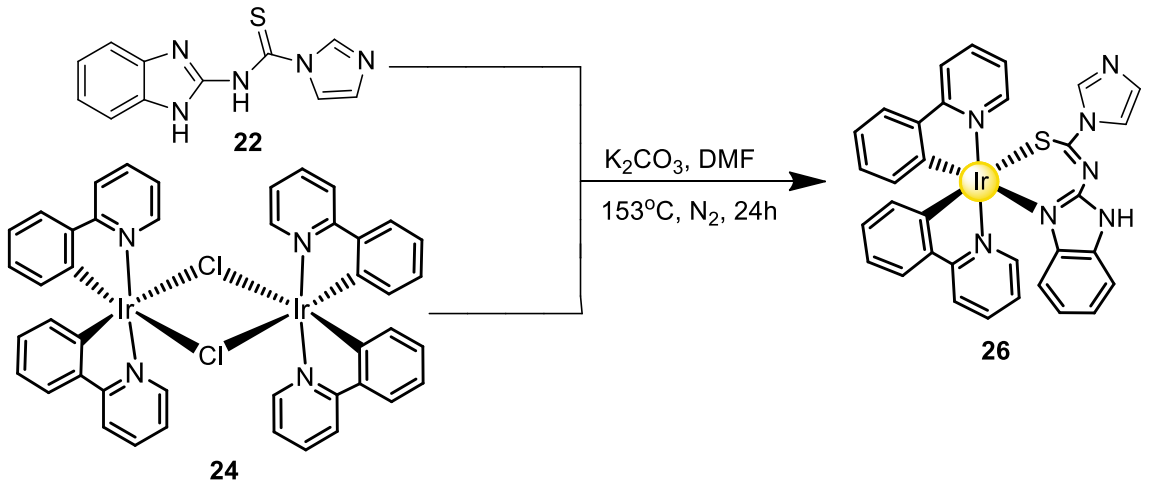

Figure 3.7: Reaction scheme for the synthesis of compound **26**.

Compound **26** – To a solution of compound **24** (0.2 g, 0.18 mmol, 1eq) in DMF (~15 mL) was added K_2CO_3 (0.248 g, 1.8 mmol, 10eq), and compound **22** (0.919 g, 0.38 mmol, 2.1eq). The reaction mixture was stirred for 24 hours under a nitrogen atmosphere at 153°C. After cooling to room temperature, the solvent was removed in vacuo and the remaining solid was redissolved in ethyl acetate. The organic phase was washed with water (2 x 20 mL), dried with $MgSO_4$, and filtered. Column chromatography was performed in hexanes/ethyl acetate to give the final product in 24% yield.

^{1}H NMR (400 MHz, DMSO-d6) δ: 12.53 (s, 1H), 9.35 – 9.32 (m, 1H), 8.49 – 8.45 (m, 1H), 8.23 (d, J = 8.3 Hz, 1H), 8.15 – 8.12 (m, 1H), 8.09 (d, J = 8.3 Hz, 1H), 7.94 – 7.89 (m, 1H), 7.89 – 7.75 (m, 4H), 7.29 (ddd, J = 13.1, 9.5, 4.6 Hz, 2H), 7.23 – 7.18 (m, 1H), 7.00 – 6.91 (m, 3H), 6.87 – 6.81 (m, 2H), 6.69 (td, J = 7.4, 1.2 Hz, 1H), 6.57 – 6.51 (m, 1H), 6.29 – 6.24 (m, 2H), 6.10 – 6.07 (m, 1H).

^{13}C NMR (101 MHz, DMSO-d6) δ 168.36, 167.60, 161.83, 157.12, 150.54, 150.21, 149.76, 148.56, 144.65, 144.53, 142.46, 138.25, 137.94, 135.79, 132.81, 131.83, 131.54,

129.84, 129.63, 129.51, 125.21, 124.58, 123.50, 123.34, 122.77, 121.88, 121.53, 121.49, 120.14, 119.65, 118.18, 118.00, 110.83.

HRMS m/z calculated: 744.1521. Found: 744.1508 [M+]

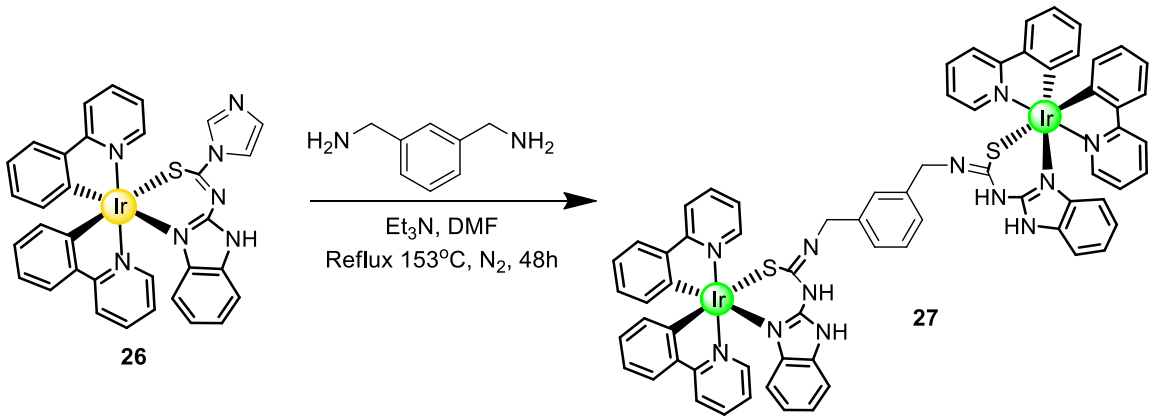

Figure 3.8: Reaction scheme for the synthesis of compound **27**.

Compound **27** – To a solution of compound **26** (0.0366 g, 0.05 mmol, 2.1eq) in DMF was added m-xylylenediamine (3.1 µL, 0.023 mmol, 1eq), and triethylamine (excess). The reaction mixture was stirred for 48 hours under a nitrogen atmosphere at 153°C. After cooling to room temperature, the solvent was removed in vacuo and the remaining solid was redissolved in ethyl acetate. The organic phase was washed with water (2 x 20 mL), dried with $MgSO_4$, and filtered. Column chromatography was performed in hexanes/ethyl acetate to give the final product in 27% yield.

^{1}H NMR (400 MHz, DMSO-d6) δ: 9.49 (d, 1H), 8.36 (m, 1H), 7.88 (m, 1H), 7.72-7.63 (m, 2H), 7.61-7.51 (m, 3H), 7.03-6.96 (m, 2H), 6.93-6.76 (m, 5H), 6.72 (td, 1H), 6.55 (ddd, 1H), 6.43 (m, 1H), 6.24 (m, 1H), 3.25 (s, 4H)

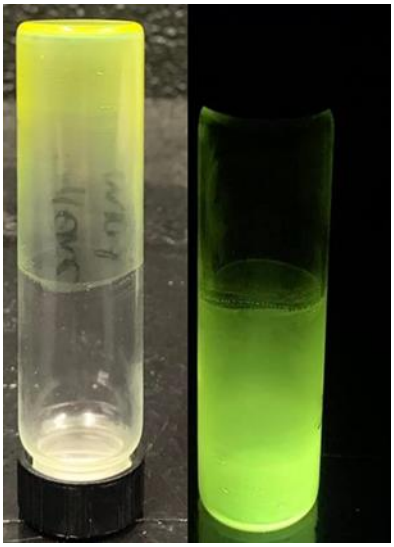

Figure 3.9: Left: Compound **27** and a yellow solid, right: compound under UV light.

3.3 Results and Discussion

Photophysical Studies:

Photophysical studies were conducted on compounds **25** and **27**. Iridium (III) complexes are known to be useful as bioimaging dyes due to their high quantum yields, long lifetimes, and resistance to photobleaching and our complexes follows these trends as indicated in Table 1. Both complex **25** and **27** display large Stokes shifts of $\Delta\lambda = 148$ and $\Delta\lambda = 118$, respectively. They also display good quantum yields. The quantum yield measurements were done in triplicate and averaged to obtain the most accurate result giving yields of 6.29% for complex **25**, and 9.87% for complex **27**. The excited-state lifetimes for the Ir(III) complexes **25** and **27** are given in Table 1 and are in the low ns range

Table 1: Photophysical properties of iridium (III) complexes.

	Compound 25	**Compound 27**
PL λmax / nm	366 nm, 514 nm	406 nm, 524 nm
Quantum Yield / ϕ	6.29%	9.87%
Lifetime τ / ns	53.47 ns	47.48 ns

Biomimetic Studies:

To evaluate the utility of our new iridium (III) complexes to function as bioimaging dyes, GUVs were electroformed in the presence of the complexes, allowing them to integrate within their lipid bilayer. These GUVs were then imaged when excited with a 488 nm source, as well as using bright-field mode on a confocal microscope. GUVs in these experiments were anchored to MOF UiO-67 to immobilize them to obtain clearer images. Experiments were conducted using dye concentrations of 0.4 mol%, and the concentration of dye within the lipid bilayer appeared to have no effect on the number of GUVs formed and did not appear to alter the integrity of their lipid bilayer as can be seen in Figures 3.10 and 3.11. The luminescence intensity of labelled GUVs also remained constant for several hours, confirming that our complex displays high photochemical stability.

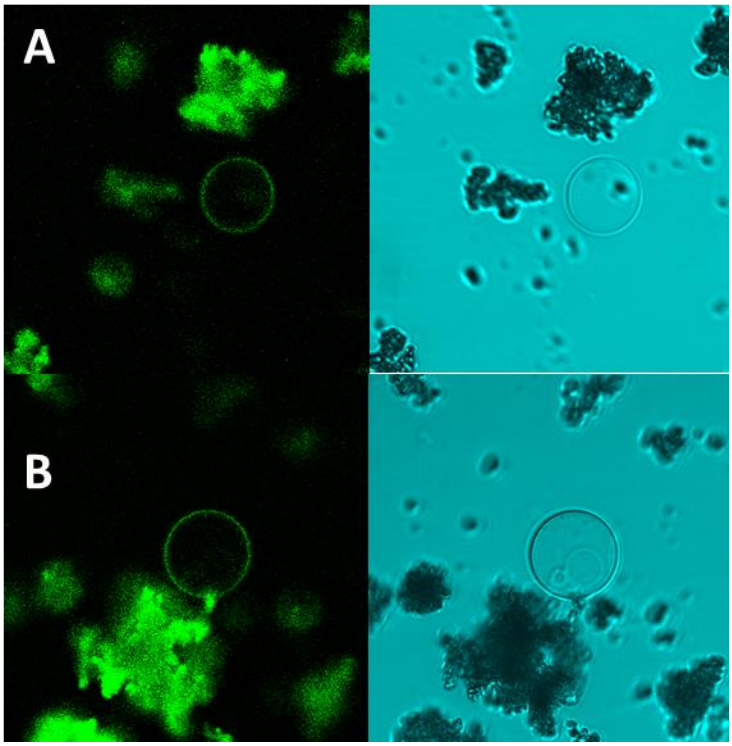

Figure 3.10: Confocal (left) and brightfield (right) images taken at 488 nm of compound **25** as a bioimaging dye in the lipid bilayer of GUVs.

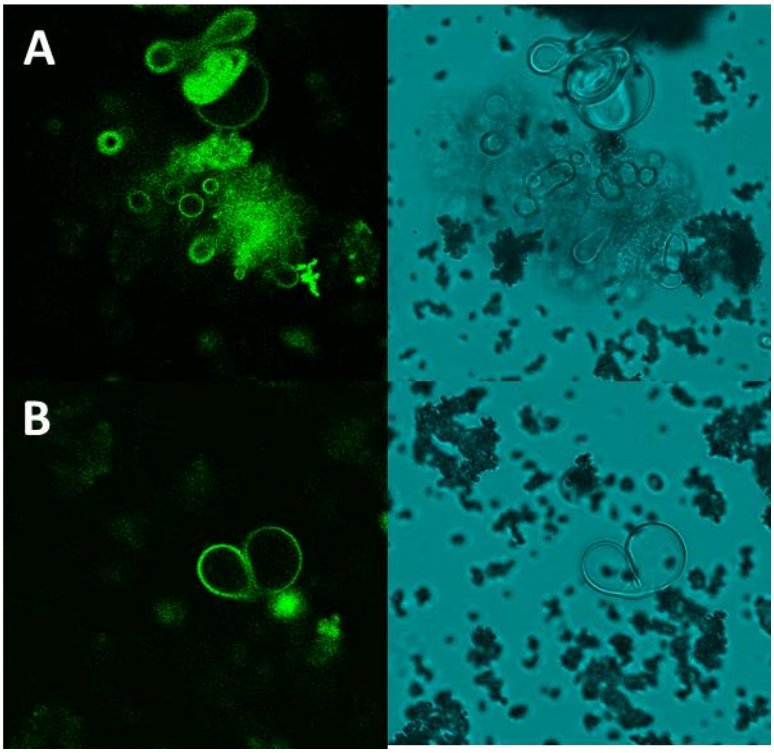

Figure 3.11: Confocal (left) and brightfield (right) images taken at 488 nm of compound **27** as a bioimaging dye in the lipid bilayer of GUVs.

In comparing compound **25** and compound **27** as bioimaging dyes, we anticipated that compound **27** might be slightly more fluorescent as a bioimaging dye due to it being a dimer with two iridium centers within the molecule. However, when analyzing the images, it does not appear that compound **27** is any brighter within the lipid bilayer than compound **25**. We also considered that this discrepancy may be because compound **25** is more lipophilic than compound **27**, so it may be possible that there is a higher concentration of compound **25** that is able to integrate within the lipid bilayer than compound **27**.

Control Experiments:

Control experiments were conducted to confirm that any decrease in fluorescence of lucigenin dye within the GUVs was from chloride ion transport. GUVs were formed in the presence of the chloride sensitive lucigenin dye, however in the first control experiment there were no iridium complexes inserted into the lipid bilayer. Chloride was added to the imaging slide with the GUVs and imaged on the confocal microscope. There was no observable change in fluorescence which proves that the lucigenin dye does not leak from the GUVs due to the addition of chloride ions causing defects in the lipid bilayer and does not photo bleach over the 20 minutes imaging session. This control experiment was done in triplicate, GUVs A and B were imaged within the same session (Figure 3.12), whereas GUV C was imaged individually (S23). As shown in the confocal images in Figure 3.12, GUVs A and B show no change in fluorescence 20 minutes after the chloride was added. Normalized fluorescence was then plotted against time for all three GUVs, as shown in Figure 3.13. There was little to no change in fluorescence of the lucigenin dye after 20 minutes. This suggests that the decrease in fluorescence observed during the chloride transport experiments using ion transporters was not due to dye leaking from the GUVs from the addition of chloride ions causing defects in the lipid bilayer or from photobleaching of the dye.

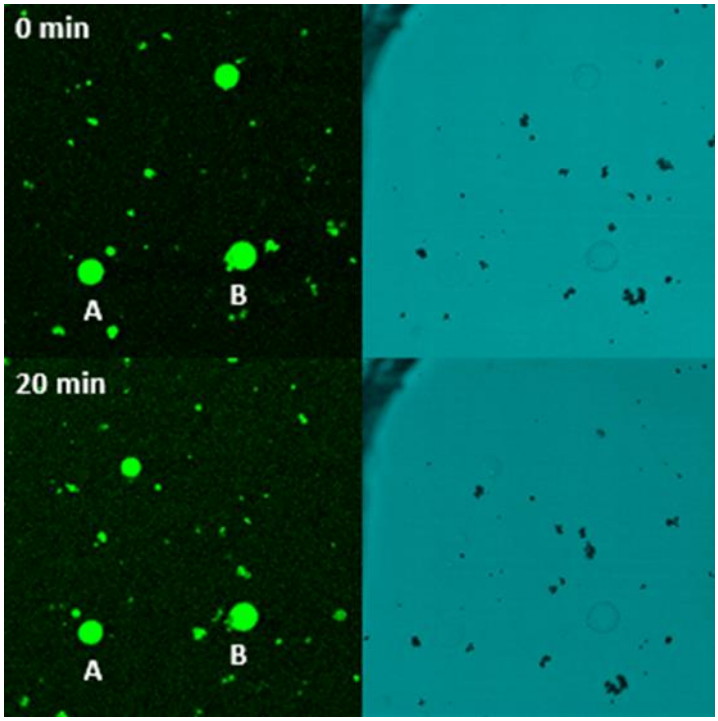

Figure 3.12: Confocal fluorescence images of GUVs without anion transporters at 0 minutes, and 20 minutes after addition of NaCl, Right: Brightfield images taken at 0 minutes, and 20 minutes after addition of NaCl.

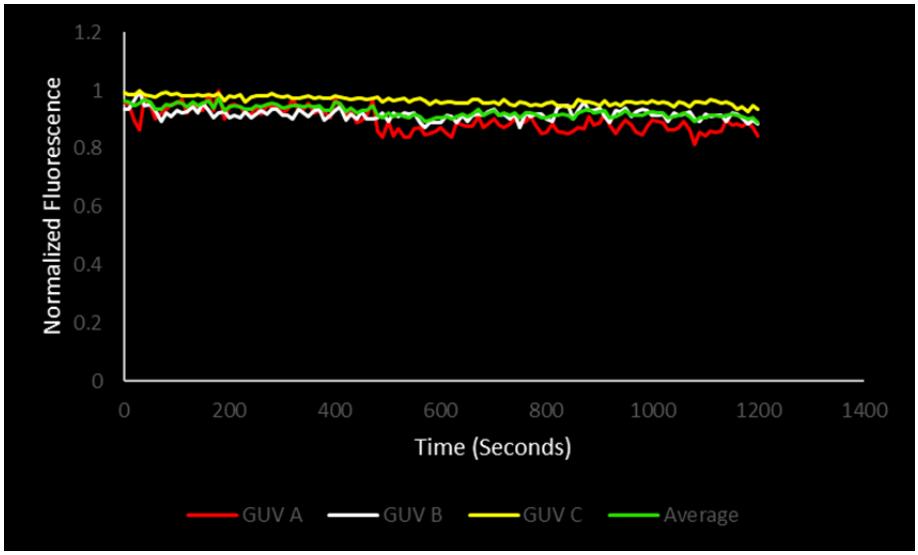

Figure 3.13: Plot of Time (seconds) vs Normalized Fluorescence for the decrease in fluorescence of lucigenin dye within GUVs without anion transporters after the addition of NaCl.

Another control experiment was conducted to rule out the possibility that an interaction between the GUVs and the iridium complexes within the lipid bilayer might cause the lucigenin dye to leak causing the appearance of the dye quenching. To prove that the dye was not leaking from the GUVs the control experiment was conducted using lucifer yellow dye rather than lucigenin dye. Lucifer yellow is a commonly used bioimaging dye however it is not sensitive to chloride ions, so in the presence of chloride it will not quench. Chloride ions were added to the solution of lucifer yellow filled GUVs and imaged for 20 minutes. The lucifer yellow dye is not chloride sensitive, so if the lucigenin dye was quenching due to the iridium complexes causing the dye to leak, then there would be a decrease in fluorescence of the lucifer yellow dye as well. If ion transport was occurring, the fluorescence of the lucifer yellow dye should remain consistent, but the fluorescence of the lucigenin dye should decrease under the same conditions. This control experiment was conducted for both compound **25** and compound **27** as seen in Figures 3.14 and 3.16. When normalized fluorescence was plotted vs time as seen in Figures 3.15 and 3.17, there was a negligible decrease in fluorescence with both experiments indicating that the presence of compounds **25** and **27** in the lipid bilayer were not causing the appearance of dye quenching by allowing the dye to leak out of the GUVs.

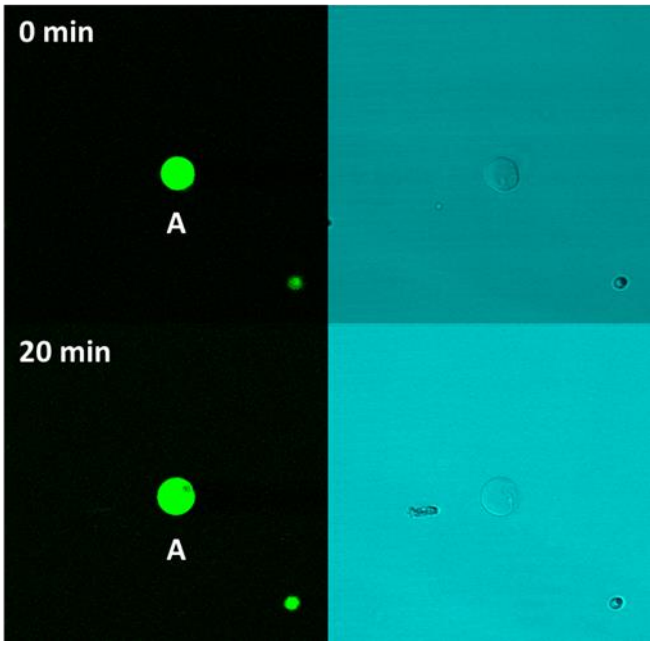

Figure 3.14: Confocal fluorescence images of GUVs filled with lucifer yellow dye and compound **25** at 0 minutes, and 20 minutes after addition of NaCl, Right: Brightfield images taken at 0 minutes, and 20 minutes after addition of NaCl.

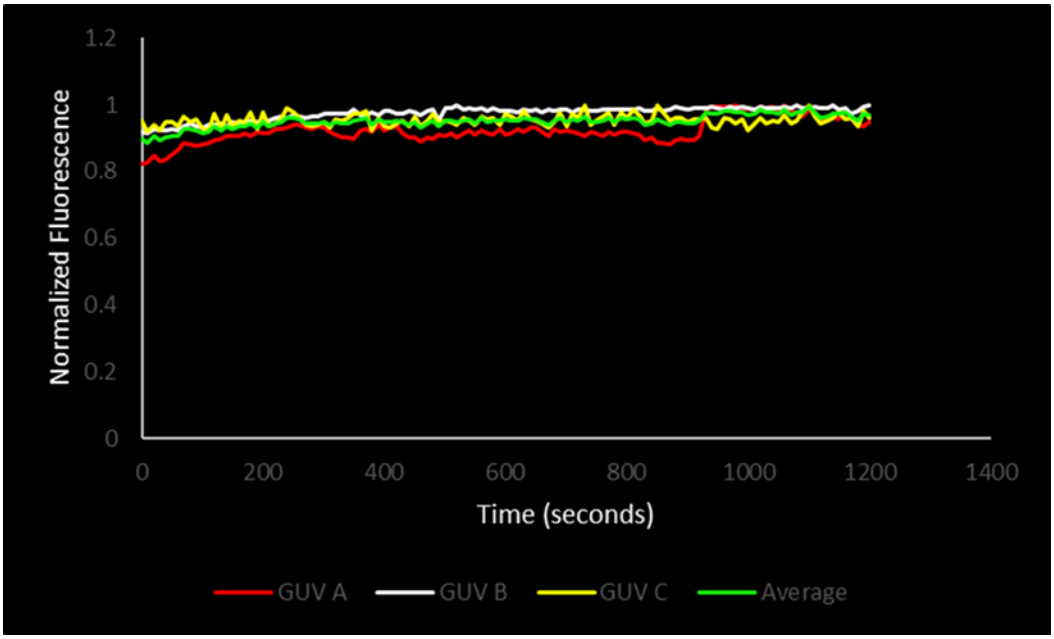

Figure 3.15: Plot of Time (seconds) vs Normalized Fluorescence for the decrease in fluorescence of lucifer yellow dye within GUVs with compound **25** after the addition of NaCl.

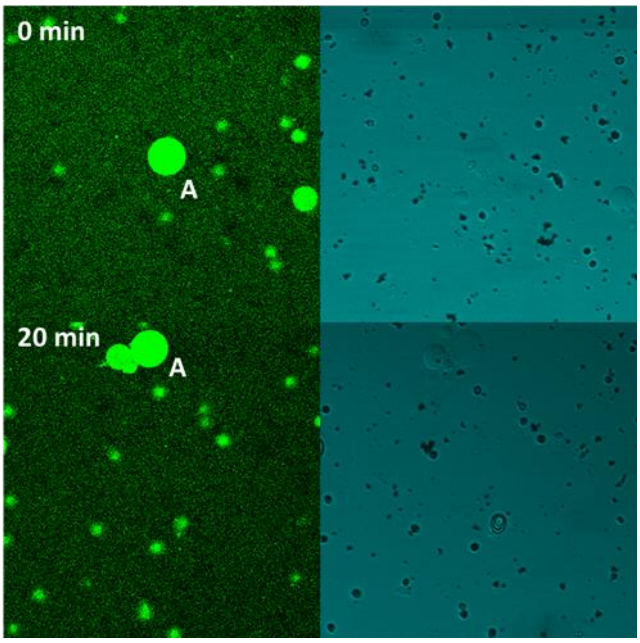

Figure 3.16: Confocal fluorescence images of GUVs filled with lucifer yellow dye and compound **27** at 0 minutes, and 20 minutes after addition of NaCl, Right: Brightfield images taken at 0 minutes, and 20 minutes after addition of NaCl.

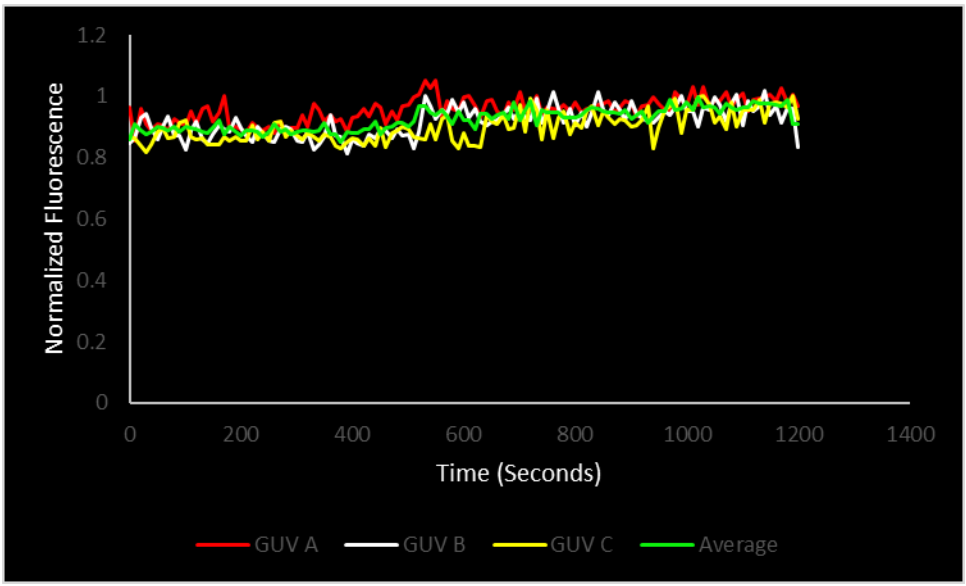

Figure 3.17: Plot of Time (seconds) vs Normalized Fluorescence for the decrease in fluorescence of lucifer yellow dye within GUVs with compound **27** after the addition of NaCl.

Ion Transport Studies:

The ion transport studies were conducted by electroforming GUVs in the presence of lucigenin, a halogen sensitive dye, which then became trapped within the GUVs. A peristaltic pump was then used to replace the supernatant in which the GUVs were formed with a clean resuspension solution to provide a clear background for imaging. The ion transport process involves the iridium (III) complexes hydrogen bonding to chloride ions using the protons of the ancillary thiourea ligand to pull them across the lipid bilayer. Once inside the GUVs, the chloride ions quench the fluorescence of the lucigenin dye resulting in a visual indication of ion transport. In conducting these experiments, we received visual confirmation that ion transport was occurring with both iridium (III) complexes after watching the lucigenin dye within the GUVs quench shown

in Figures 3.18 and 3.20. To quantify the decay in fluorescence we observed, a program called ImageJ was used to measure the average fluorescence intensity within the GUVs for every image taken during a 20-minute imaging session and plotted the normalized fluorescence vs time. There was a steady decrease in the fluorescence of the lucigenin dye which indicates the presence of chloride ion transport as seen in Figures 3.19 and 3.21. The decay in fluorescence eventually started to level off indicating that an equilibrium between the chloride concentrations inside and outside the GUVs had been reached.

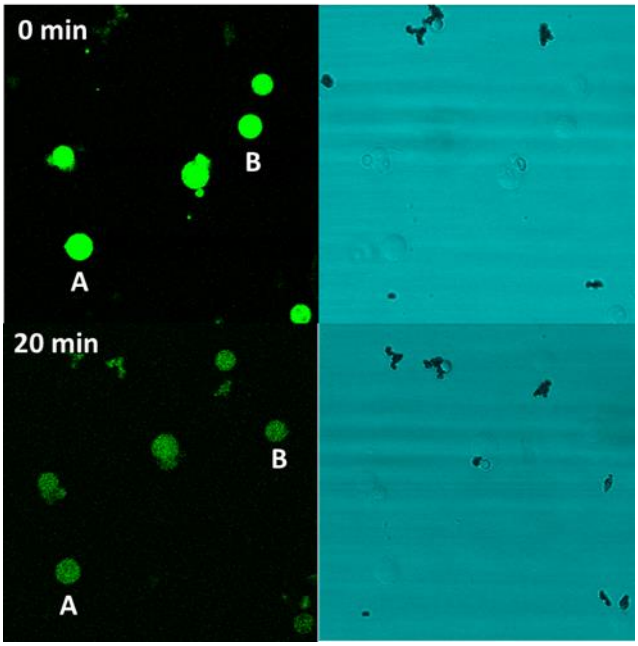

Figure 3.18: Left: Confocal fluorescence images of GUVs with compound **25** at 0 minutes, and 20 minutes after addition of NaCl, Right: Brightfield images taken at 0 minutes, and 20 minutes after addition of NaCl.

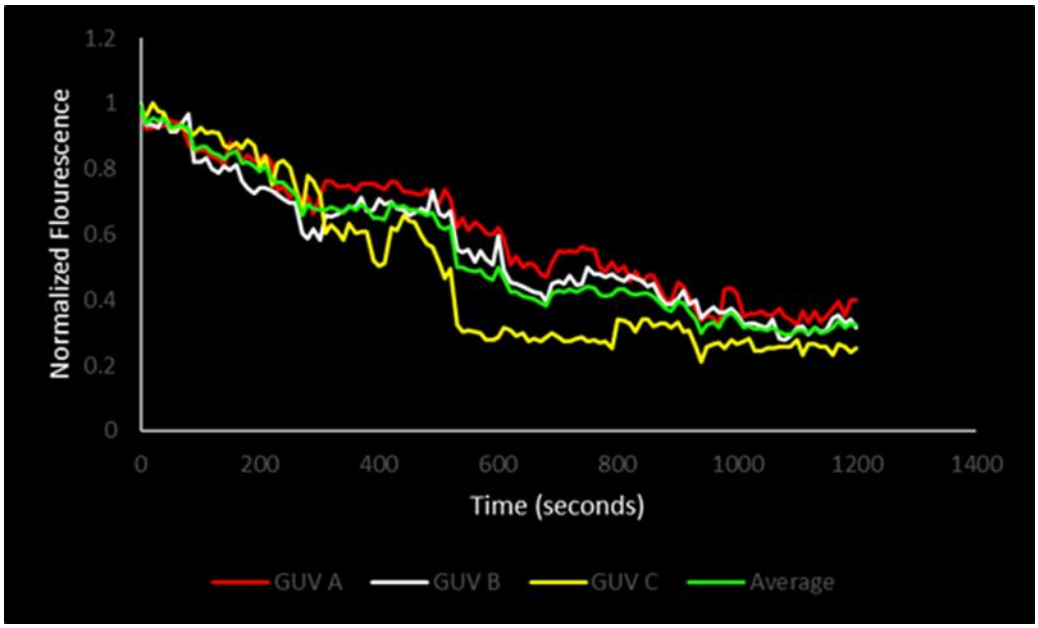

Figure 3.19: Plot of normalized fluorescence vs time over a period of 20 minutes for chloride ion transport studies conducted on compound **25**.

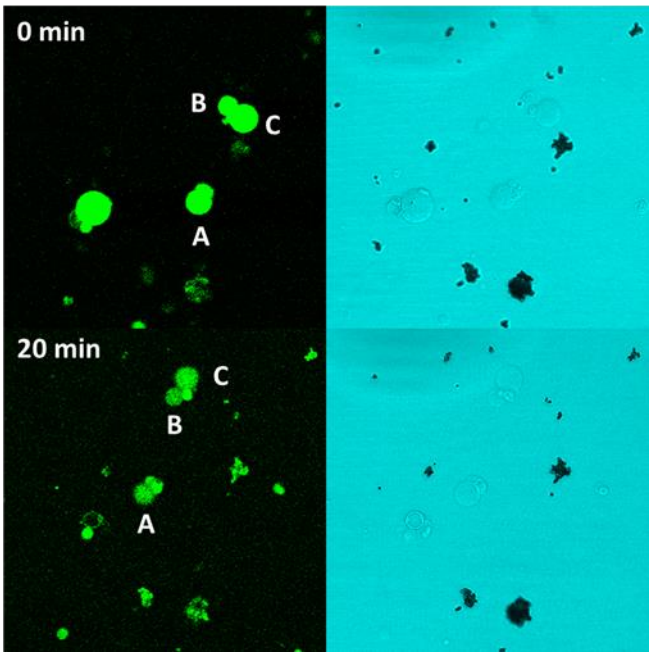

Figure 3.20: Left: Confocal fluorescence images of GUVs with compound **27** at 0 minutes, and 20 minutes after addition of NaCl, Right: Brightfield images taken at 0 minutes, and 20 minutes after addition of NaCl.

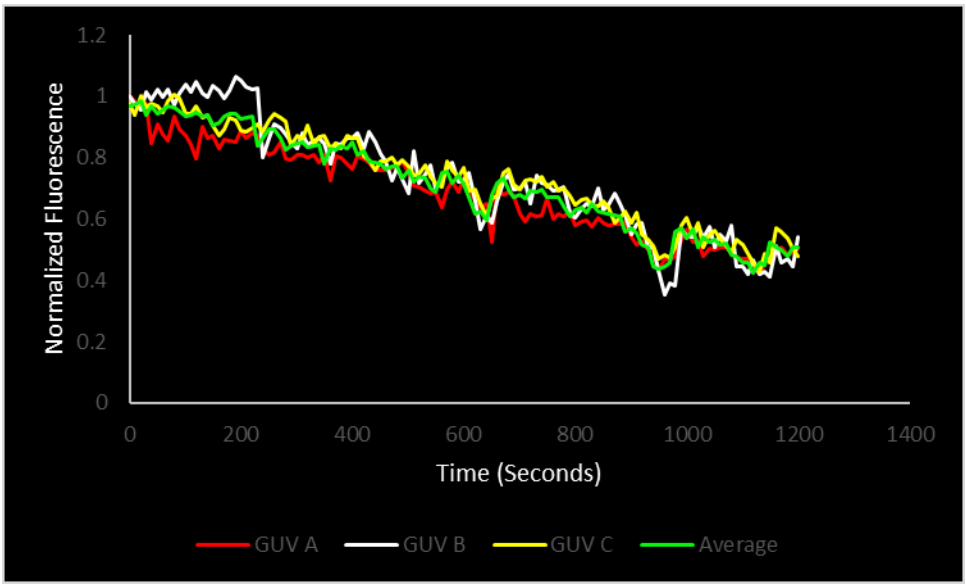

Figure 3.21: Plot of normalized fluorescence vs time over a period of 20 minutes for chloride ion transport studies conducted on compound **27**.

The ion transport experiments were completed in triplicate for both compound **25** and **27**, and the trials yielded similar fluorescence vs time curves, allowing us to use this data to find the average rate of ion transport. The fluorescence decay data was analyzed using a procedure previously used for large unilamellar vesicles (LUVs).[11] Normalized fluorescence[10] values were fitted to a single exponential decay function. This data was then converted to chloride ion concentrations by assuming that the limiting chloride concentration within the vesicles was 50 mM, the concentration of chloride ions within the imaging wells after addition. The initial rate of chloride transport per transporter molecule was then calculated using this information.[13] This was done for all three ion transport trials (all with 0.4 mol% transporter), yielding an average initial rate per transporter of approximately 3.1 $Cl^- s^{-1}$ per molecule for compound **25** and 2.6 $Cl^- s^{-1}$ per molecule for compound **27**. This rate of ion transport is significantly lower than those of

known highly active ion transporters such as bisthioureado decalin,[10] which transports chloride ions at a rate of approximately 860 $Cl^- s^{-1}$. In comparing to the highly efficient ion transporter synthesized by Davis et al., this indicates that despite having four times the ratio of transporter to lipid in our GUVs, our iridium (III) complexes function at less than 1% of the capacity. This could be due to our ancillary thiourea ligand not having as much of an affinity for chloride ions as other known ion transporters but in the future these ligands could be altered to lead to complexes that can transport ions at rates comparable to known transporters. Despite their slow rate of ion transport in comparison to know ionophores, these molecules are the first ion transporters that can also fluoresce.

3.4 Conclusion

In summary, we have developed two novel iridium (III) complexes that can function as both a bioimaging dyes as well as ion transporters. By inserting these complexes into the lipid bilayer of GUVs we were able to prove that they are fluorescent enough to be used as a dye at concentrations as low as 0.4 mol%, and that they transport chloride ions into GUVs at a low rate. These complexes do not transport ions as efficiently as known chloride ion transporters; however, they serve to prove that we can synthesize molecules that can function in two roles. We hope that demonstrating that these two characteristics can coexist within the same molecule will lead to the development of new molecules that can be used to both treat and image cancer cells simultaneously.

3.5 Future Work

The development of two new iridium (III) complexes as dual anion transporters and bioimaging dyes is also intriguing but there is more work to be done in this area to prove their usefulness. These complexes have only been tested on the transportation of chloride ions, but it is likely that they have the potential to function as transporters for other anions as well. Testing these complexes for their ability to transport other anions such as iodide, bromide, and bicarbonate would add more depth to their functionality and potential applications. In addition to anion transporters, cation transporters have been known to be used as anticancer drugs as well as for other applications. There is the potential to develop the first ever dual cation transporters and bioimaging dyes simply by changing the structure of the ancillary ligand on the iridium (III) complexes.

3.6 References

1. V. Kaushik, J. S. Yakisich, A. Kumar, N. Azad, A. K. V. Iyer, *Cancers*. **2018**, 10, 360.

2. N. Busschaert, S. Park, K. Baek, Y. P. Choi, J. Park, E. N. W. Howe, J. R. Hiscock, L. E. Karagiannidis, I. Marques, V. Félix, W. Namkung, J. L. Sessler, P. A. Gale, and I. Shin, *Nat Chem*. **2017**, 9(7), 667.

3. H. Sudath, A. Dmitri, *Front. Oncol*. **2020**, 10, 1131.

4. L. M. Quan, A. I. Mechler, P. J. Barnard, *J. Inorg. Biochem*. **2020**, 206.

5. T. Etrych, H. Lucas, O. Janoušková, P. Chytil, T. Mueller, K. Mäder, *J. Controlled Release.* **2016**, 226, 168.

6. S. Baas, V. Saggiomo, Ender3 3D printer kit transformed into Open, Programmable Syringe Pump set.

7. B. Balónová, D. Rota Martir, E. R. Clark, H. J. Shepherd, E. Zysman-Colman, B. A. Blight, *Inorg. Chem*. **2018**, 57(14), 8581.

8. M. Nonoyama, Bull., *Chem.Soc. Jpn*., **1974**, 47, 767-768.

9. C. S. Jennings, J. S. Rossman, B. A. Hourihan, R. J. Marshall, R. S. Forgan, and B. A. Blight, *Soft Matter*. **2021**, 17, 2024.

10. A. P. Davis, A. Kros, N. L. Mora, H. Valkenier, *Angew. Chem. Int. Ed*. **2015**, 54(7), 2137.

11. H. Valkenier, L.W. Judd, H. Li, S. Hussain, N. Sheppard, A. P. Davis, *J. Am. Chem. Soc*. **2014**, 136, 12507.

12. Aamod V. Desai, Sujit K. Ghosh, in Metal-Organic Frameworks (MOFs) for Environmental Applications, 2019.

13. Hills, RD Jr, McGlinchey, N., J Comput Chem. 2016, 37(12), 1112-1118.

Chapter 4
Conclusions and Future work

4.1 Conclusions

In summary, this thesis outlines the development of two potential new methods of ion transport into cells. We have demonstrated the first reported evidence of MOFs being used as anion transporters, as well as the first ever case of fluorescent iridium (III) complexes that can function as dual bioimaging dyes and anion transporters simultaneously.

In Chapter two, three different MOFs were tested, MOF 808, UiO-67, and Zr-BTDZ, for their ability to anchor to GUVs and then facilitate the transport of chloride ions. Using a literature procedure, GUVs were formed in the presence of lucigenin, a chloride sensitive dye, which subsequently became trapped within the GUVs aqueous interior, as well as MOFs which caused the GUVs to become anchored. These GUVs were then imaged under a fluorescence confocal microscope while sodium chloride was added. The lucigenin dye within the GUVs visibly quenched after the addition of chloride ions for both MOFs 808 and UiO-67. This suggested the capability of both MOFs 808 and UiO-67 to transport chloride ions across the lipid bilayer of GUVs. There was no indication that MOF Zr-BTDZ was able to transport the chloride ions into GUVs, but this suggests that not all MOFs can function as ion transporters, but rather that there are specific characteristics of the MOFs that allow them to function in this role. Control experiments were also conducted, including adding chloride to lucigenin filled GUVs not anchored to MOFs. This experiment was conducted in triplicate and demonstrated that

the addition of chloride to the solution with the GUVs does not alter their lipid bilayer allowing the chloride to pass through, thus causing the lucigenin dye to quench. Another control experiment was conducted using lucifer yellow dye in the place of the lucigenin dye. This was done to prove that the interaction between the MOFs anchored to GUVs did not cause a disruption in the lipid bilayer which allowed the dye to leak out. These control experiments served to prove that the quenching of lucigenin dye we were witnessing was due to the transport of chloride ions, by MOFs, through the lipid bilayer of the GUVs. This data altogether proves the first ever reported evidence that MOFs, when anchored to GUVs, can function as efficient ion transporters and could have fascinating implications for the potential future treatment of channelopathies like cystic fibrosis.

In Chapter three, two new iridium (III) complexes were synthesized based on the structure of known anion transporters and iridium (III) bioimaging dyes. These complexes were then tested for the ability to function as bioimaging dyes and as chloride ion transporters. To test their ability to perform as bioimaging dyes, GUVs were formed with the iridium complexes in their presence allowing them to integrate within the lipid bilayer of the GUVs. These GUVs were then imaged using a confocal fluorescence microscope. These images proved that both iridium complexes were highly visible in the lipid bilayer of the GUVs at a concentration of only 0.4 mol %, and that their addition did not affect the structural integrity of the GUVs membrane. To test these complexes for ion transport, GUVs were formed both in the presence of the iridium complexes and the chloride sensitive dye lucigenin. These GUVs were then imaged on a fluorescence confocal microscope while chloride ions were introduced to the GUVs, and the

quenching of the lucigenin dye indicated the capability to the two new iridium complexes to function as ion transporters. Both complexes performed as effective bioimaging dyes and consistent chloride ion transporters. Control experiments were also conducted, including adding chloride to lucigenin filled GUVs without the iridium complexes in their lipid bilayer. This experiment was conducted in triplicate and demonstrated that the addition of chloride to the solution with the GUVs does not alter their lipid bilayer allowing the chloride to pass through, thus causing the lucigenin dye to quench. Another control experiment was conducted using lucifer yellow dye in the place of the lucigenin dye. This was done to prove that the addition of the iridium complexes to the lipid bilayer of the GUVs did not cause a disruption in the lipid bilayer which allowed the dye to leak out. These control experiments served to prove that the quenching of lucigenin dye was due to the transport of chloride ions by the iridium anion transporters through the lipid bilayer of the GUVs. In conclusion, the data obtained proves the capability of two new iridium (III) complexes to function as effective anion transporters and bioimaging dyes, research within this area could have potential future applications in the treatment of various cancers.

4.2 Future work

MOFs as anion transporters is a novel and fascinating discovery yet there is still much work that needs to be done to continue to prove this concept. Only three MOFs have been tested, all of which are zirconium MOFs. It would be useful to test a variety of other MOFs using other metal nodes such as iron, copper, and zinc, as these are some of the most used metal nodes in MOFs. It would also be useful to test a variety of MOFs

with varying organic linker molecules as well to see how these might affect the MOFs ability for anion transport.

We have also only tested MOFs for anion transport using chloride ions; it would be beneficial to test MOFs for their ability to transport other anion as well, including the bicarbonate ion as it and chloride are among the most important anions transported into and out of cells within the human body. Although not as important biologically, it would also be useful to test other anions such as iodide, and even bromide ions. MOFs could also have the potential to transport cations across the lipid bilayer of GUVs. Sodium, potassium, calcium, and even proton transport within cells is imperative for their functions, so it would be useful to test these MOFs for cation transport in addition to the already proven study of anion transport.

Finally, we are not completely certain of the mechanism that underlies the ability of MOFs 808 and UiO-67 to transport chloride ions, so control experiments need to be developed to discover what characteristic of MOFs allows them to function as anion transporters.

The development of two new iridium (III) complexes as dual anion transporters and bioimaging dyes is also intriguing but there is more work to be done in this area of research as well. These complexes have only been tested on the transportation of chloride ions, but it is likely that they have the potential to function as transporters for other anions as well. Testing these complexes for their ability to transport other anions such as iodide, bromide, and bicarbonate would add more depth to their functionality and potential applications. In addition to anion transporters, cation transporters have been known to be used as anticancer drugs as well as for other applications. There is the

potential to develop the first ever dual cation transporters and bioimaging dyes simply by changing the structure of the ancillary ligand on the iridium (III) complexes.

Fluorescent red dyes are widely used for biological applications, as they are highly efficient for deep tissue imaging.[1] Iridium (III) complexes are well known for their ability to fluoresce different colours depending on the structure of their cyclometalated ligands[2], so this project could also be expanded into the development of red iridium (III) complexes that can also act as ion transporters and bioimaging dyes. Red versions of both iridium complexes used in Chapter 3 have been synthesized by changing the cyclometalated ligands for one with more electron-donating properties. These complexes have yet to be fully characterized or tested for their abilities as anion transporters, however, as the ancillary ligand is the part of the structure that we would expect to play the biggest role in the complexes ability to transport ions, and this ligand remains the same in the red complexes, it could be assumed that they should have a similar capacity for transporting chloride ions.

After proving these iridium (III) complexes can work as chloride ion transporters and bioimaging dyes as intended, the next step would be to evaluate their performance when used in actual cells. Following literature procedures used by Balonova et al.[3] and Busschaert et al.[4], these complexes can be tested for both cytotoxicity against healthy cells and cancer cells, to determine their efficacy as potential cancer drugs, as well as for their ability to transport ions within living cells rather than synthetic vesicles. These studies are necessary as these complexes have thus far only been tested on GUVs, and to move forward in studying their potential use in the treatment of cancers they need to be tested on actual living cells.

Another remaining problem is if these complexes are used in the future as tumor imaging dyes, they need to selectively seek out cancer cells rather than normal healthy cells. According to Pearce et al., drugs synthesized with the purpose of seeking out cancer cells whether for imaging or treatment are often equipped with ligands that have a specific affinity for the target cells.[5] If these complexes show promise in causing cancer cell death, then it is possible that they would need to undergo further derivatization to be fixed with a ligand that would allow them to specifically target cancer cells within the body.

In summary, there are a variety of fascinating routes that these projects could follow if there is continued success in their abilities to be used as bioimaging dyes and anion transporters.

4.3 References

1. E. Oliveira, E. Bértolo, C. Núñez, V. Pilla, H. M. Santos, J. Fernández-Lodeiro, A. Fernández-Lodeiro, J. Djafari, J. L. Capelo, C. Lodeiro. *ChemistryOpen*. **2017**, 7(1), 9-52.

2. C. Caporale, M. Massi, *Coordination Chemistry Reviews*, **2018**, 363, 71-91.

3. S. J. Thomas, B. Balónová, J. Cinatl, M. N. Wass, C. J. Serpell, B. A. Blight, M. Michaelis, *ChemMedChem*, **2020**, 15 (4), 349-353.

4. N. Busschaert, S. Park, K. Baek, Y. P. Choi, J. Park, E. N. W. Howe, J. R. Hiscock, L. E. Karagiannidis, I. Marques, V. Félix, W. Namkung, J. L. Sessler, P. A. Gale, I. Shin, *Nat. Chem*. **2017**, 9, 667–675.

5. A. K. Pearce, R. K. O'Reilly, *Bioconjugate Chem*. **2019**, 30, 9, 2300–2311.

Appendix I

Supporting Information for Chapter 2

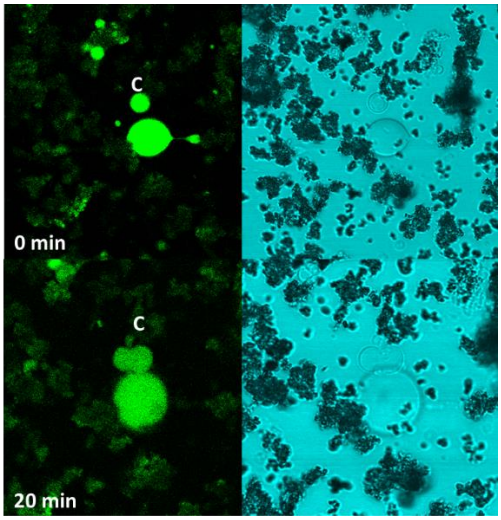

S1: Left: Confocal fluorescence images of GUVs anchored to MOF-808 at 0 minutes, and 20 minutes after addition of NaCl, Right: Brightfield images taken at 0 minutes, and 20 minutes after addition of NaCl.

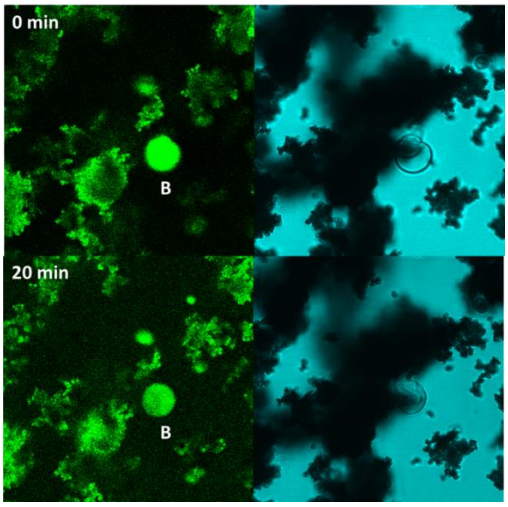

S2: Left: Confocal fluorescence images of GUV B anchored to MOF UiO-67 at 0 minutes, and 20 minutes after addition of NaCl, Right: Brightfield images taken at 0 minutes, and 20 minutes after addition of NaCl.

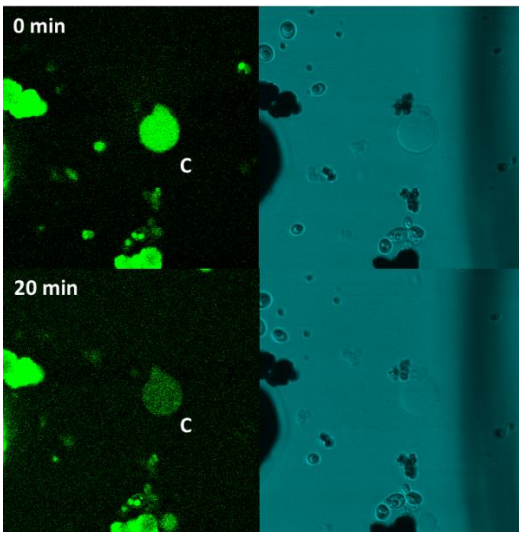

S3: Left: Confocal fluorescence images of GUV C anchored to MOF UiO-67 at 0 minutes, and 20 minutes after addition of NaCl, Right: Brightfield images taken at 0 minutes, and 20 minutes after addition of NaCl.

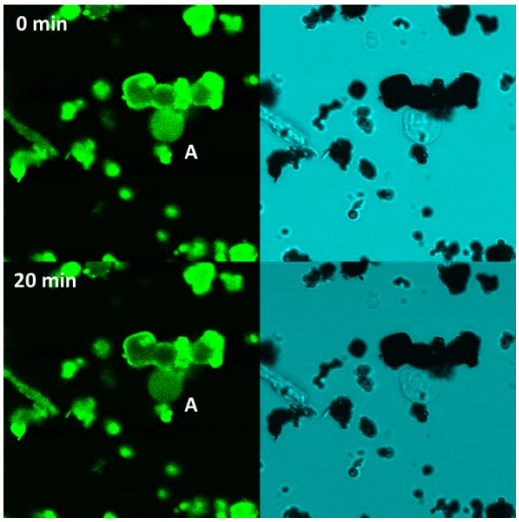

S4: Left: Confocal fluorescence images of GUV A anchored to MOF Zr-BTDZ at 0 minutes, and 20 minutes after addition of NaCl, Right: Brightfield images taken at 0 minutes, and 20 minutes after addition of NaCl.

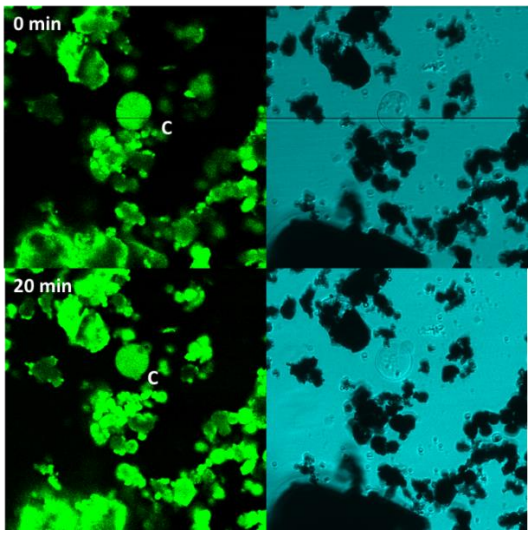

S5: Left: Confocal fluorescence images of GUV C anchored to MOF Zr-BTDZ at 0 minutes, and 20 minutes after addition of NaCl, Right: Brightfield images taken at 0 minutes, and 20 minutes after addition of NaCl.

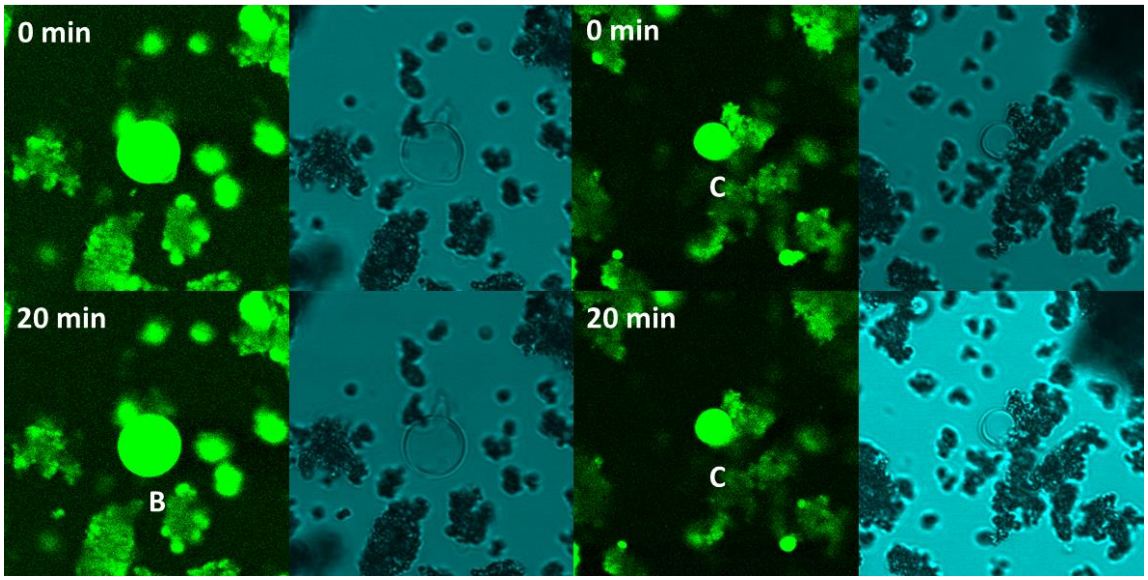

S6: Confocal fluorescence images of GUVs B and C filled with lucifer yellow dye and anchored to MOF-808 at 0 minutes, and 20 minutes after addition of NaCl, Right: Brightfield images taken at 0 minutes, and 20 minutes after addition of NaCl.

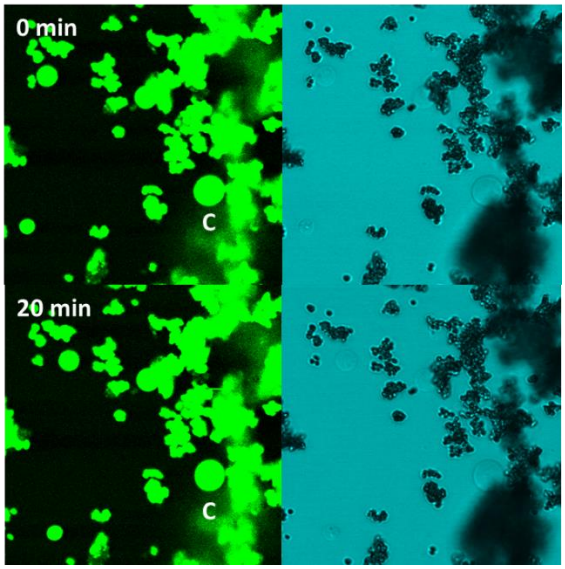

S7: Confocal fluorescence images of GUV C filled with lucifer yellow dye and anchored to MOF UiO-67 at 0 minutes, and 20 minutes after addition of NaCl, Right: Brightfield images taken at 0 minutes, and 20 minutes after addition of NaCl.

Supporting Information for Chapter 3

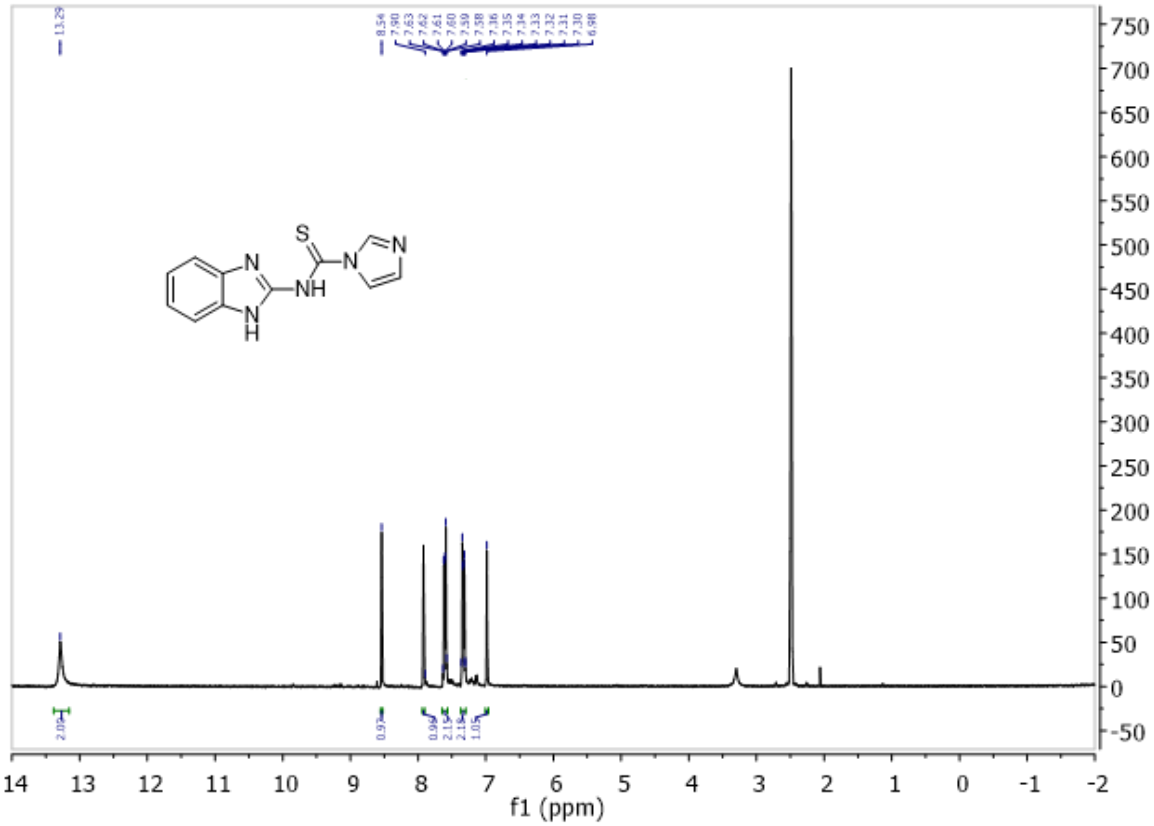

S8: ^{1}H NMR spectrum of compound **22**, 400 MHz. d6-DMSO (2.49) and water contaminant (3.3)

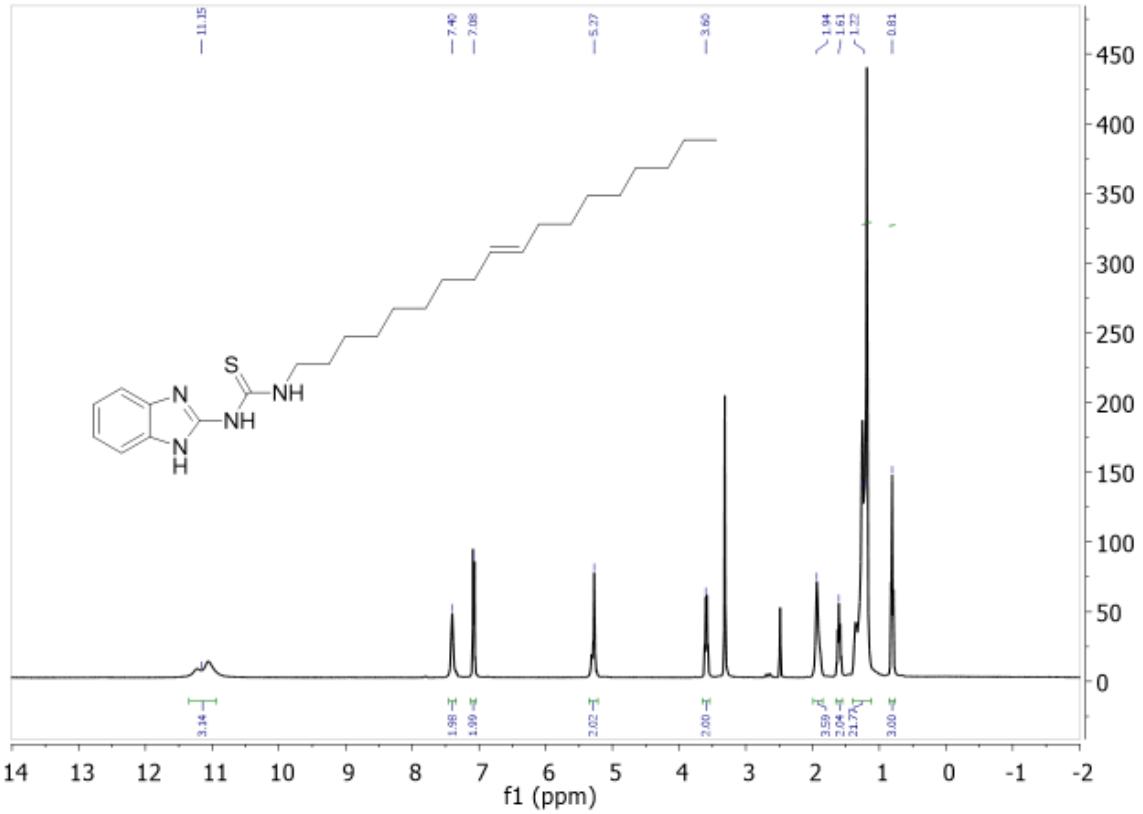

S9: ^{1}H NMR spectrum of compound **23,** d6-DMSO (2.49) and water contaminant (3.3)

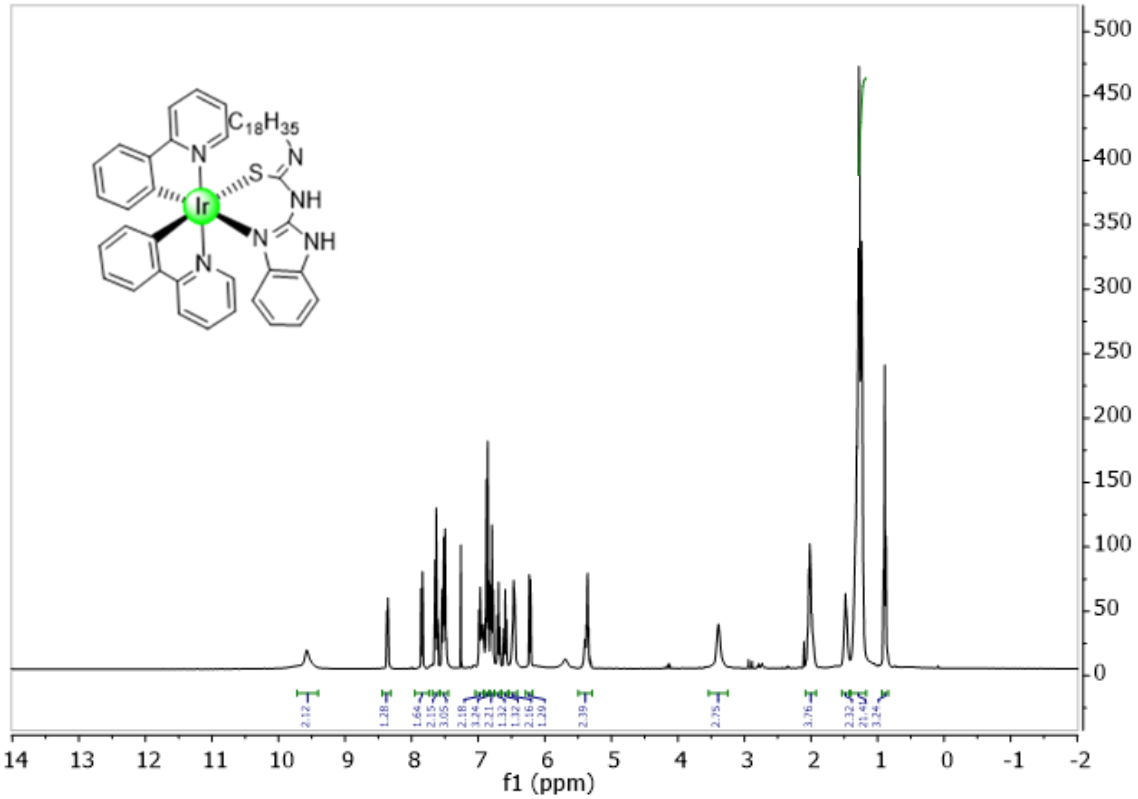

S10: ^{1}H NMR spectrum of compound **25**, 400 MHz, $CDCl_3$ (7.26)

Mass Spectrum SmartFormula Report

Analysis Info

Analysis Name	D:\Data\Xiao\Aug 04 2022000013.d	Acquisition Date	8/4/2022 3:19:41 PM
Method	Xiao all 1.m	Operator	x
Sample Name	BH-64	Instrument	compact 8255754.20059
Comment			

Acquisition Parameter

Source Type	ESI	Ion Polarity	Positive	Set Nebulizer	0.5 Bar
Focus	Not active	Set Capillary	3500 V	Set Dry Heater	180 °C
Scan Begin	50 m/z	Set End Plate Offset	-500 V	Set Dry Gas	4.0 l/min
Scan End	1500 m/z	Set Charging Voltage	2000 V	Set Divert Valve	Source
		Set Corona	0 nA	Set APCI Heater	0 °C

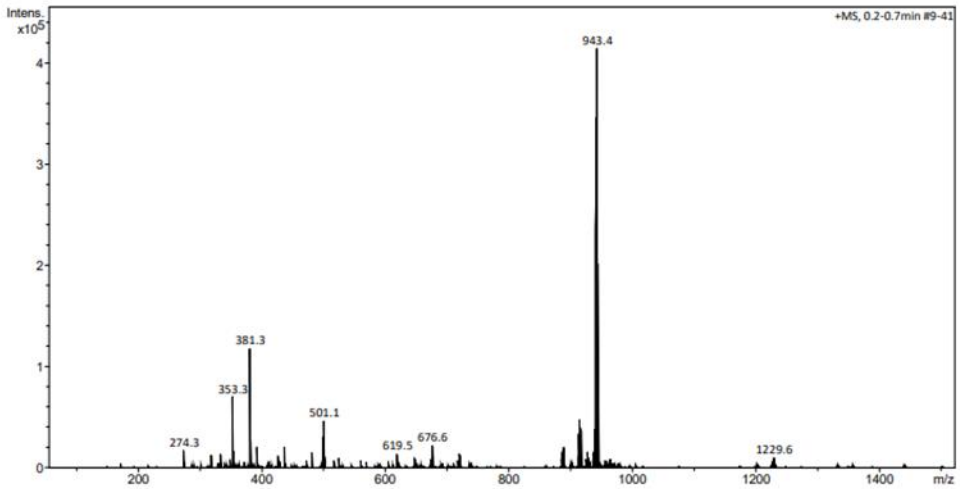

S11: Mass spectrum of compound **25**.

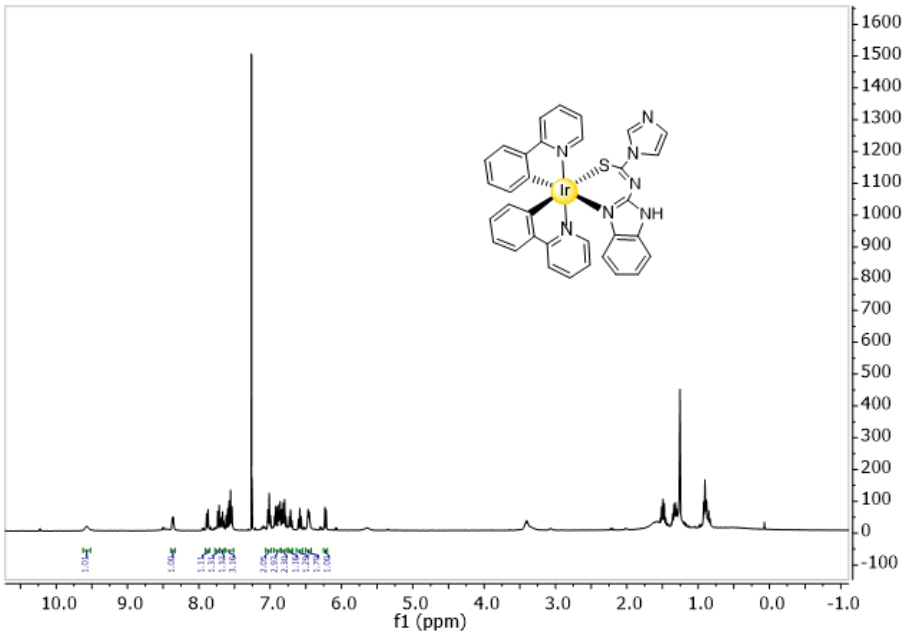

S12:^{1}H NMR spectrum of compound **26**, 400 MHz, $CDCl_3$ (7.26)

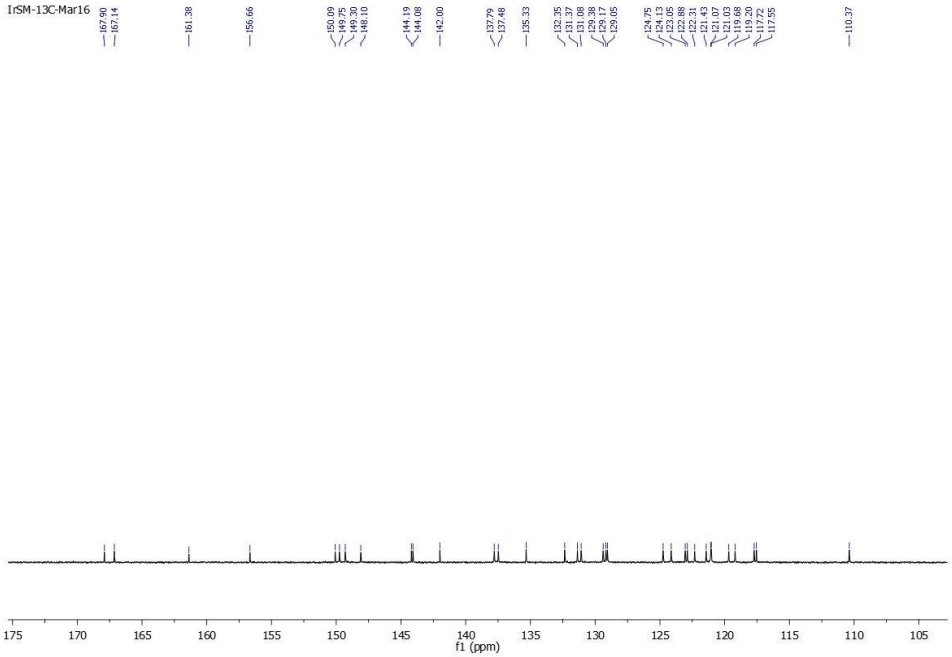

S13: ^{13}C NMR spectrum of compound **26**

Mass Spectrum SmartFormula Report

Analysis Info

Analysis Name	D:\Data\Xiao\Jan 07 2022000009.d	Acquisition Date	1/7/2022 9:50:35 AM
Method	Xiao all 1.m	Operator	x
Sample Name	Iridium Primer	Instrument	compact 8255754.20059
Comment			

Acquisition Parameter

Source Type	ESI	Ion Polarity	Positive	Set Nebulizer	0.5 Bar
Focus	Not active	Set Capillary	3500 V	Set Dry Heater	181 °C
Scan Begin	50 m/z	Set End Plate Offset	-500 V	Set Dry Gas	4.0 l/min
Scan End	1500 m/z	Set Charging Voltage	2000 V	Set Divert Valve	Source
		Set Corona	0 nA	Set APCI Heater	0 °C

Meas. m/z	Ion Formula	m/z	err [ppm]
744.150838	C33H25IrN7S	744.151593	1.0

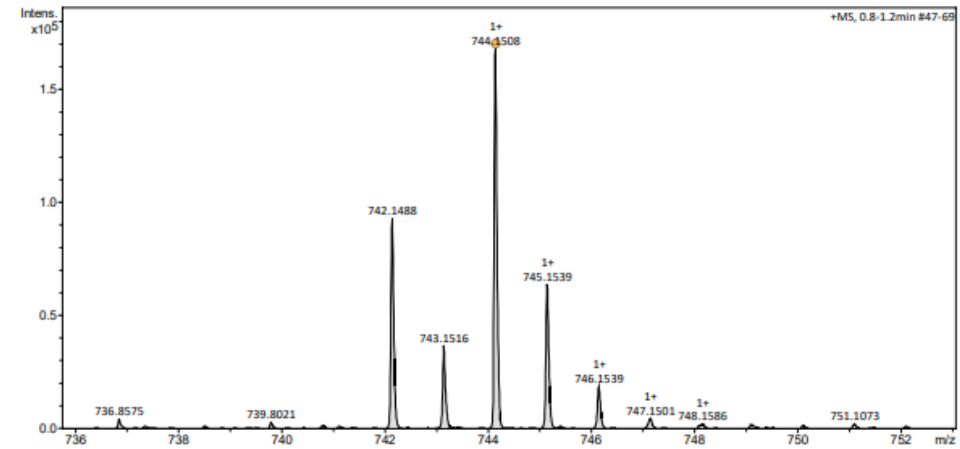

S14: Mass spectrum of compound **26**

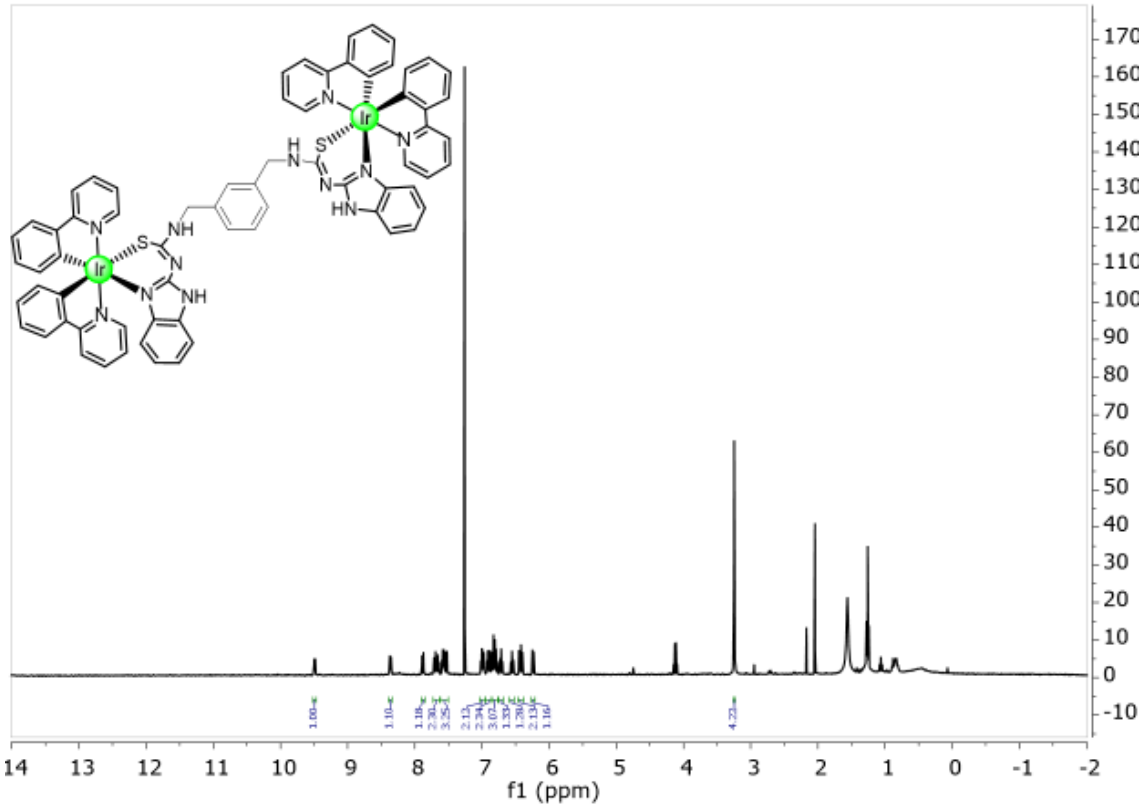

S15: ^{1}H NMR spectrum of compound **27**, $CDCl_3$ (7.26)

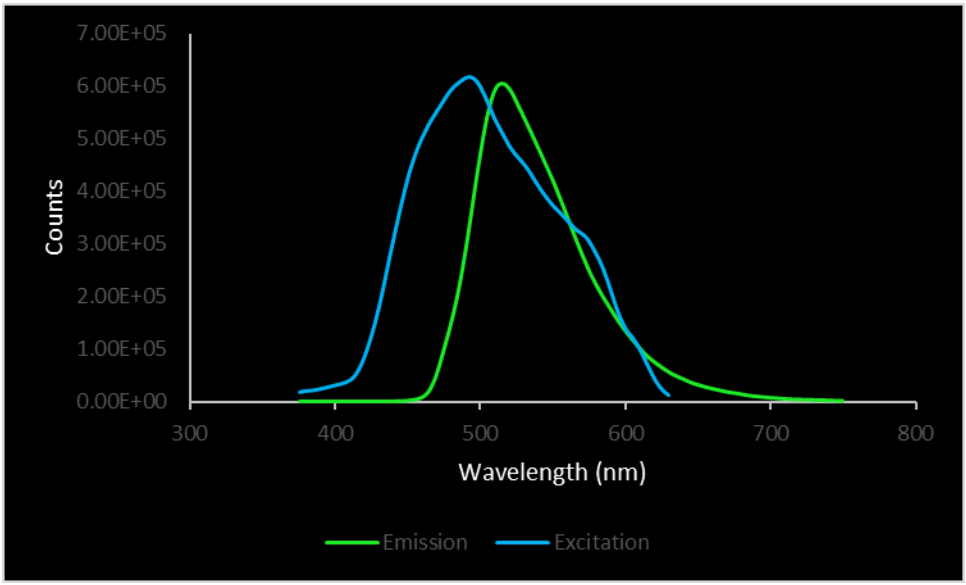

S16: Emission and excitation maxima for compound **25**.

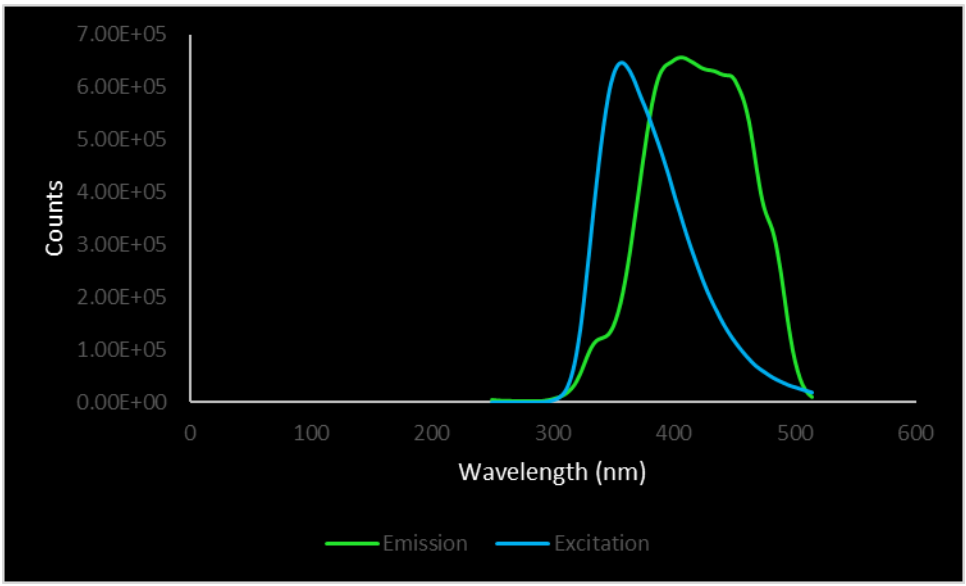

S17: Emission and excitation maxima for compound **27**.

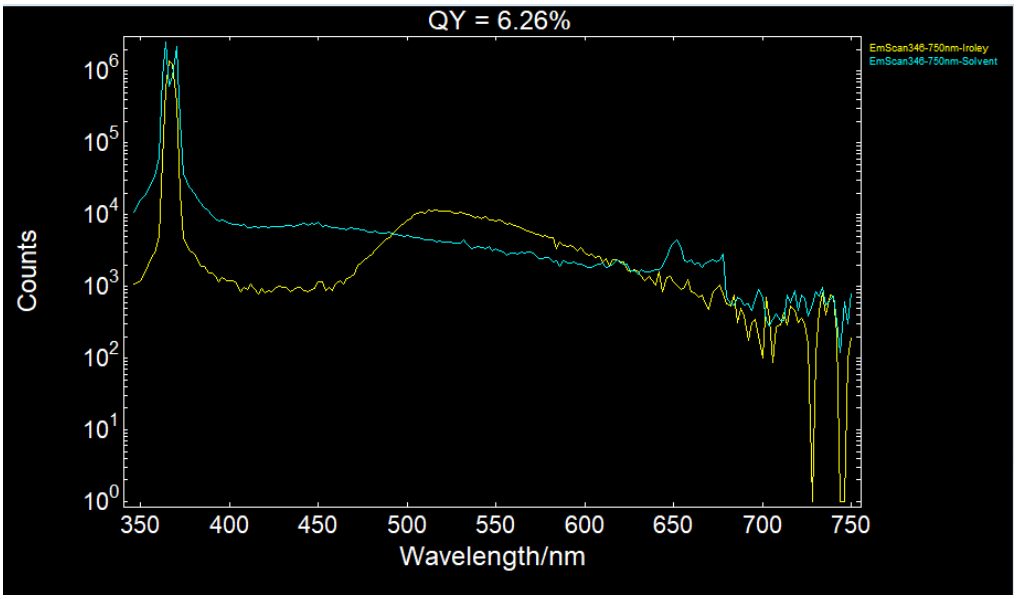

S18: Quantum yield spectra #1 for compound **25**, at 350 – 750 nm.

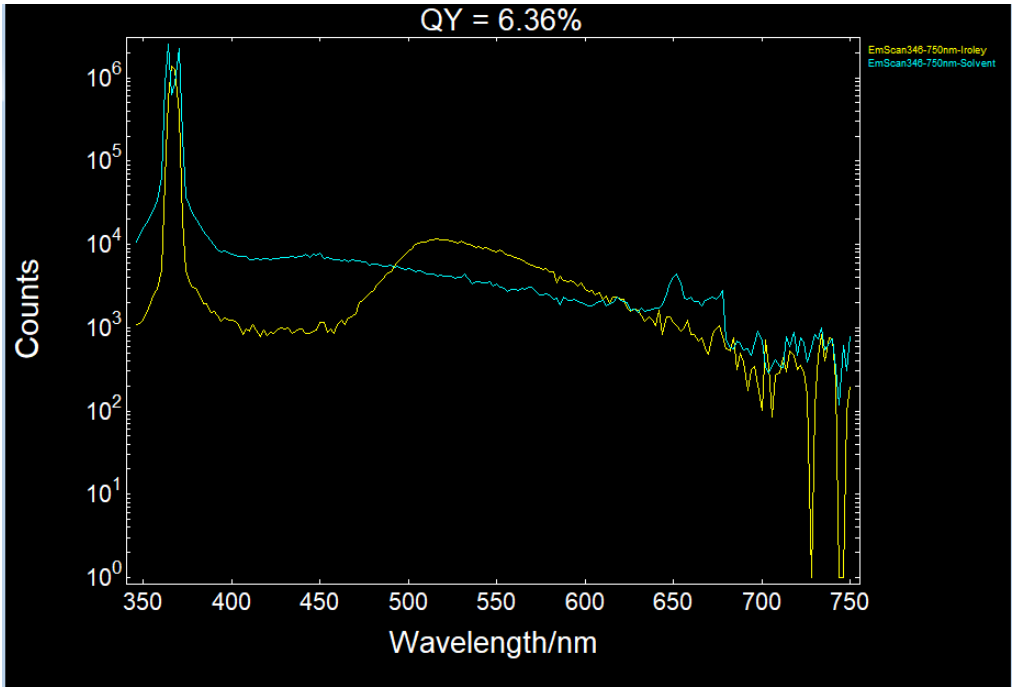

S19: Quantum yield spectra #2 for compound **25**, at 350 – 750 nm.

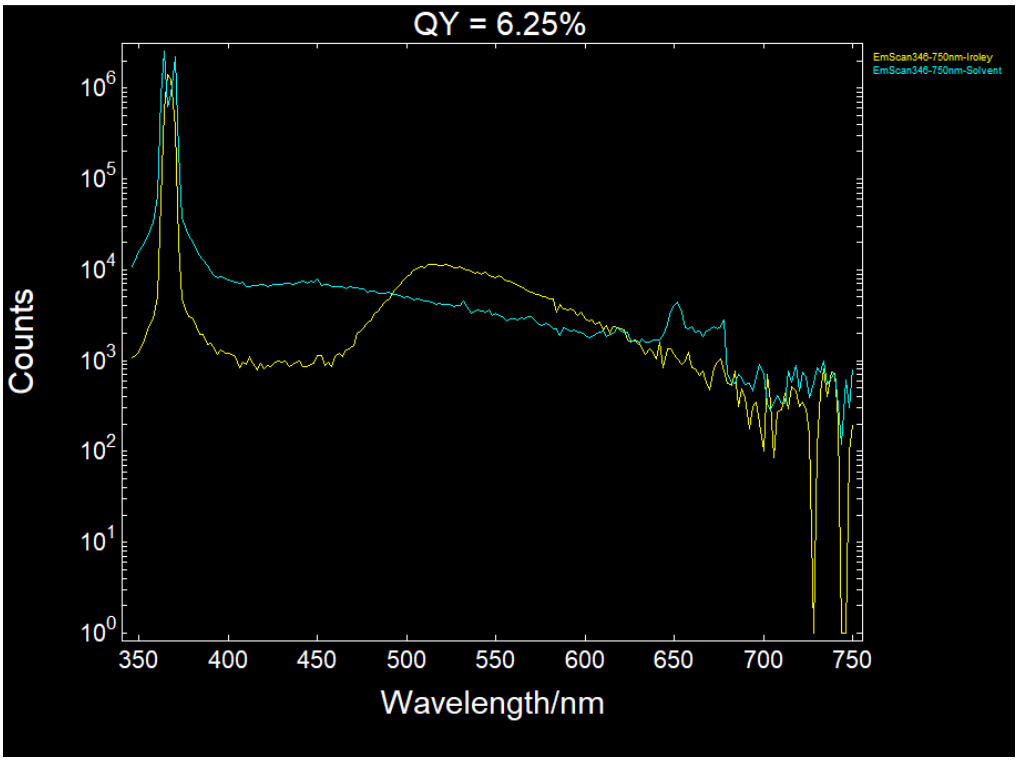

S20: Quantum yield spectra #3 for compound **25**, at 350 – 750 nm.

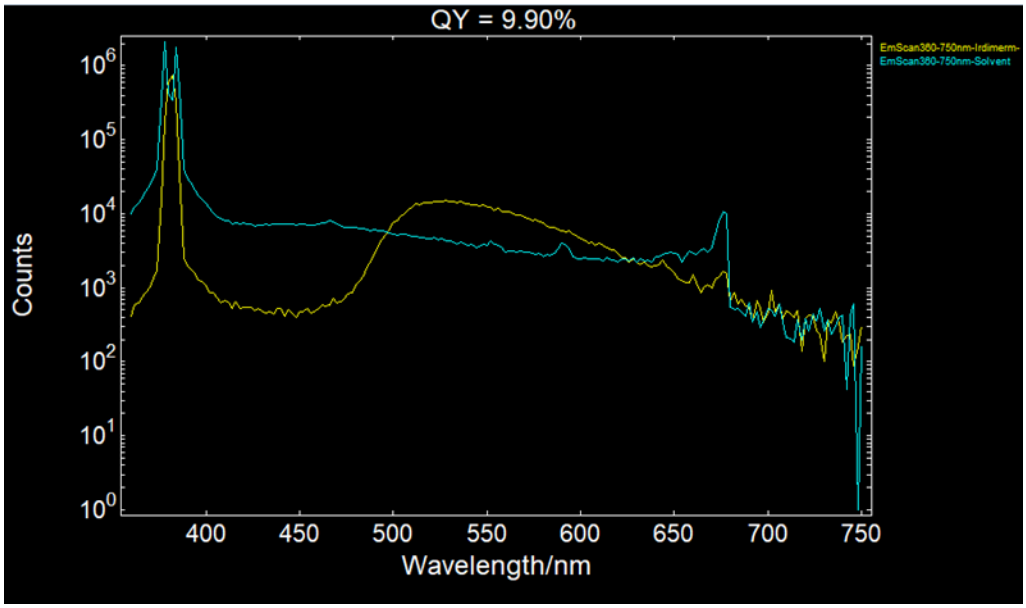

S21: Quantum yield spectra #1 for compound **27**, at 350 – 750 nm.

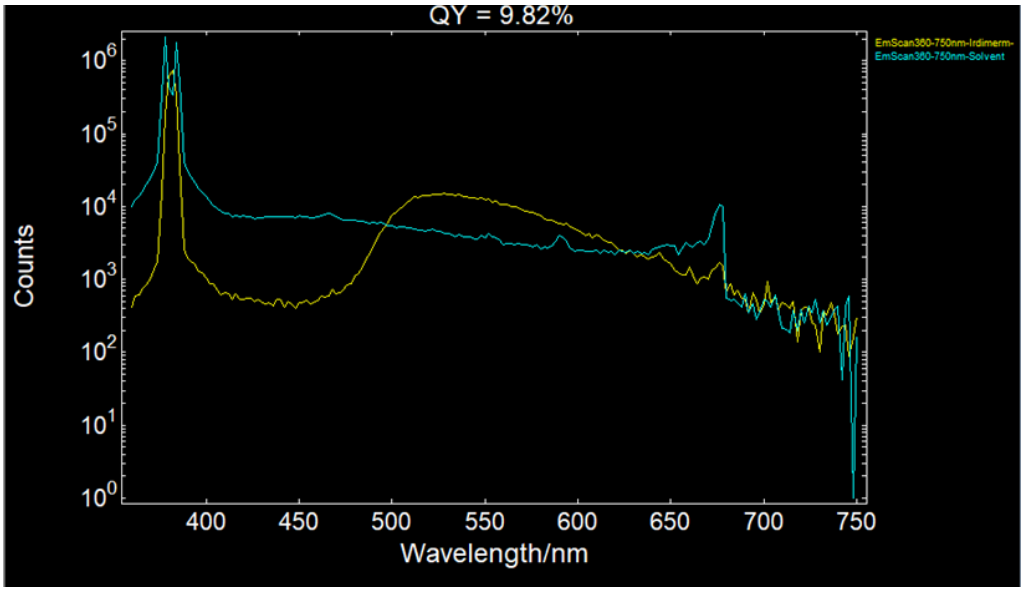

S22: Quantum yield spectra #2 for compound **27**, at 350 – 750 nm.

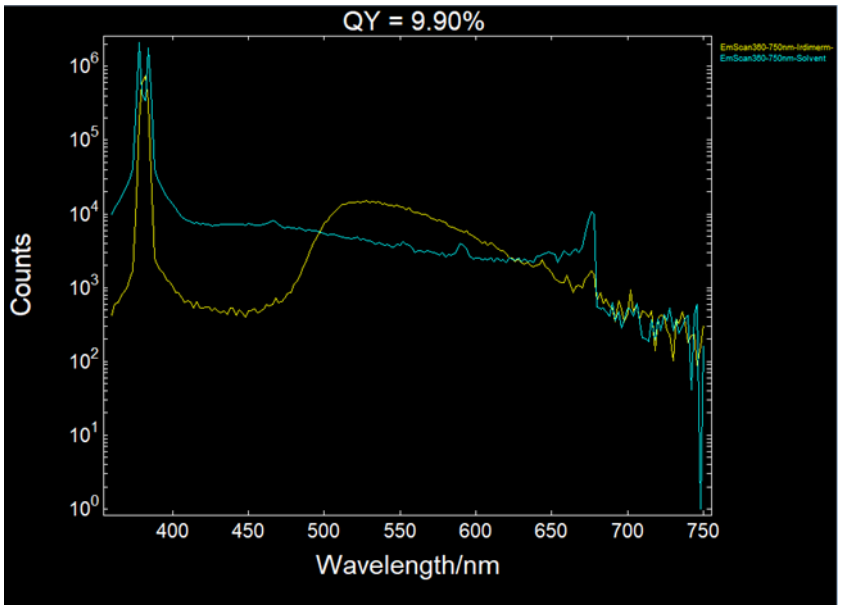

S23: Quantum yield spectra #3 for compound **27**, at 350 – 750 nm.

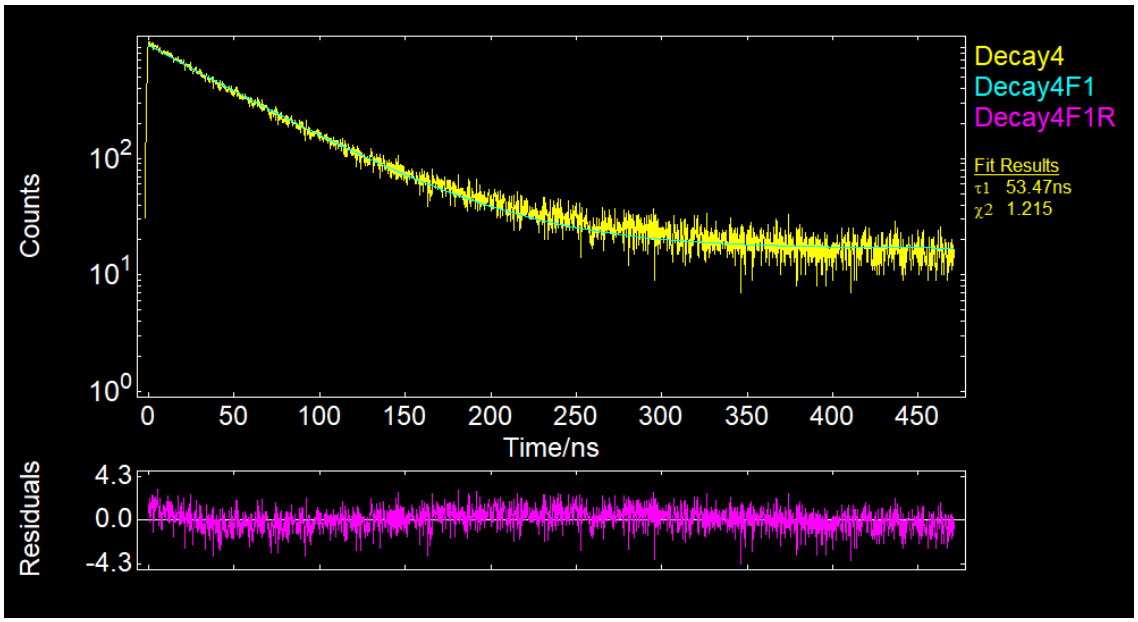

S24: Lifetime decay of compound **25** after excitation at 366 nm at 298 K. Data collected at Λ = 514 nm.

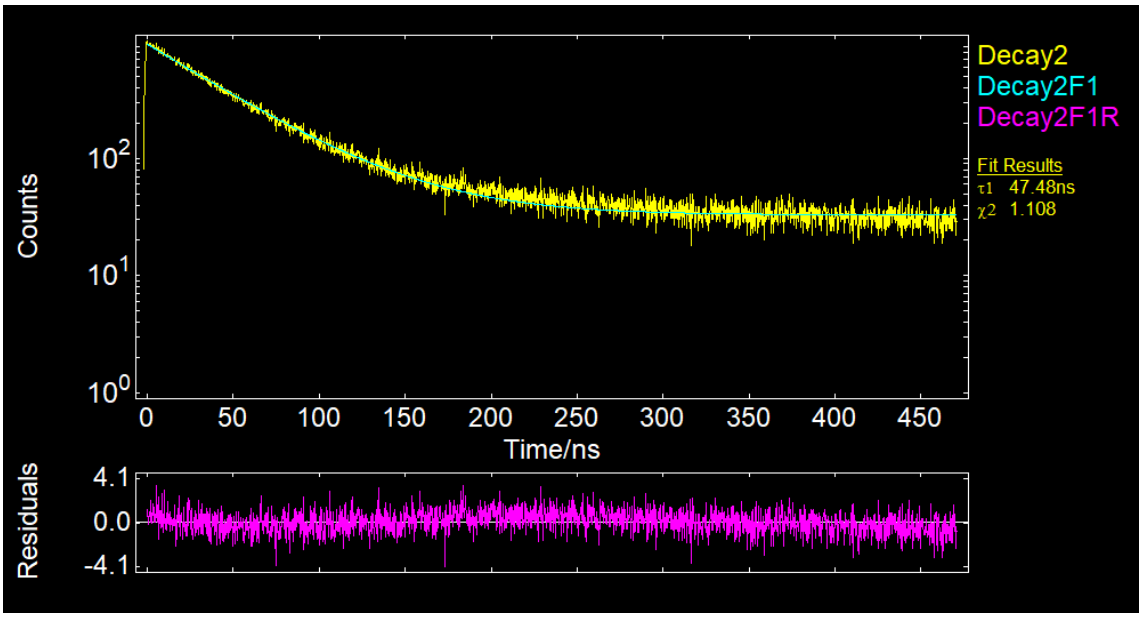

S25: Lifetime decay of compound **27** after excitation at 406 nm. Data collected at Λ = 524 nm.

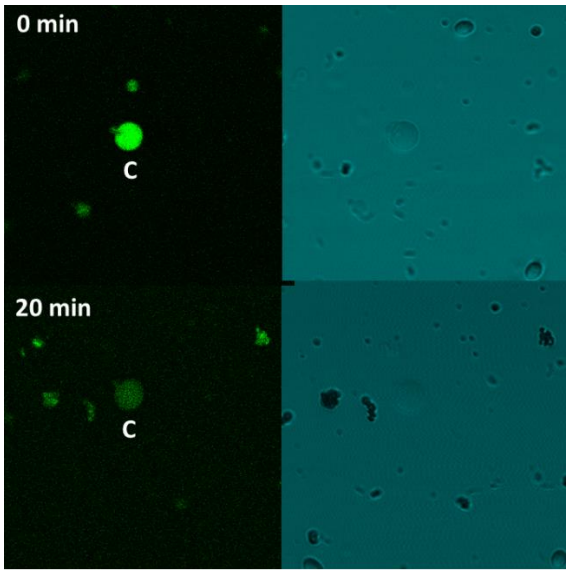

S26: Confocal fluorescence images of compound **25** in GUV C at 0 minutes, and 20 minutes after addition of NaCl, Right: Brightfield images taken at 0 minutes, and 20 minutes after addition of NaCl.

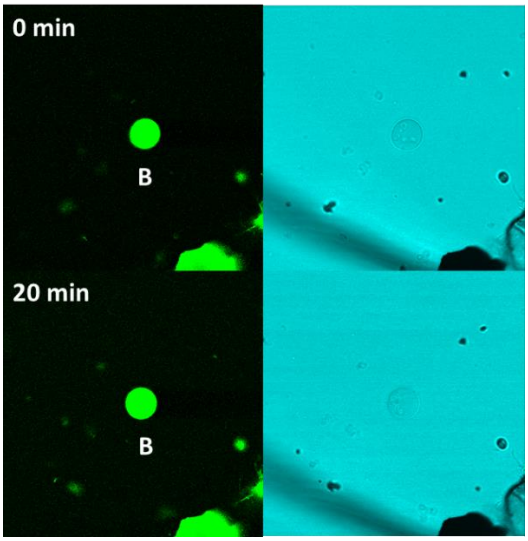

S27: Confocal fluorescence images of compound **25** in GUV B filled with lucifer yellow dye at 0 minutes, and 20 minutes after addition of NaCl, Right: Brightfield images taken at 0 minutes, and 20 minutes after addition of NaCl.

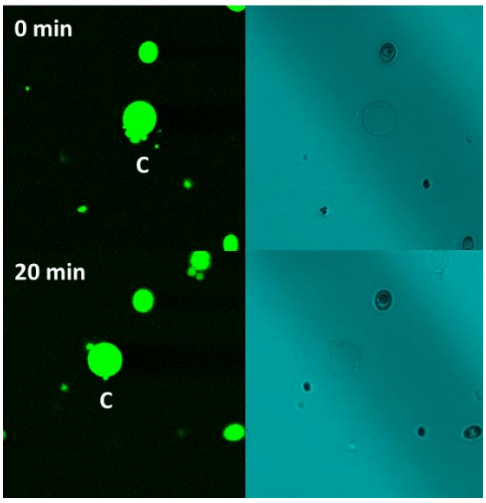

S28: Confocal fluorescence images of compound **25** in GUV C filled with lucifer yellow dye at 0 minutes, and 20 minutes after addition of NaCl, Right: Brightfield images taken at 0 minutes, and 20 minutes after addition of NaCl.

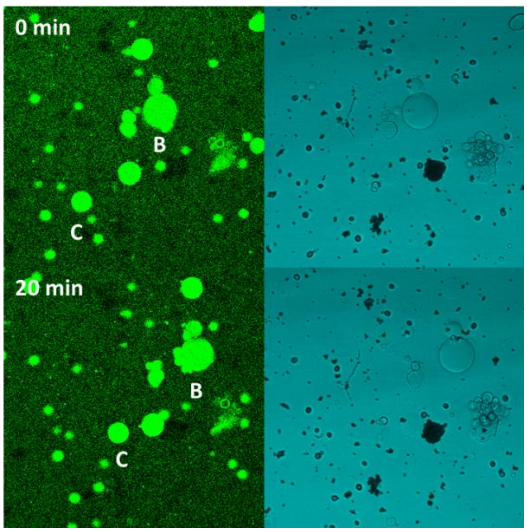

S29: Confocal fluorescence images of compound **27** in GUVs B and C filled with lucifer yellow dye at 0 minutes, and 20 minutes after addition of NaCl, Right: Brightfield images taken at 0 minutes, and 20 minutes after addition of NaCl.

Curriculum Vitae

Braeden Hourihan

Education

2022-Present **PhD Chemistry**

University of Ottawa, ON, Canada

2021-Present **MSc. Chemistry – Focus: Inorganic Chemistry**

University of New Brunswick, NB, Canada

2017-2021 **B.Sc. Chemistry**

University of New Brunswick, NB, Canada

Journal Publications

1. Jennings, Christopher S.; Rossman, Jeremy s.; **Hourihan, Braeden A**.; Marshall, Ross; Forgan, Ross S.; Blight, Barry A.* "Immobilizing Giant Unilamellar Vesicles with Zirconium Metal-Organic Framework Anchors." Soft Matter, 2021, 17, 2024-2027 DOI: 10. 1039/D0SM02188A

Conference Presentations

- N/A

Awards and Grants

- UOttawa PhD Entrance Scholarship (fall 2022-present)
- NBIF STEM & Social Innovation Award (2021-2022)
- G. Vernon and Leila M. Ashfield Memorial Scholarship (2020 – 2021)
- Betts/Wilbur Memorial Scholarship (2017-2021)